Polynuclear Ni(II) Complexes with Schiff Bases as Bridging Ligands:

A Molecular Approach to Nanoscience

Angeliki A. Athanasopoulou

A thesis submitted to the Department of Chemistry in partial fulfillment of the

requirements for the Degree of Master of Science

Brock University

St. Catharines Ontario, Canada

September 2015

Abstract

The initial employment of *N*-salicylidene-2-amino-5-chlorobenzoic acid ($sacbH_2$) in metal cluster chemistry has provided access to five new polynuclear Ni^{II} complexes with large nuclearities, unprecedented metal core topologies, and interesting magnetic properties.

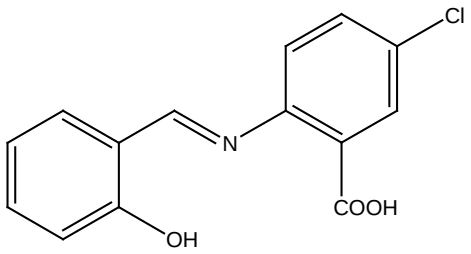

N-salicylidene-2-amino-5-chlorobenzoic acid ($sacbH_2$)

The obtained results are presented in two projects. The first project includes the investigation of the general $Ni^{2+}/RCO_2^-/sacbH_2$ reaction system (where R = CH_3, Bu^t, Bu^tCH_2) in which the nature of the carboxylic acid was found to be of crucial importance, affecting enormously the nuclearity of our complexes. $\{Ni_{26}\}$ (**1**), $\{Ni_{18}\}$ (**2**) and $\{Ni_{11}\}$ (**3**) compounds were obtained. The second project includes the study of the $Ni^{2+}/X^-/sacbH_2$ reaction system (X^- = inorganic anions) under basic conditions. Two new complexes, $\{Ni_4\}$ (**4**) and a $\{Ni_8\}$ (**5**), were obtained and characterized. The magnetic properties of **1**-**5** were thoroughly studied. The plethora of coordination modes demonstrated by $sacb^{2-}$ ligand justifies the usefulness of Schiff bases in the field of molecular nanoscale magnetism.

Acknowledgements

First and foremost, I would like to thank my supervisor, Prof. Theocharis C. Stamatatos, whose encouragement, guidance and support enabled me to finish this Thesis. I would also like to thank him for assigning this very interesting and enjoyable project to me and for teaching me so many things and perspectives of coordination chemistry and molecular magnetism. Besides my research advisor, I would also like to thank the members of my research committee, Prof. Melanie Pilkington and Prof. Art van der Est for their continuous encouragement, helpful advice, and insightful comments. My thanks also go to all our research collaborators because without their hard work none of these interesting compounds would have been thoroughly studied and eventually published in prestigious peer-reviewed international journals. More specifically, I am utterly grateful to Dr. Catherine P. Raptopoulou, Dr. Vassilis Psycharis, and Prof. Melanie Pilkington for solving and refining the structures of all the reported complexes, as well as Prof. Albert Escuer who performed the magnetic studies of all synthesized Ni(II) cluster compounds.

The members of Prof. Stamatatos' research group have been my family for the past two years at Brock University. They have my endless gratitude for enduring me over the years and for being my friends. After all, we all had the same cause: A snow day! Lab work is fun but it will never be the same without you guys. My special gratitude goes to the PhD student in our group, Dimitrios Alexandropoulos, who taught me many synthetic hints in the lab and guided me whenever I was facing difficulties. I must also thank my uncle, Prof. Spyros P. Perlepes, because he was the first person who pushed me to reach

my limits, leave the security of my home and country, and move to Canada for pursuing graduate studies. For these reasons, I am very grateful!

The foundations of who I am can only be traced back to my parents. From them I have learned more than I can recall, and they helped me to become the person I am today. Although geographically distant, their constant support and advice have been the driving force for me all this time. I dedicate my Thesis to them because without them I would have done nothing in my life; I want to say that I am more than grateful being your daughter. Finally, I would like to thank my beloved sister, Gina, for the funniest Skype discussions ever and for her unrestrained sense of humor. Her support has meant everything to me and helped me moving on.

Table of Contents

Chapter 1: Introduction

Chapter 2: Investigation of the General $Ni^{2+}/RCO_2^-/sacbH_2$ Reaction System

Chapter 3: Study of the General $Ni^{2+}/X^-/sacbH_2$ (X^- = inorganic anions) Reaction System

List of Schemes

List of Figures

List of Tables

List of Publications

Chapter 2:

A. A. Athanasopoulou, C. P. Raptopoulou, A. Escuer, Th. C. Stamatatos,

"Rare nuclearities in Ni(II) cluster chemistry: A Ni_{11} cage-like cluster from the initial use of *N*-salicylidene-2-amino-5-chlorobenzoic acid", *RSC Advances*, **4**, 12680, 2014.

A. A. Athanasopoulou, M. Pilkington, C. P. Raptopoulou, A. Escuer, Th. C. Stamatatos,

"Structural aesthetics in molecular nanoscience: A unique Ni_{26} cluster with a 'rabbit-face' topology and a discrete Ni_{18} 'molecular chain'", *Chemical Communications*, **50**, 14942, 2014.

Chapter 3:

P. S. Perlepe, A. A. Athanasopoulou, K. I. Alexopoulou, C. P. Raptopoulou, V. Psycharis, A. Escuer, S. P. Perlepes, Th. C. Stamatatos,

"Structural and magnetic variations in tetranuclear Ni^{II} clusters: the effect of the reaction solvent and ligand substitution on the product identity", *Dalton Transactions*, **43**, 16605, 2014.

List of Abbreviations

1-D	One-dimensional
2-D	Two-dimensional
3-D	Three-dimensional
Å	Angstrom
ac	Alternating Current
acacH	Acetylacetone
$^{n}Bu_3N$	Tributylamine
chpH	6-chloro-2-pyridone
$citH_4$	Citric Acid
CH_2Cl_2	Dichloromethane
cm^{-1}	Wavenumbers
D	Axial Zero-Field Splitting Parameter
dc	Direct Current
DMF	Dimethylformamide
E	Transverse Anisotropy
Et_3N	Triethylamine
EtOH	Ethanol
G	Gauss
g	Gyromagnetic Factor
hmpH	2-(hydroxymethyl)pyridine
HSAB	Hard Soft Acid Base principle

Hz	Hertz
η^1, η^2, η^3	Coordination Modes of Ligands
H	Applied Magnetic Field
IR	Infrared
J_1, J_2, …	Magnetic Exchange Coupling Constants
k	Boltzman Constant
K	Kelvin
L	Ligand
M	Metal Ion
M	Magnetization
μ, μ_3, …, μ_5	Bridging Modes of Ligands
μ_B	Bohr Magneton
m_s	Microstates
$mpoH_4$	2-methylpyrazolinone
MeOH	Methanol
MeCN	Acetonitrile
Me-	Methyl Group
Me_3N	Trimethylamine
N_3^-	Azides
o	Ortho Position
QTM	Quantum Tunneling of Magnetization
RCO_2H	Carboxylic Acid
RCO_2^-	Carboxylate Anion

SMMs	Single-Molecule Magnets
S	Spin Ground State
SQUID	Superconducting Quantum Interference Device
T	Tesla
T	Temperature
τ	Relaxation Time
τ_0	Pre-exponential Factor
THF	Tetrahydrofuran
$tmpH_3$	1,1,1-tris(hydroxymethyl)propane
$thmeH_3$	1,1,1-tris(hydroxymethyl)ethane
U	Energy Barrier of Magnetization Reversal
WOC	Water Oxidizing Complex
ZFS	Zero-Field Splitting
χ	Magnetic Susceptibility
χ_M	Molar Magnetic Susceptibility
ω	Angular Frequency

CHAPTER 1: Introduction

1.1 Polynuclear Metal Complexes – Molecular Nanoscience

The construction of new devices and machines require more and more the miniaturization of the assembled components. This process has been achieved for years through the use of traditional top-down synthetic approaches. The latter have been very successful and contributed the most to the recent foundations of our modern society. Scientists, engineers and technicians from different disciplines have managed to fabricate small to tiny pieces of matter using top-down techniques such as photolithography.[1] The latter, however, is a technique that cannot be actually applied to materials with dimensions smaller than 100 nm. Undoubtedly though, this size is still small, when compared to the sizes of the everyday life devices and machines, but also very large on scale of molecules and atoms which are as large as few nanometers. Thus, although Feynman elegantly said that 'there is plenty of room at the bottom', it is quite difficult for the top-down approaches to undertake and accomplish the new technological challenges.[2] In order to proceed towards further miniaturization, both science and technology have to develop new synthetic ways.

The molecular, or bottom-up, approach can provide the means of overcoming the above discussed problems. Therefore, a feasible way to make components/materials smaller in size is through the synthesis of large in nuclearity molecular compounds that

could be used in the new generations of nanoscale machines, devices and technological applications. The bottom-up approach deals with the use of molecules and the fabrication of molecule-based devices that will be small in size (i.e., miniaturization) and will consist of nanoscale components assembled from the 'bottom' (i.e., atoms, molecules). This is why such a molecular approach to the nanoscale has been recently dubbed as 'Molecular Nanoscience', i.e., to highlight the connection of two different but at the same time closely related areas of science; molecular chemistry and materials science. This approach builds on sources of individual elements or small molecules and utilizes them to construct molecular nanostructures with the optimized and targeted applications for the desired goal. At this point, it would be more useful to define the word 'molecule' from the chemical point of view: a molecule is sufficiently stable, discrete, electrically neutral, a finite-sized group of at least two atoms in a definite arrangement held together by strong chemical bonds. The discreteness of molecules distinguishes them from polymers, i.e. one-dimensional chains, two-dimensional sheets, and three-dimensional networks, and their neutrality distinguishes them from 'ionic salts' such as common table salt, sodium chloride (NaCl), which is composed of Na^+ and Cl^- charged species (ions) and is thus not a molecular substance. However, these strict definitions are often blurred, particularly in biochemistry; for example, DNA is often referred to as the 'molecule of life' but it is strictly speaking not a molecule but a one-dimensional polymer of linked repeating units, and it is not electrically neutral. It and other polymers such as proteins are perhaps best described as 'macromolecules'.

Hence, a molecule-based device can be defined as an array of different molecular components that are assembled together to accomplish a targeted function. Each

molecular component is capable to performing a particular or a collection of different actions. The result of all components joined together is a nanometer-sized, supramolecular or multi-molecular assembly which has the ability to carry out more complex functions than the individual components.[3] Similar to the well-known macroscopic devices, the molecular devices operate via atomic and electronic communication and thus they require energy and the appropriate stimulus to achieve such an operation. The extension of the long-term goal of making devices at the molecular level is of great interest not only for fundamental research, but also for the progress of nanoscience and nanotechnology.[4]

Molecular nanoscience is heavily relying on the ability of synthetic chemists to construct the desired molecules from small in size and relatively simple starting reagents. As a result the complex assemblies shall exhibit the desired and targeted properties and potential applications. It therefore becomes apparent that new synthetic strategies and extended methodologies are required to develop the appropriate molecule-based devices, and it is this reason why synthetic chemistry is considered one of the most enjoyable and challenging areas of science and technology. It would be necessary at this point to emphasize at the advantages a bottom-up approach brings to the field of traditional nanoscale materials and/or nanotechnology. In general lines, we can definitely say that molecular synthesis is almost always performed under mild conditions and at ambient temperatures, or nearly so. These ‘low cost, low energy’ and accessible conditions can provide scientists with synthetic control and an enhanced ability to ‘manipulate’ and ‘adjust’ the molecules at will, and according to the targeted applications. In particular, the most important advantages of molecular compounds are the following:[5] (i) in a purified

sample, all molecular species in the material are identical. Such a monodisperse collection of nanometer-sized species is almost impossible to accomplish with traditional top-down synthetic approaches. This is a significant task given the greater variation of the properties with size at the nanoscale level compared with the more standard properties of the everyday macroscale materials. Therefore, a distribution of nanoparticle sizes in traditional materials reflects in an important distribution of properties. In contrast, each molecule in a monodisperse collection will have identical properties (i.e., electronic, magnetic and/or conductivity); (ii) the periphery of the molecules is organized by various organic groups as a result of the low-energy synthetic methods which are applied for the construction of such materials. These organic groups, usually attached to the metal ions, are called 'ligands' and can be altered at will. Such a chemical manipulation can provide the means to adjust accurately very important properties of the molecular materials, such as their crystallinity, solubility (important for their purification), crystal lattice energies, kinetics, and thermodynamics; (iii) solubility of molecular species is a major benefit compared to the classical nanoparticles which regularly form colloidal suspensions. True solubility provides huge advantages for purification, processing, deposition on various conductive and electrical surfaces, removal from surfaces, modification, and controlled alteration; (iv) growth of single-crystals suitable for X-ray diffraction studies reflects in the formation of beautiful, three-dimensional arrays of identical and ordered, monodisperse species, which often possess the same orientation as well (Figure 1.1).[6] As a result, all the molecules in the crystal display the same response to an external stimulus, such as an applied magnetic field, pressure, heat, or light. In contrast, crystallization of traditional nanoparticles is very difficult to achieve, especially under ambient conditions;

(v) the molecules are well-separated in the crystal due to the presence of the peripheral organic groups (ligands), which provide a protective shell and do not allow significant interactions between adjacent molecules. The ligands also guarantee the absence of surface defects, distortions and other variations which are common with traditional nanoparticles. From all of the above, and more, it becomes apparent that there is a continuous need for new molecular materials with nano-sized dimensions and improved, or even new, properties compared with the bulk and traditional materials of the top-down approach. When the interest is concentrated on the magnetic properties and consequently into the area of molecular electronics, then the desired nanoscale molecular compounds must be constituted of many paramagnetic metal ions surrounded and linked through flexible and multifunctional bridging ligands. Such high-nuclearity metal species are known as polynuclear metal complexes, and their synthesis and applications have become the focal point of a large number of research groups worldwide during the last three decades.

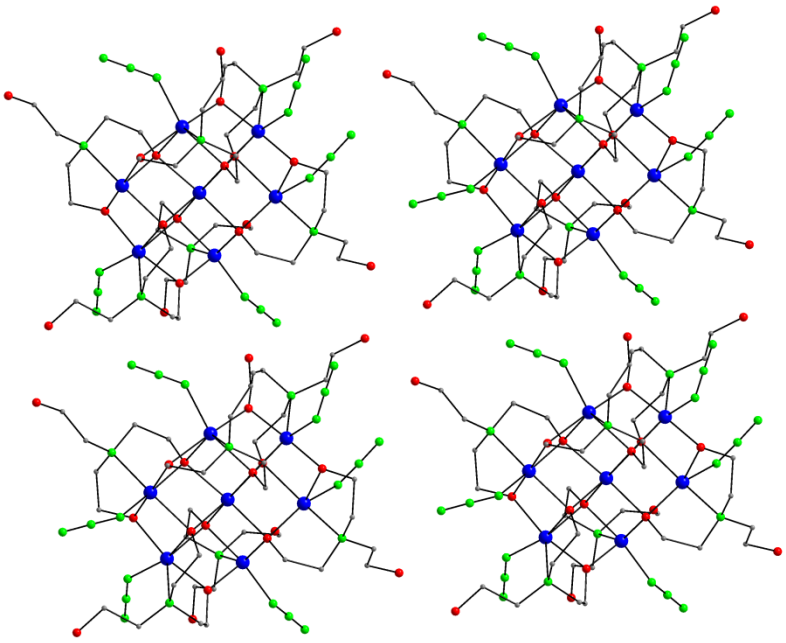

Figure 1.1 A three-dimensional, ordered array of monodisperse, identically oriented molecules within a crystal. Each molecule comprises seven manganese atoms (blue) connected by oxygen atoms (red) and surrounded by organic groups (grey and green).

Polynuclear metal complexes or "coordination clusters", or simply "clusters", are generally composed of a large number of metal ions (M^{n+}; "n" varies), a class of bridging ligands (L), and various terminal, chelating or simply monodentate, ligands (L′). A general formula for polynuclear complexes is $[M_x(L)_y(L')_z]^n$, where "x" is an integer number larger or equal to three, "y" and "z" are also integer numbers, and "*n*" can be any integer number, including zero; if "*n*" is negative, the cluster compound is anionic, if it is positive, it is cationic, and if it is zero the complex is neutral.[7] In polynuclear Werner-type compounds, the metal ions are mostly in moderate-to-high oxidation states and they are considered, according to the Pearson HSAB principle, as relatively hard acids, fostering the formation of molecular species with moderate-to-hard bases as ligands. Hence, such paramagnetic metal cluster compounds are frequently bridged by elements of the *p*-block, such as oxygen bridges, and any type of exchange interactions (magnetic, electronic, etc.) between the spin carriers is propagated through the bridging ligand(s). These compounds are different from the metal-metal bonded complexes,[8] also termed "clusters" by many groups.

The nuclearity of a metal cluster is associated with its size, some of which have nanoscale dimensions. The smallest classical nanoparticles fabricated to date via the top-down approach are of the same order of magnitude as the largest molecule-based metal

clusters synthesized by bottom-up methods.[9] However, the synthesis and crystallization of such species has been always a challenging task for coordination chemists. Christou, Winpenny, Brechin, and others,[10] have shown that *3d*-metal clusters can indeed reach the size regimes of small nanoparticles, and apart from their architectural beauty, they can also exhibit interesting physicochemical properties.[11] Although very high-nuclearity, *3d*-metal clusters are of precedence, their size limit has definitely not been reached to date and new record nuclearities for a given metal ion await discovery. Very recently Powell and coworkers reported a beautiful $\{Cu^{II}_{27}\}$ cluster which possesses a "chicken-in-a-basket" structural motif (Figure 1.2).[12] Record nuclearities for other homometallic *3d*-metal clusters to date are the $\{Mn^{III}_{84}\}$ torus (Figure 1.3),[13] the $\{Fe^{III}_{168}\}$ and $\{Co^{II/III}_{36}\}$ cages (Figure 1.4),[14,15] while in Ni(II) coordination chemistry the record in size was held for many years by the structurally impressive $\{Ni_{24}\}$ clusters of Winpenny[16] and Christou[17] (Figure 1.5, left and right, respectively).

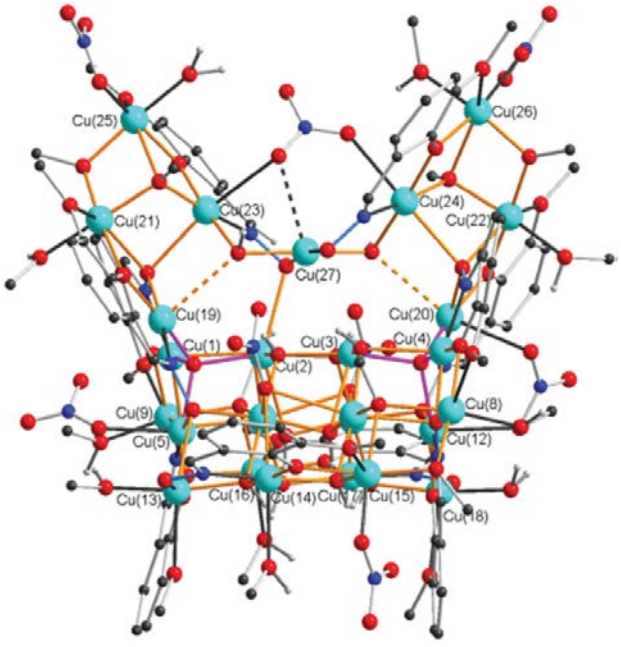

Figure 1.2 Molecular structure of the $\{Cu^{II}_{27}\}$ cluster. Cu cyan, O red, N blue, C dark grey, H grey; H-atoms riding on organic groups are omitted for clarity. Cu-O bonds to μ_2 or μ_3-bridges are shown in orange color, while $(\mu_4$-O)-Cu bonds are highlighted with purple. Bonds within the 2.8 > Cu–O > 2.6 Å range are shown in dashed lines. Reproduced from Ref. 12 with permission from the Royal Society of Chemistry.

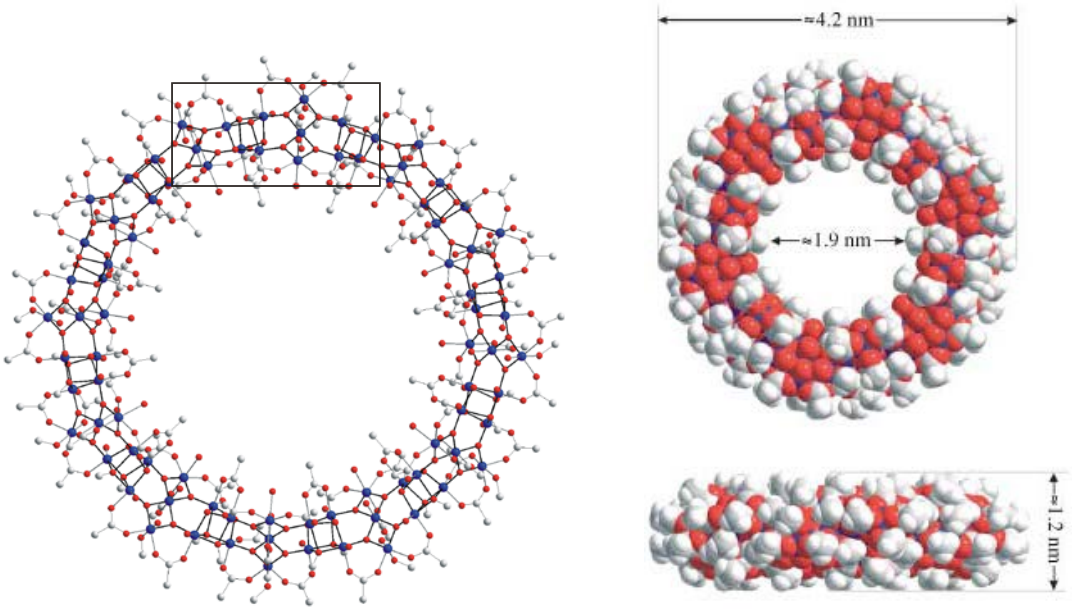

Figure 1.3 (left) Molecular structure of the $\{Mn_{84}\}$ torus-like cluster, excluding hydrogen atoms. The rectangle indicates the repeating $\{Mn_{14}\}$ unit of the molecule. (right) Space-filling representations showing that the torus has a diameter of about 4.2 nm and a thickness of about 1.2 nm, with a central hole of diameter 1.9 nm. Color scheme: Mn^{III} blue, O red, C grey. Reproduced from Ref. 13 with permission from John Wiley and Sons.

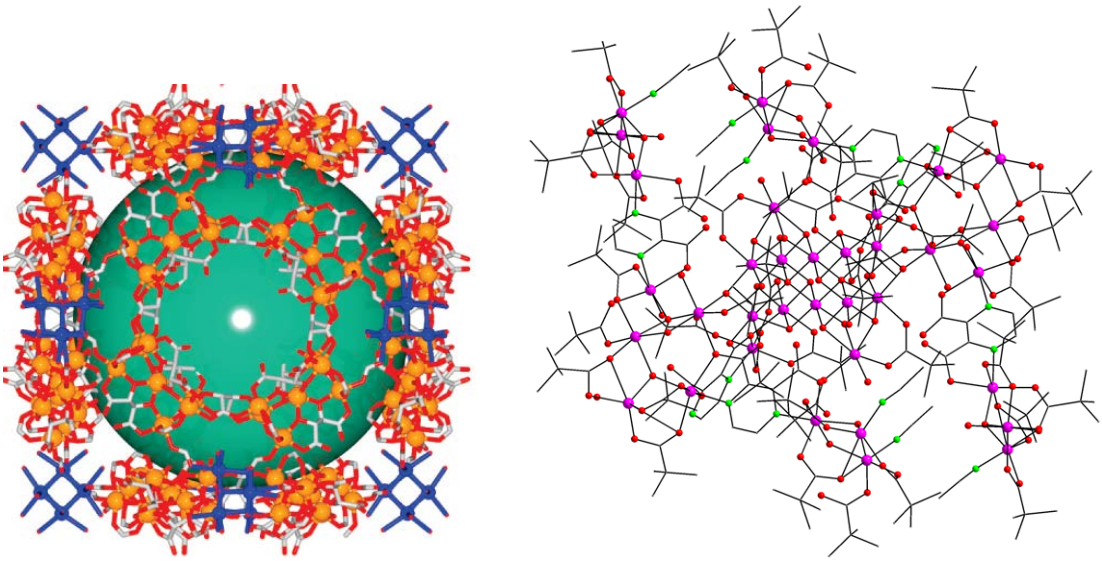

Figure 1.4 (left) Structure of the anion of the {Fe_{168}} cage-like cluster; the central green sphere indicates the void space. Color scheme: Fe^{III} orange, Na blue, O red, C grey. Reproduced from Ref. 14 with permission from the American Chemical Society. (right) Molecular structure of the {Co_{36}} cage. H atoms are omitted for clarity. Color scheme: Co purple, N green, O red, C grey.

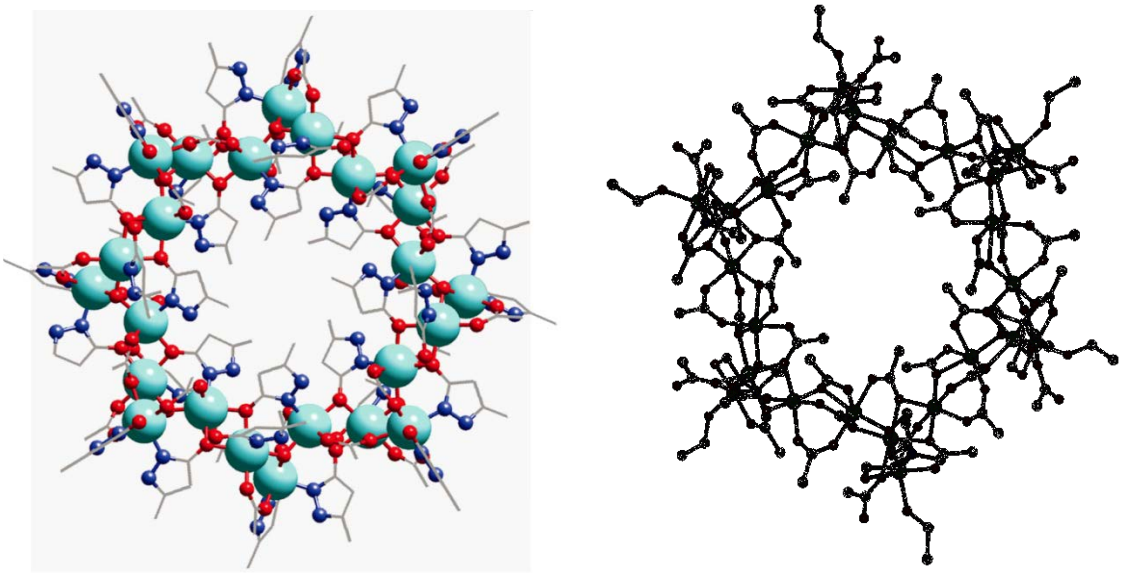

Figure 1.5 Complete structures of the $\{Ni^{II}_{24}\}$ wheel-like clusters reported by Winpenny (left) and Christou (right). H atoms are omitted for clarity. Color scheme: Ni^{II} turquoise or green, O red, N blue, C grey. Reproduced from Refs. 16 and 17 with permission from John Wiley and Sons and Royal Society of Chemistry, respectively.

1.2 Applications of Transition Metal Cluster Compounds in Bioinorganic Chemistry and Molecular Magnetism

Polynuclear *3d*-metal complexes continue to attract the interest of the scientific community due to their potential applications in various fields of research such as bioinorganic chemistry and molecular magnetism. Among the reasons for the interest in biological inorganic chemistry is the search for various, high-nuclearity oxide-bridged metal clusters to model the M_x sites in biomolecules. Such efforts include the understanding of the assembly of the multinuclear Fe^{III}/O^{2-} core of the iron-storage protein ferritin,[18] the structural and/or functional role of Ni^{II} ions in the active site of urease, which catalyzes the hydrolysis of urea to ammonia and carbamate,[19] and the elucidation of the nature and mechanism of action of the Mn_4Ca core of the water oxidizing complex (WOC) within the photosynthetic apparatus of green plants and cyanobacteria.[20]

It is well-known that nickel is an essential element for plants, animals and humans. Despite the fact that the role of that metal has not yet been determined precisely in the

biochemistry of animals, it has been seen that nickel exists in the active site of four bacterial enzymes. These enzymes are:[21]

- Hydrogenase,
- CO-dehydrogenase from photosynthetic bacteria,
- Urease, and
- Methyl-S-coenzyme-M-reductase, which uses a Ni-containing metal cofactor (Ni-F430).

The coordination environment of Ni in each of the above proteins is different, and it is believed that Ni exists in the active site of those enzymes by playing an important role in their catalytic cycles. The chemistry of Ni in biological systems is rather unusual compared to its well-known coordination chemistry. Most of the above mentioned enzymes include redox-active Ni centers, with the oxidation state of the metal varying from +III, +II and/or +I when it is found in an environment with thiolate or tetrapyrrole ligands. The reactions that are catalyzed by these enzymes, and more specifically the oxidation of H_2 and the reduction of H^+ (hydrogenase), the conversion of CO to CO_2 and the formation or the cleavage of the C-S and C-C bonds (CO-dehydrogenase), are completely unusual in non-organometallic complexes of nickel. An exception to this rule is urease in which Ni(II) acts as a Lewis acid. The latter enzyme has been characterized by single crystal X-ray crystallography and its structural characteristics are well-known. For all the other enzymes the functional and structural characteristics of their active sites are still debated.

Due to the importance of urease in the development of enzymology, in combination with the elucidation of its crystal structure (Figure 1.6) and the discovery of nickel[19] in its active site, we decided to refer extensively to its role and functional activities. Urease catalyzes the hydrolysis of urea in plants, algae, fungi, and several microorganisms[22] in the final step of organic nitrogen mineralization to produce ammonia and carbamate, as is shown by equation 1.1.

$$H_2NCONH_2 + H_2O \longrightarrow NH_2CO_2^- + NH_4^+ \xrightarrow{H_2O} 2\,NH_4^+ + HCO_3^- \qquad (1.1)$$

The hydrolysis of the reaction products induces an overall pH increase that has negative implications both in human and animal health as well as in the ecosphere. Urea decomposes into cyanic acid and ammonia with a half-life of 33 years through an ammonia elimination mechanism, while the half-life for spontaneous hydrolysis to yield ammonia and carbamate is 520 years.[23] In the case of enzyme urease, the half-life for the catalytic hydrolysis is 20 ms, resulting in a rate enhancement of 3×10^{15}, much higher than that of all other known hydrolases enzymes.

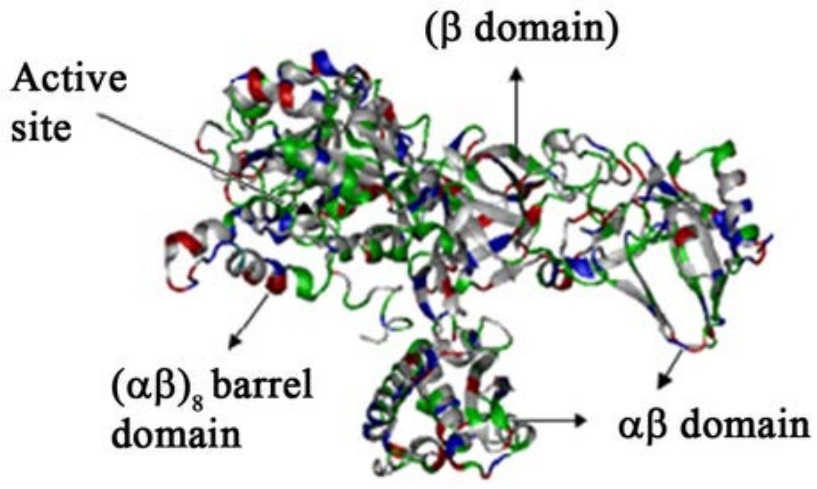

Figure 1.6 Overall structure of the Jack bean urease monomer, highlighting the three different domains and the location of the active site.[24] Reproduced from Ref. 24 with permission from Nature Publishing Group.

The structure of the active site of urease is shown in Figure 1.7. It contains two Ni^{2+} ions separated from each other by 3.5-3.7 Å. The metal ions are bridged by the oxygen atoms of a carbamylated lysine residue and are additionally bound to two terminal histidine residues. One Ni^{2+} ion is further bound to a carboxylate oxygen atom from an aspartate residue. The coordination geometries of the Ni^{2+} ions are completed by a water molecule terminally bound to each metal ion and a doubly-bridging hydroxido ion. The terminal H_2O molecules are hydrogen-bonded to histidine and alanine residues that are found in the vicinity of the active site. The overall ligand conformation yields a five-coordinate Ni^{2+} ion with a distorted square-pyramidal geometry and a six-coordinate Ni^{2+} ion with a distorted octahedral geometry. There are clear indications by various inhibitor complexes that bridging OH^- group and bound H_2O ligands are extremely labile, while the remaining protein ligands are rigidly maintained to the Ni^{2+} ions.

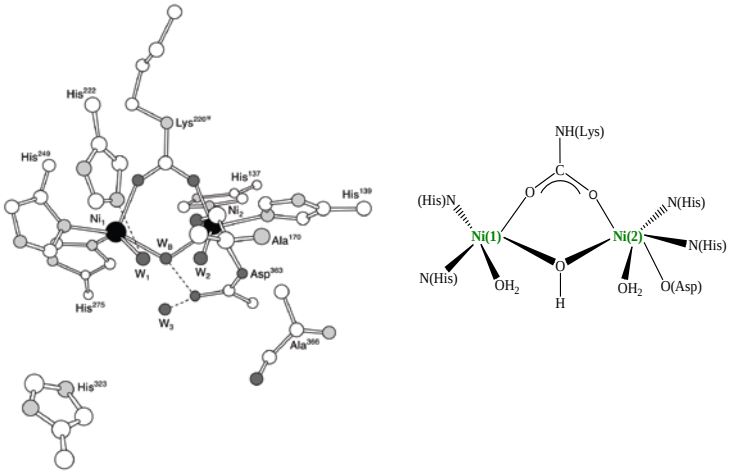

Figure 1.7 (left) Complete structural and (right) short schematic representations of the structure of the active site of urease from *B. pasteurii* (BPU).[19a] Reproduced from Ref. 25 with permission from John Wiley and Sons.

There have been many catalytic mechanisms proposed for the hydrolysis of urea by the Ni_2 complex of urease enzyme. The most recognized and studied mechanism is the one analyzed herein and presages a direct role of both Ni^{2+} ions in binding and activating the urea substrate (Figure 1.8).[25] Firstly, urea enters the active site by replacing W1/2/3 (Figure 1.7) located in positions matching its molecular shape and dimensions. Urea binds with the carbonyl O and amide N atoms to both Ni^{2+} ions; this binding mode brings urea C atom in close proximity to the $\{Ni_2\text{-}(\mu\text{-}OH)\}$ unit. The OH^- ion acts as a nucleophile and fosters the formation of the 'tetrahedral' $\{Ni_2\text{-}OH\text{-}urea\}$ transition state *via* bonding to the urea C atom (Figure 1.8). Once the C_{urea}-OH bond is formed, the proton needed by the distal urea NH_2 group -in order to form NH_3 by cleavage of the C-N bond- could easily be provided by the nucleophile OH^- itself. An open-to-close, flap-like conformational change of the active site is necessary to move His323 (Figure 1.7) from the vicinity into close proximity to the transition state so that it would act as a general base by stabilizing, in its deprotonated form, the positive charge that develops on the distal N_{urea} atom during formation of nascent NH_3. This mechanism is in complete agreement with the pH dependence of urease activity.[26] To date, many research groups are attempting to synthesize various Ni(II) dimers, bridged by carboxylate and hydroxido groups, in order to mimic the structure and catalytic function of the active site of the

native urease enzyme.[27] Unfortunately, there are no structural models yet that approach the catalytic activity and potency of the native enzyme.

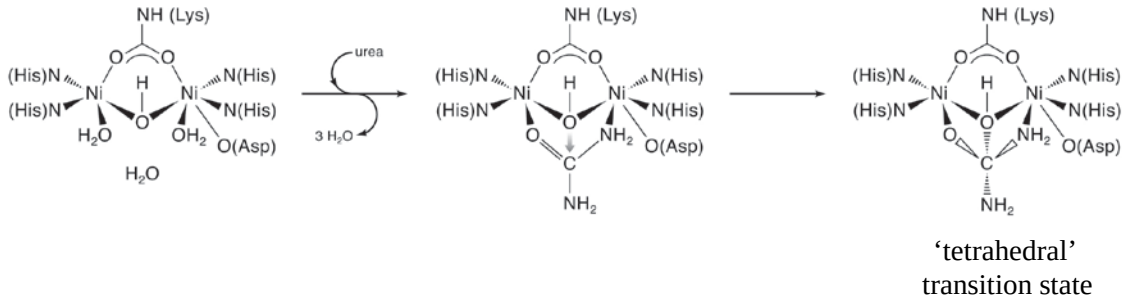

Figure 1.8 A proposed mechanism for the binding of urea to the active site of urease, followed by its hydrolysis to ammonia and carbamate.[25] Reproduced from Ref. 25 with permission from John Wiley and Sons.

In the field of molecular magnetism, polynuclear complexes of paramagnetic 3*d*-metal ions have received tremendous attention over the last three decades or so, especially after the discovery that they can function as single-molecule magnets (SMMs). Single-molecule magnets, like all traditional magnets, are species that retain their magnetization in the absence of an external magnetic field.[28] However, an SMM is capable of maintaining its magnetization for an extensive amount of time as long as it is kept below its characteristic blocking temperature.[29] SMMs are also known as molecular nanomagnets or magnetically bistable compounds. The blocking temperature is dependent on the magnitude of the energy barrier, U, for the magnetization reversal. The magnitude of the energy barrier is proportional to $S^2|D|$ for integer spin systems and $(S^2-1/4)|D|$ for half-integer spin systems. Thus, in order to observe single-molecule magnetic

behaviour in a transition-metal molecular compound that must possess two properties; a large spin ground state (*S*) and a significant magnetic anisotropy of the Ising (or easy-axis) type, the latter being reflected in a large and negative zero-field splitting parameter, *D*.[30] A large spin ground state, *S*, for a polynuclear 3*d*-metal compound results from the ideal situation where all the metals' spin vectors are aligned parallel to each other; such entirely ferromagnetic (or ferrimagnetic) systems are called high-spin molecules and their synthesis and isolation are among the most difficult tasks to achieve in synthetic coordination chemistry. Furthermore, high-spin molecules can also derive when spin frustration effects from the presence in certain M_x (M = metal) topologies of competing antiferromagnetic exchange interactions prevent (frustrate) the preferred antiparallel spin alignments that would normally yield low-spin species.[31] Zero-field splitting (ZFS), however, is a parameter that a synthetic chemist cannot really account for its sign and size; it mainly depends on the nature of the paramagnetic metal ion, the single-ion anisotropy of the metal of choice, the structural motif of the resulting polynuclear compound, and the presence of spin-orbit coupling.[32] Ultimately, the magnetic bistability of SMMs could find use in potential applications such as high-density information storage, quantum computing and spin-based molecular electronics.[33]

Figure 1.9 shows a tutorial example of the energy barrier of an SMM with a spin ground state of $S = 10$. The latter has been observed in the first SMM ever reported, which is the dodecanuclear $[Mn^{III}_8Mn^{IV}_4O_{12}(O_2CMe)_{16}(H_2O)_4]$ cluster, in short Mn_{12}ac, described as an internal $\{Mn^{IV}_4\}$ cubane linked to an external cyclic array of 8 Mn^{III} ions (Figure 1.9, top).[34] The $S = 10$ ground state results from the antiferromagnetic interactions between eight ferromagnetically-coupled Mn^{III} ions ($S_{local1} = 8 \times 2 = 16$) and

four ferromagnetically-coupled Mn^{IV} ions (S_{local2} = 4 × 3/2 = 6). The antiferromagnetic interaction between the two S_{local1} and S_{local2} spin carriers leads to a total spin ground state of $S = S_{local1} - S_{local2} = 10$. There is a splitting of the previously degenerate m_s microstates induced by the axial anisotropy. Because the value of the axial ZFS parameter, D, for an SMM is negative (-0.50 cm^{-1} for Mn_{12}ac), the $m_s = \pm 10$ sublevels lie lowest in energy while the $m_s = 0$ sublevel lies highest (Figure 1.9). Consequently, there is a potential energy barrier, U, between the "spin-up" (m_s = -10) and "spin-down" (m_s = +10) orientations of the magnetic moment. To cross the magnetization reversal barrier, an electron travels up each subsequent spin microstate, since the selection rule for the change in m_s states only allows for a change of ±1. The reason that SMMs are only capable of retaining their magnetization at low temperatures (i.e., below liquid N_2 temperatures) is that at higher temperatures they possess more thermal energy, which is large enough to overcome the energy barrier for the magnetization reversal. The value of the ground state spin has a significant effect on the spin-reversal mechanism, which further rationalizes the motivation in research towards the synthesis of high-spin molecules. The spin-reversal barrier can also be described as a double-well, where the two "wells" are separated by a barrier of potential energy, U. An alternative spin-reversal pathway can also be achieved by the quantum tunneling of the magnetization through the energy barrier.[35] Tunneling is a process where a particle enters an area that is classically forbidden or in this case the particle passes through an area with greater potential energy that surpasses the particles' energy.[30] Quantum tunneling of magnetization (QTM) provides an additional pathway for overcoming the energy barrier; this effect leads to even faster magnetization relaxation times. QTM can be reduced by making new SMMs

with larger energy barriers than the ones currently known, since the rate of quantum tunneling increases with decreasing the potential energy barrier.[36]

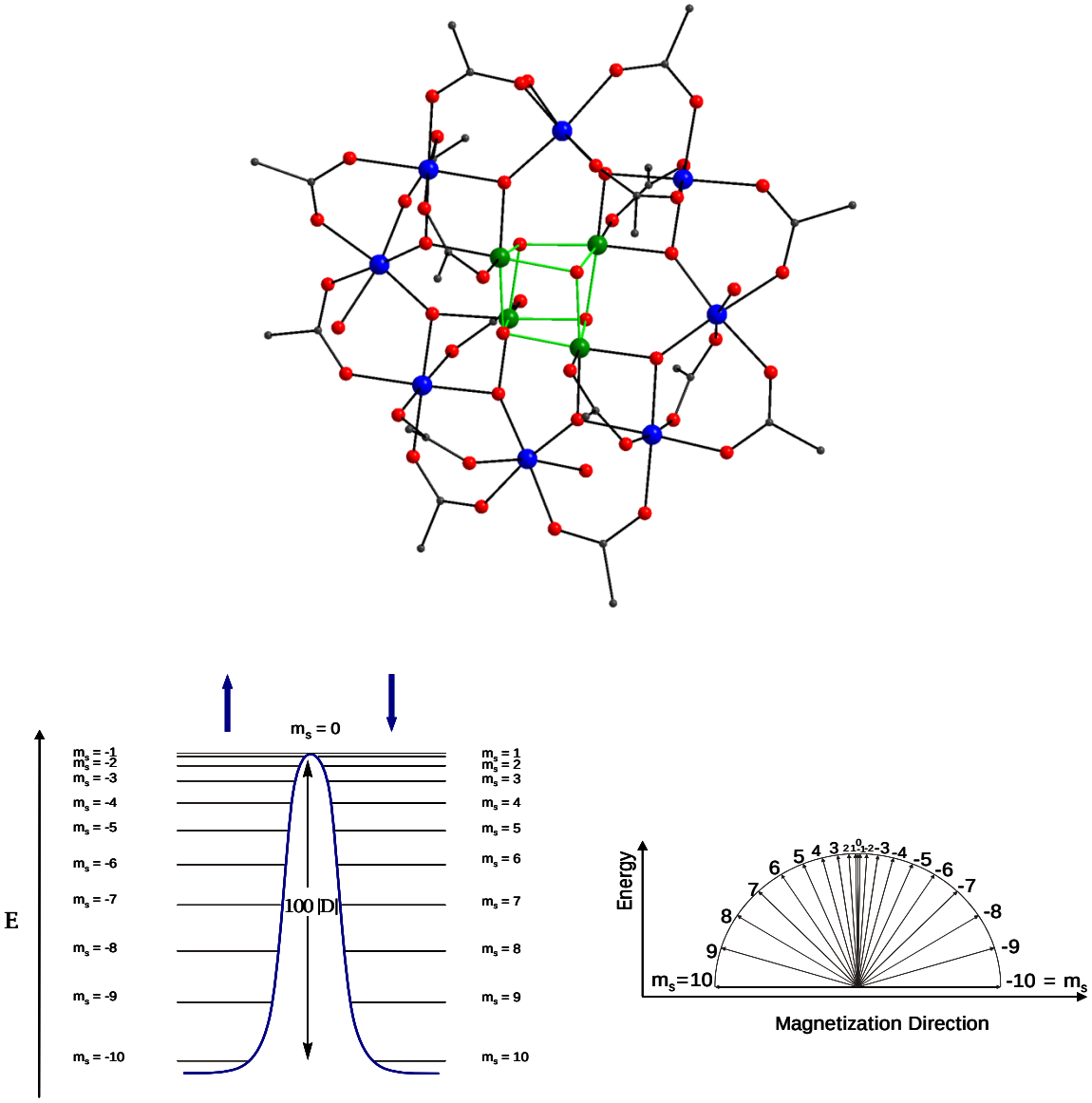

Figure 1.9 (top) Structure of the archetypal Mn_{12}ac SMM. Color scheme: Mn^{III} blue, Mn^{IV} green, O red, C grey. H atoms are not shown for clarity. (bottom) Two different views of the same double-well diagram of the Mn_{12}ac SMM with $S = 10$.

The relaxation rate of magnetization can be monitored and quantitatively determined from the use of alternating current (*ac*) magnetic susceptibility measurements. *Ac* measurements are used to probe the dynamic susceptibility (equation 1.2), otherwise magnetic dynamics, of a sample by applying an oscillating magnetic field. The dynamic susceptibility, χ, is a complex quantity with real (dispersion) and imaginary (absorption) components that are dependent on the angular frequency, ω, of the ac field.[37] Note that ω is often converted to $2\pi\nu$ units, where ν is the ordinary frequency.

$$\chi(\omega) = \chi'(\omega) - i\chi''(\omega) \tag{1.2}$$

The relaxation of magnetization is a kinetic process and, as such, it follows an Arrhenius relationship (equation 1.3) for the thermally activated region,

$$\tau = \tau_0 \exp(U_{\text{eff}} / kT) \tag{1.3}$$

where τ is the relaxation time [$\tau = (\omega)^{-1}$], τ_0 is the pre-exponential factor, k is the Boltzmann constant, and U_{eff} is the mean effective barrier to magnetization relaxation. Thus, from the slope of an Arrhenius diagram of $\ln(\tau)$ *vs.* $(1/T)$ the energy barrier (U_{eff}) can be accurately determined.[38] As the *ac* frequency approaches the relaxation rate of the molecules, the observed in-phase susceptibility (χ') reduces. Therefore, the out-of-phase component (χ'') will increase. For SMMs where a single relaxation process takes places, a graph of χ'' *vs.* temperature will show a peak maximum at the temperature where $\omega = (\tau)^{-1}$. When the *ac* frequency increases, the peak maxima are shifted to higher temperatures,[35a,39] as is clearly seen in the corresponding diagram of the Mn_{12}ac SMM (Figure 1.10).

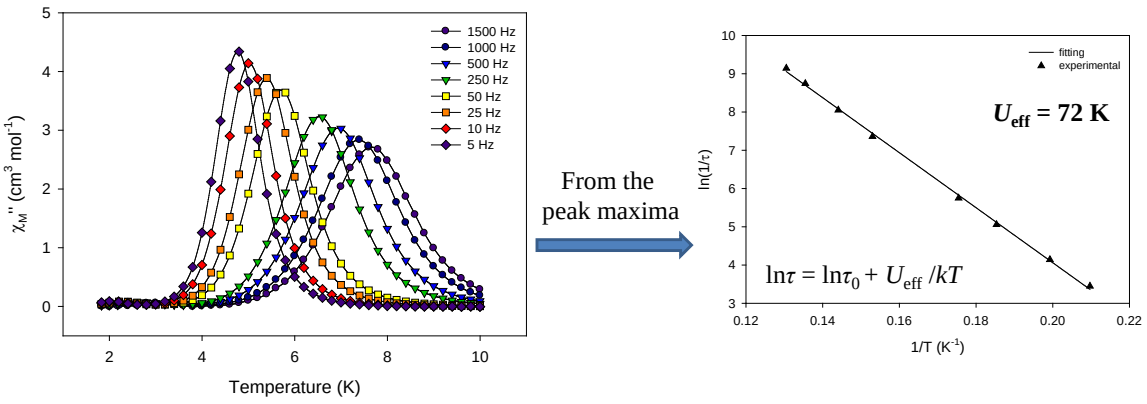

Figure 1.10 (left) Frequency-dependent peaks of the χ_M'' *ac* signals of Mn_{12}ac and (right) the corresponding Arrhenius plot constructed from the peak maxima and their given temperatures. Note that Mn_{12}ac possesses an effective barrier for the magnetization reversal of 72 K, one of the highest yet reported for any transition metal-based SMM.

In addition to the χ_M'' *ac* signals, a single molecule magnet often displays magnetization *vs.* field hysteresis loops, as shown in Figure 1.11 (left). The hysteresis loops frequently show steps which are characteristic of the quantum tunneling of magnetization (QTM) through the energy barrier (see Figure 1.9).[35a] QTM is the quantum property of molecular nanomagnets and results from the presence of transverse anisotropy which gives a superposition of states of both sides of the barrier with a tunneling splitting. The axial anisotropy (described by the *D* term) splits the m_s levels, while the transverse (or rhombic zero-field splitting) anisotropy (*E* term), together with other Zeeman terms, mixes the m_s states. The greater the transverse anisotropy is, the greater the mixing of states will be on either sides of the anisotropy barrier, leading to increased rates of QTM and fast magnetization relaxation. To tackle this problem, an

external direct current (*dc*) magnetic field can be applied, altering the relative energies of the m_s states. QTM is only possible when the energy levels on both sides of the barrier are aligned and can therefore only occur at certain points as the field is swept, thus creating steps in the hysteresis loops (Figure 1.11, right). Pure QTM results from the alignment of the same energy levels on both wells (i.e., from $m_s = \pm 10$ states, Figure 1.11a), while resonant quantum tunneling can occur from the alignment of different m_s states (i.e., $m_s = 10$ and $m_s = -8$, Figure 1.11b). SMM hysteresis loops are temperature- and sweep rate-dependent, with the coercivities of loops increasing with decreasing temperature and increasing field sweep rates.

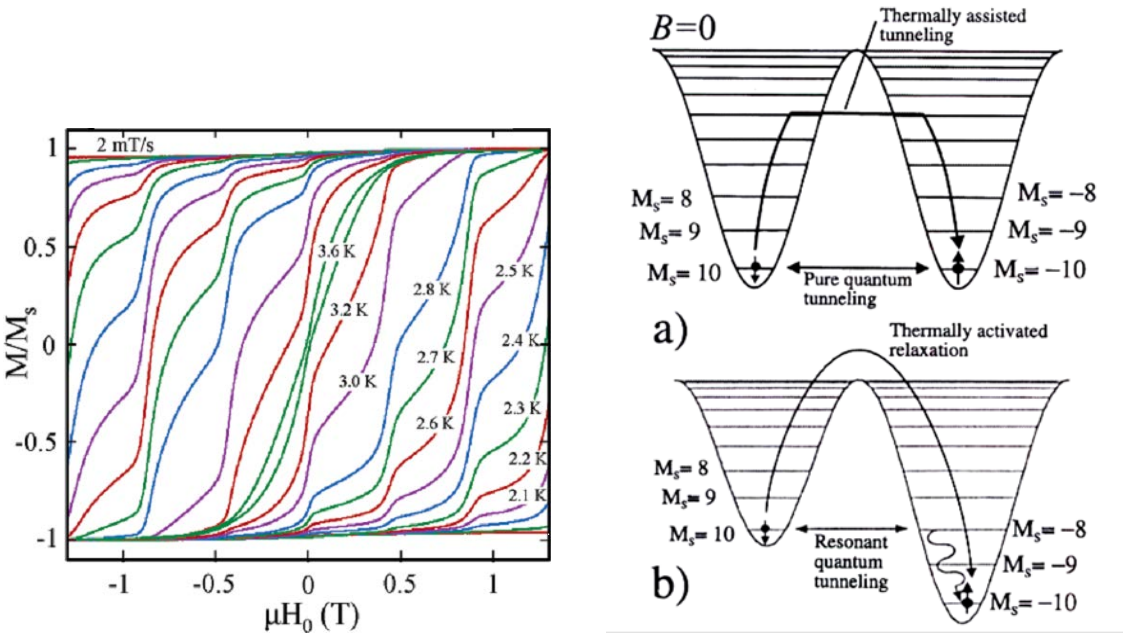

Figure 1.11 (left) Magnetization (*M*) *vs.* field hysteresis loops for a single-crystal of Mn_{12}ac showing the temperature dependence at a fixed sweep rate of 2 mT/s. (right) Possible tunneling mechanisms for *3d*-metal SMMs. Reproduced from Ref. 34 with permission from the Royal Society of Chemistry.

The coordination chemistry of nickel(II) with various N- and O-donor ligands has been well developed and explored the last three decades, and it includes several polynuclear complexes with various nuclearities from 3 up to 26.[40] Considering the ability of Ni^{II} ion (d^8, $S = 1$) to form high-spin complexes, in conjunction with the large single-ion anisotropy that it possesses ($|D| > 10$ cm^{-1}),[41] it makes it an ideal candidate for the construction of single-molecule magnets. Despite the continuous synthetic efforts and the structural characterization of numerous Ni(II) complexes reported to date, there are only five different structural types that exhibit SMM behavior; these are collected in Table 1.1 for convenient comparison of their structural and magnetic features. The lack of appreciable energy barriers for the magnetization reversal in Ni^{II}-based SMMs stems from the co-existence, together with *D*, of a large transverse anisotropy, *E*, which results in a strong and fast QTM that hinders the relaxation of magnetization over the barrier (thermally-activated relaxation).

Table 1.1 Chemical formulas, as well as the nature of predominant magnetic exchange interactions and values of the spin ground state, *S*, of all the up to date structurally characterized, homometalic Ni(II) SMMs

Complex[a]	Magnetic Interactions	S[b]	Reference
$[Ni_4(hmp)_4(MeOH)_4Cl_4]$	ferromagnetic	4	[42a]

$[Ni_4(hmp)_4(EtOH)_4Cl_4]$	ferromagnetic	4	[42a]
$[Ni_4(hmp)_4(C_4H_9CH_2CH_2OH)_4Cl_4]$	ferromagnetic	4	[42a]
$[Ni_4(thmeH_2)_4(MeCN)_4(NO_3)_4]$	ferromagnetic	4	[42b]
$[Ni_8Na_2(N_3)_{12}(O_2CPh)_2(mpo)_4(mpoH)_6(EtOAc)_6]$[c]	ferromagnetic	8	[43]
$[Ni_{10}(N_3)_8(tmp)_2(acac)_6(MeOH)_6]$	ferromagnetic	10	[44]
$[Ni_{12}(chp)_{12}(O_2CMe)_{12}(THF)_6(H_2O)_6]$	ferromagnetic	12	[45]
$Na_8(NMe_4)_8[Ni_{21}(cit)_{12}(OH)_{10}(H_2O)_{10}]$[c]	antiferromagnetic	3	[46]

[a] The formulas of the compounds are shown without the solvate molecules for simplicity.

[b] The spin ground state, *S*, values were derived from simulation of magnetization data at low temperatures and/or EPR spectroscopy.

[c] Na^+ ions are diamagnetic, and thus we consider their complexes with Ni^{II} as homometallic, based on the fact that Na^+ ions do not contribute into the magnetic properties of the reported compounds.

Abbreviations: hmpH = 2-(hydroxymethyl)pyridine, $thmeH_3$ = 1,1,1-tris(hydroxymethyl)ethane, $citH_4$ = citric acid, mpoH = 2-methylpyrazolinone, $tmpH_3$ = 1,1,1-tris(hydroxymethyl)propane, acacH = acetylacetone, chpH = 6-chloro-2-pyridone, THF = tetrahydrofuran.

The first Ni(II) SMM was reported in the literature by the group of Winpenny and its structure revealed a dodecanuclear, cyclic complex $[Ni_{12}(chp)_{12}(O_2CMe)_{12}(THF)_6(H_2O)_6]$ (Figure 1.12).[45] The compound lies on a crystallographic $\bar{3}$ axis with two nickel atoms present in the asymmetric unit, each bound to six oxygen atoms in a distorted octahedral

geometry. For Ni(1), three of these oxygen atoms derive from acetate groups, two from chp^- ligands, and one from a water molecule. For Ni(2), there are six O atoms from two acetate, two chp^-, one water, and a THF molecules. All of these ligands but the THF molecules are involved in bridging of the metal atoms. Ni(1) is bridged to Ni(2) through two μ-O atoms derived from chp^- ligands, thus forming an Ni_2O_2 ring. The two metal ions in the asymmetric unit are further bridged by an $\eta^1{:}\eta^2{:}\mu_3$ acetate ligand which lies inside the $\{Ni_{12}\}$ metallocycle. Ni(1) is also bridged to Ni(2′) [a symmetry-equivalent of Ni(2) generated by the $\bar{3}$ axis] by two additional μ-O atoms which are derived from an internal acetate group and water molecule. Ni(1) and Ni(2′) are also bridged by an $\eta^1{:}\eta^1{:}\mu$ $MeCO_2^-$ group on the exterior of the ring. The structure therefore consists of a closed-chain of intersecting Ni_2O_2 rings, with each ring being further strapped by an acetate ligand. The methyl group of the internal acetate ligand efficiently fills the cavity of the $\{Ni_{12}\}$ metallo-based macromolecule. There are no significant intermolecular interactions, but there are strong intramolecular H-bonds between the water molecules and chp^- ligands.

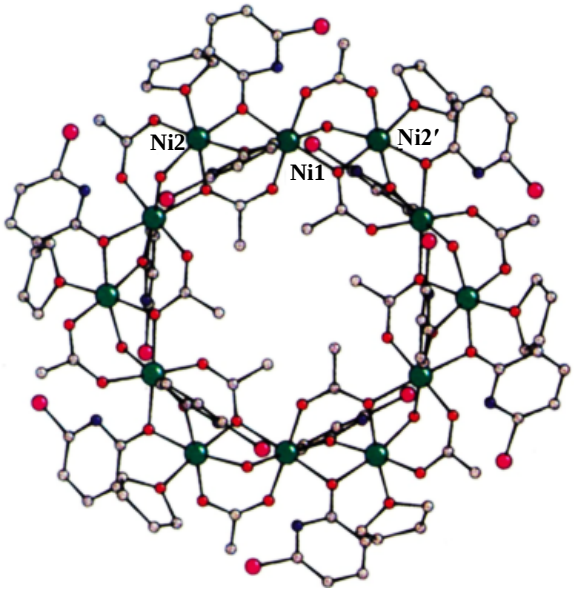

Figure 1.12 The structure of $[Ni_{12}(chp)_{12}(O_2CMe)_{12}(THF)_6(H_2O)_6]$ complex in the crystal. Color scheme: Ni green, O red, N blue, Cl magenta, C grey.[45] Reproduced from Ref. 45 with permission from the Royal Society of Chemistry.

Magnetic studies revealed the presence of predominant ferromagnetic exchange interactions between the 12 Ni^{II} ions and a resulting spin ground state of S = 12. Isothermal magnetization, M, *vs.* field, H, studies were also performed and confirmed the S = 12 ground state accompanied with a very small zero-field splitting parameter, D = -0.05 cm^{-1}. The combination of a large S and a negative value of D gave rise to a barrier for the magnetization relaxation of an SMM, which was evidenced by the appearance of hysteresis loops below 0.4 K (Figure 1.13), the classical property of any magnet. As expected, the coercivities of the loops increase as the temperature decreases for constant field sweep rates. The hysteresis loops become more pronounced as the temperature is lowered, and below 0.2 K the steps become resolved due to resonant quantum tunneling of magnetization. The dodecanuclear complex possesses to date the largest S value among all the reported Ni(II) SMMs.

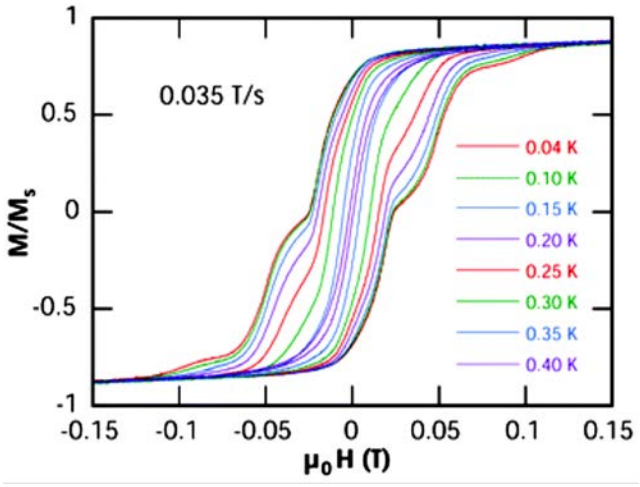

Figure 1.13 Magnetization *vs.* field hysteresis loops for a single-crystal of $[Ni_{12}(chp)_{12}(O_2CMe)_{12}(THF)_6(H_2O)_6]$ complex at different low temperatures. The steps due to quantum tunneling are clearly shown below 0.2 K, under a constant field sweep rate of 0.035 T/s.[45] Reproduced from Ref. 45 with permission from the Royal Society of Chemistry.

Another Ni^{II}-based SMM with the second largest spin ground state was reported by Brechin and coworkers, and includes the aesthetically beautiful, decanuclear complex $[Ni_{10}(N_3)_8(tmp)_2(acac)_6(MeOH)_6]$ (Figure 1.14).[44] The core of the compound contains a planar $[Ni_{10}O_{10}N_8]^{2+}$ disc-like array, with the metal ions held together by a combination of tmp^{3-} and N_3^- ligands. The azides are all bound in an end-on fashion, and are of two types: the ones in the center of the cluster bridge in a μ_3-fashion while the peripheral ones bridge in a μ-fashion (Scheme 1.1). Finally, all Ni(II) atoms are six-coordinate with distorted octahedral geometries. At this point we need to emphasize the ability of end-on azides to propagate ferromagnetic exchange interactions between the metal ions they bridge for a wide range of M-N_{azido}-M angles (M = metals). The bridging azido ligand as a central "player" in high-nuclearity 3*d*-metal cluster chemistry and magnetochemistry has been recently reviewed.[47]

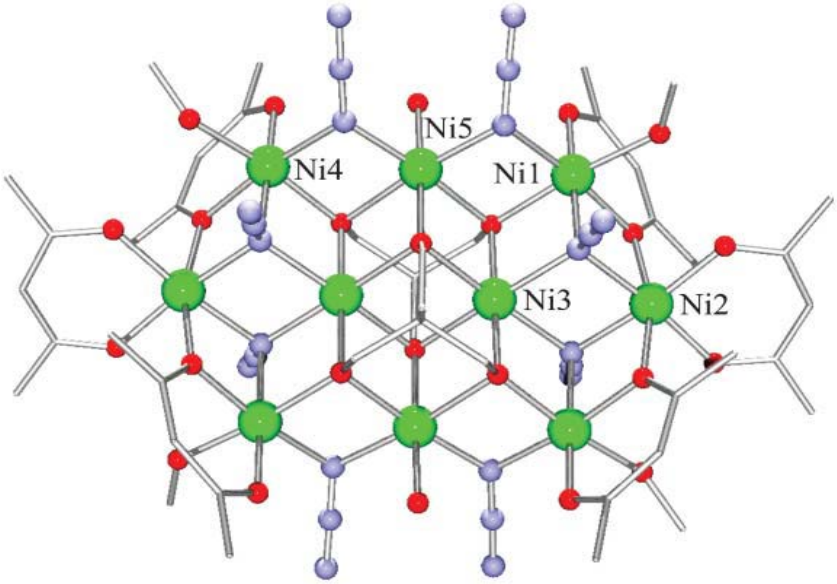

Figure 1.14 The structure of complex $[Ni_{10}(N_3)_8(tmp)_2(acac)_6(MeOH)_6]$. H-atoms are omitted for clarity. Color scheme: Ni^{II} green, O red, N blue, C grey.[44] Reproduced from Ref. 44 with permission from the Royal Society of Chemistry.

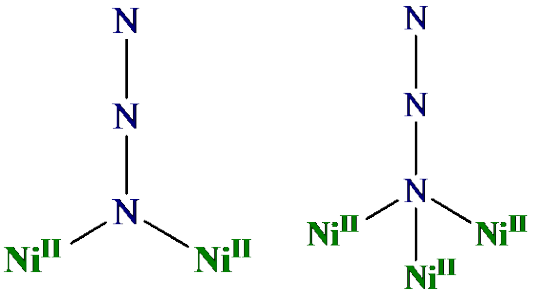

$\mu_{1,1}$-N_3^- end-on

$\mu_{1,1,1}$-N_3^- end-on

Scheme 1.1 Coordination modes of end-on azides in complex $[Ni_{10}(N_3)_8(tmp)_2(acac)_6(MeOH)_6]$.

Magnetic susceptibility studies revealed the presence of predominant ferromagnetic exchange interactions between the ten Ni^{II} atoms, leading to an $S = 10$ spin ground state. Magnetization (M) *vs.* field (H) measurements confirmed the above S value and the presence of a significant zero-field splitting parameter, D. The $\{Ni_{10}\}$ cluster exhibits SMM behavior as was confirmed by the appearance of hysteresis loops below 0.7 K (Figure 1.15). The complex possesses an effective energy barrier for the reorientation of the magnetization, U_{eff} = 14 K, which is among the largest known for any Ni-based SMM.

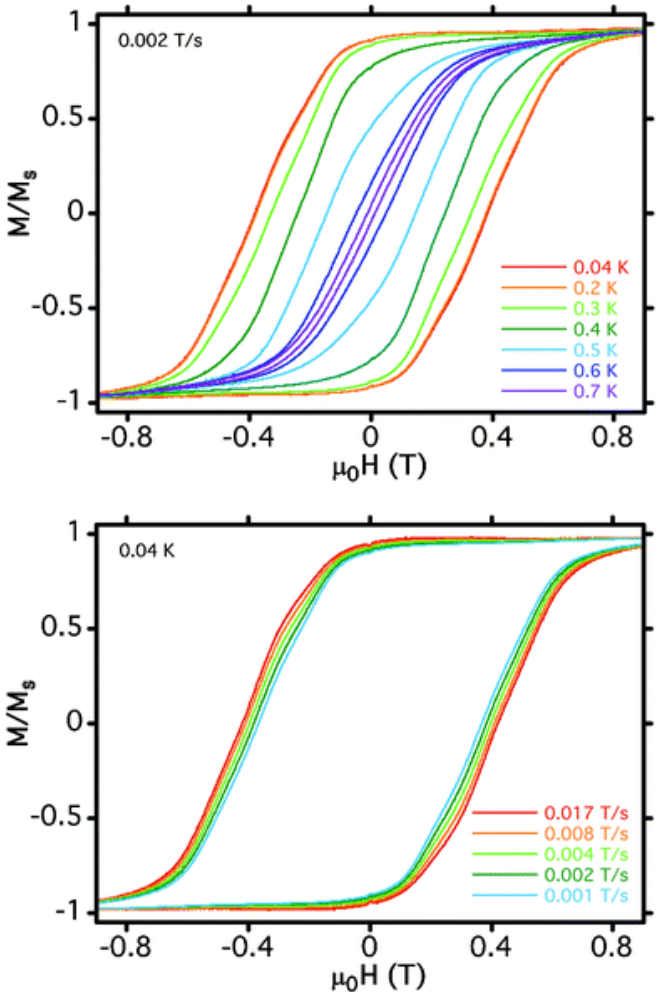

Figure 1.15 Magnetization *vs.* field hysteresis loops for a single-crystal of $[Ni_{10}(N_3)_8(tmp)_2(acac)_6(MeOH)_6]$ at different low temperatures (top) and different field sweep rates (bottom). The magnetization is normalized to its saturation value.[44] Reproduced from Ref. 44 with permission from the Royal Society of Chemistry.

1.3 Long- and Short-Term Research Objectives

The long-term objective of the present work is the synthesis and complete characterization of new nanometer-sized polynuclear Ni(II) complexes with high nuclearities and interesting magnetic properties, such as high-spin molecules and/or single-molecule magnets. For the accomplishment of the long-term objectives, our project's goals have been divided into four short-term research objectives, which are: (i) the synthesis of new, high-nuclearity Ni(II) compounds based on novel organic chelating/bridging ligands that have not been previously used in cluster chemistry, such as the Schiff base *N*-salicylidene-2-amino-5-chlorobenzoic acid ($sacbH_2$, Scheme 1.2), (ii) the growth of single-crystals of the desired Ni(II) products suitable for X-ray diffraction studies in order to elucidate their crystal structures; this is a very difficult and demanding process given the fact that large in nuclearity cluster compounds frequently crystallize in irregular shapes and tiny sizes, (iii) the complete spectroscopic and physicochemical characterization of the synthesized compounds in both solid-state and solution using IR, UV/Vis and elemental analyses techniques, and (iv) the performance of

dc and *ac* magnetic susceptibility studies in order to assess the magnetic properties and dynamics of the Ni(II) complexes.

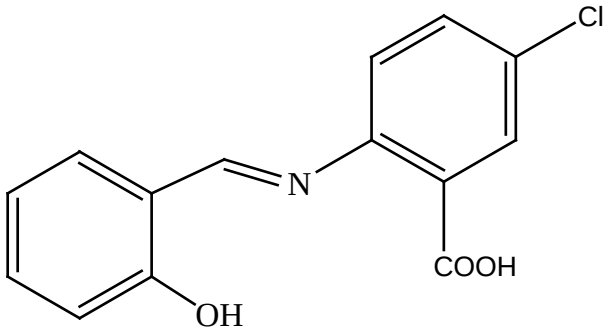

Scheme 1.2 The organic chelating/bridging ligand *N*-salicylidene-2-amino-5-chlorobenzoic acid ($sacbH_2$) used in the present Thesis.

1.4 General Synthetic Routes for the Isolation of Polynuclear 3*d*-Metal Clusters

The chances of identifying novel types of 3*d*-metal clusters with improved or new properties will benefit from the development of new reaction systems with suitable organic ligands or combinations of organic and inorganic ligands. Organic chemists have made important accomplishments the last century by developing new methods for making large and complex molecules in a systematic and more controlled way. This has inspired synthetic chemists of all different areas of research to develop methods of building molecules step-by-step. By comparison, inorganic transition metal chemists have not made large progress in discovering general synthetic approaches to preparing

complexes containing an appreciable number of metal atoms. The main reason for such discrepancy is apparently the lack of prediction in metals' coordination preference with respect to their binding with organic ligands. Moreover, the unquestioned biological relevance and commercial applications of large in nuclearity organic compounds and polymers were not matched by properties of polynuclear and polymeric coordination metal complexes. The lack of control in transition metal chemistry has led to the neologism "self-assembly" or "serendipitous assembly" being coined,[40,48] where simple metal salts or preformed small clusters (mainly containing carboxylate ligands) react with multitopic ligands under a variety of conditions.[49]

To date, the vast majority of polymetallic complexes with interesting physical properties have been created by applying serendipitous approaches. This is due to the extreme difficulty of accurately predicting the physical properties of a given structure, and the fact that even predicting structures is only possible when working with particularly predictable metal-ligand combinations. Many of the approaches to serendipitous assembly rely on creating a mismatch between either the number or type of coordination sites available on a single metal site and the donor set supplied by the ligand. This can be illustrated with two examples. The influential work of Powell and Heath has used a range of polycarboxylates,[50] such as nitrilotriacetic acid and its derivatives, where the number and disposition of the donor atoms on the ligand makes it impossible for all donor atoms to bind to a single metal center. The mismatch leads inevitably to bridging between metal centers and the degree of bridging can be elegantly controlled through pH adjustment and careful choice of the metal-to-ligand ratio. The first results of this approach were very impressive and led to a series of beautiful

{Fe^{III}_{17}}, {Fe^{III}_{19}} and {Cu^{II}_{36}} cages with unprecedented topologies and nanometer sizes.[51] Adopting a similar approach, Güdel and co-workers managed to isolate and characterize a {Ni^{II}_{21}} cage-like cluster using the fully deprotonated form of citric acid as chelating/bridging ligand (Figure 1.16).[52]

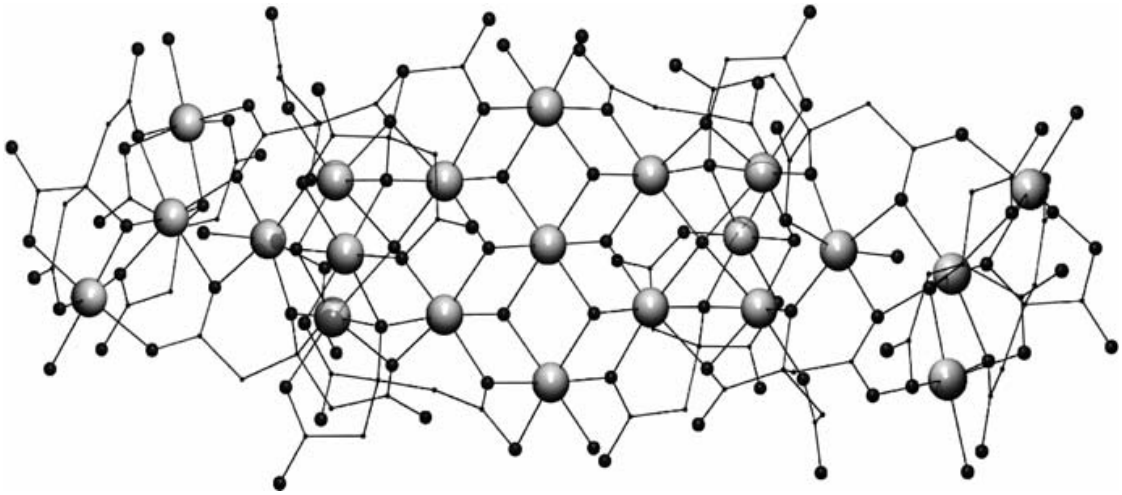

Figure 1.16 The structure of {Ni_{21}} compound. H-atoms have been omitted for clarity. Color scheme: Ni grey large spheres, O black spheres, C tiny grey spheres.[52] Reproduced from Ref. 28b with permission from Springer.

As serendipitous assembly generates unpredictable results, this influences the choice of organic ligands. Ligands that require considerable synthetic effort should be avoided, as it cannot be foreseen whether they will be useful for the construction of new and structurally interesting polynuclear compounds. Secondly, as minor variations in the ligands may influence the structure and properties of metal compounds, a series of related ligands should be ideally explored. Thirdly, as a range of solvents will need to be

examined for crystallization of metal cluster compounds, it would be useful for the ligand to have good solubility in as many solvents as possible.

In the last two decades, several groups have been introducing an element of design into the assembly process by choosing rigid ligands which have strong preferences for specific bonding modes and metal ions with preferred coordination geometries. This "designed assembly" approach has produced many beautiful clusters.[53] The structures of such compounds are moderately predictable, based on the preferred coordination geometry of the metal ion, the number of pre-organized donor sites presented by the ligand and the limited flexibility of the organic ligand. An attractive perspective of this approach for the designed synthesis of new coordination clusters is the ligand-directed rational approach, developed by Fujita[54] and Stang.[55] Rigid, multi-branched monodentate ligands and partially coordinatively saturated, labile metal centers with well-defined coordination preferences are combined in such a way that greatly reduces the complexity of the system (Figure 1.17). By avoiding ligands with multiple binding modes and metals with multiple coordination geometries, it becomes much more practical to view a self-assembling system as "molecular Meccano" (Figure 1.18).[56] It becomes apparent that "design assembly" or "molecular paneling" can be applied to metal ions with strict coordination preferences, i.e. Pd^{2+}, Ag^{+} and Pt^{2+}, but it cannot be easily employed in 3*d*-metal coordination chemistry where metal ions with moderate-to-high oxidation states are susceptible in adopting a variety of different coordination geometries and ligand environments.

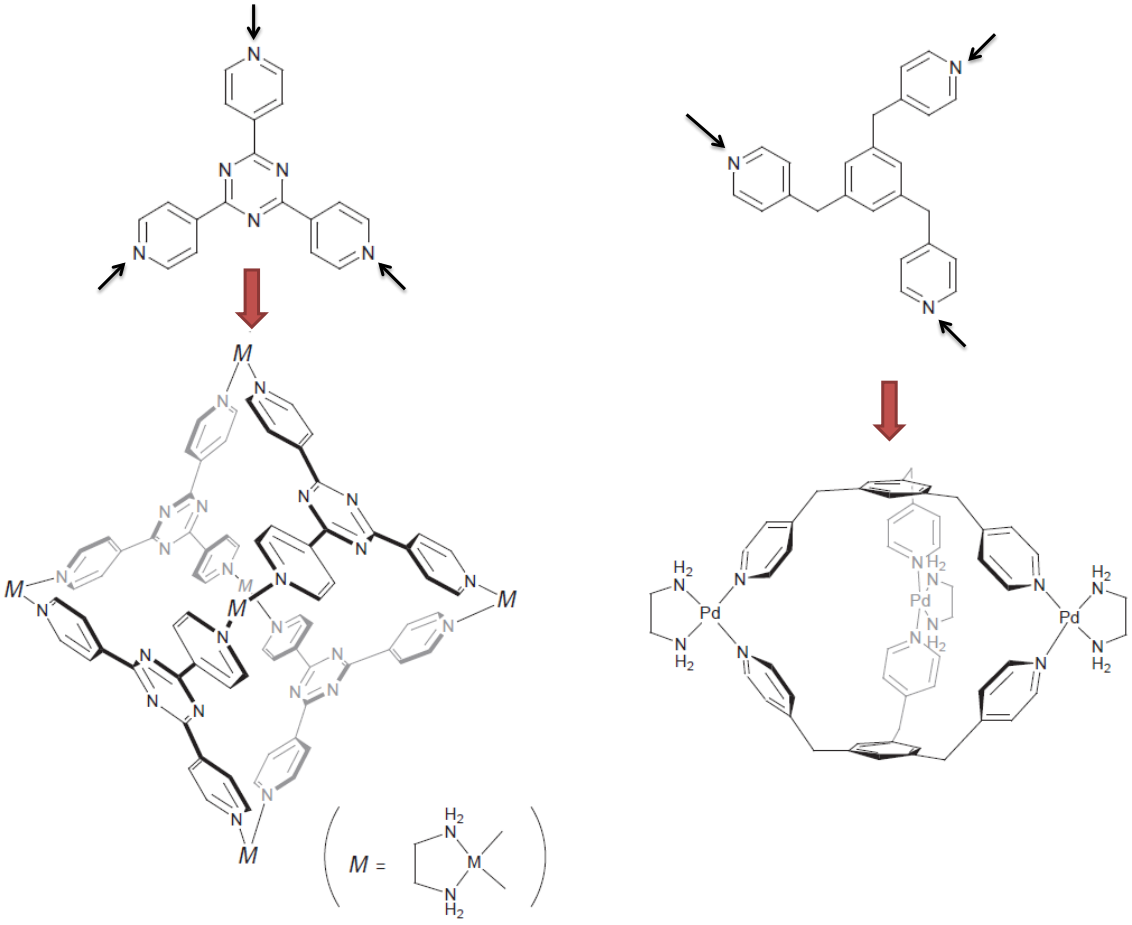

Figure 1.17 (top) Two families of rigid, N-donor polydentate ligands with specific binding abilities (indicated with black arrows), and (bottom) their corresponding nanometer-sized metal cluster compounds. "M" denotes to a divalent metal ion in the chelating unit {M(en)}, where "en" is diethanolamine.[54] Reproduced from Ref. 54b with permission from the Royal Society of Chemistry.

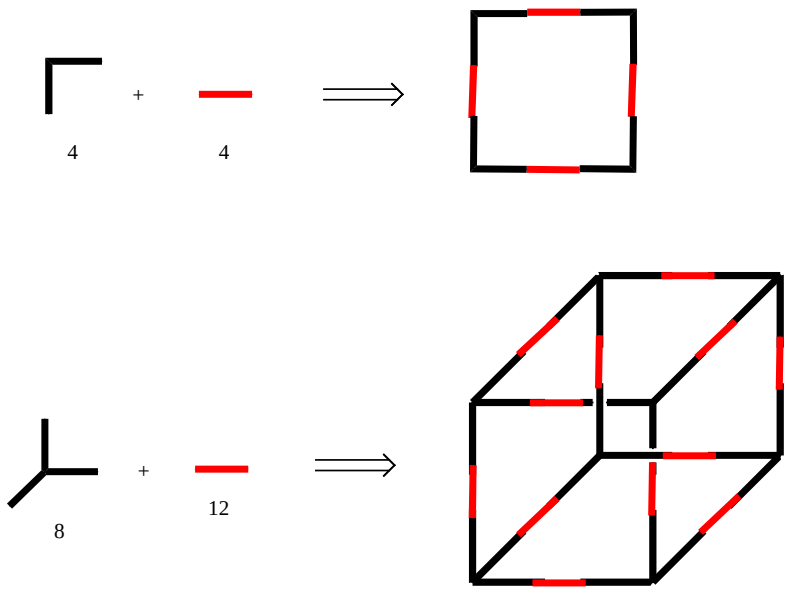

Figure 1.18 A scheme showing the assembly of a square and a cube, which require 2-D and 3-D (black bricks) 90º corner units, respectively, linked by linear spacers (red bricks).

The advantages, though, of serendipitous assembly in cluster chemistry of paramagnetic 3*d*-metal ions are considerable. Most often designed assembly requires similar coordination at each metal site, and this restricts the number of accessible structures, e.g. to Platonic solids, rings and grids in the case of cluster chemistry.[57] On the other hand, serendipitous or less designed assembly vastly increases the range of compounds available for study. The unusual structures of some of such compounds can lead to novel physicochemical (magnetic, optical and chiral) properties. It is clear, however, that we cannot simply trust to happenstance in making such clusters; there has to be considerable forethought in the ligands' choice, metals and reaction conditions (i.e., ratios of reagents, "pH", solvent, temperature, crystallization methods, etc.) for any significant progress to be made.[49] Carboxylate, poly-alcoholate, pyridyl-alcoholate,

pyridyl oximate and aromatic Schiff-base ions are frequently used as bridging and/or bridging/chelating ligands in metal cluster chemistry (Scheme 1.3).[49a,58] In all cases, the deprotonated oxygen(s) atom(s) of these ligands is(are) not coordinatively saturated by binding to one metal, and therefore acts(act) as bridge, leading to the build-up of larger in nuclearity metal clusters.

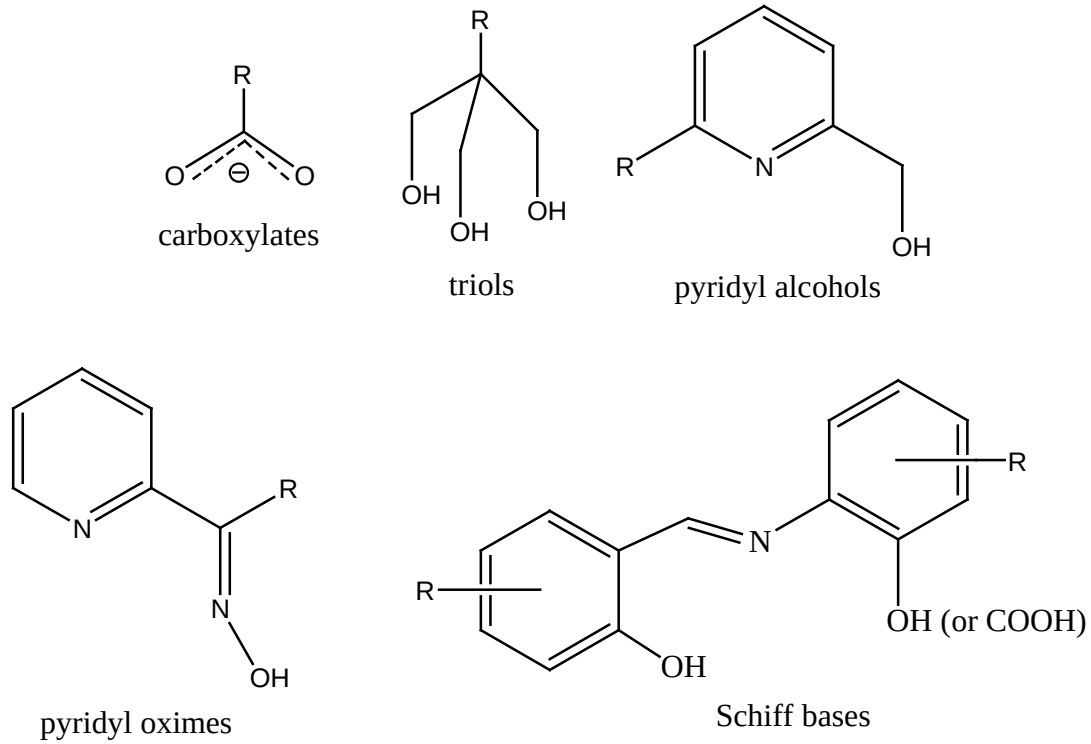

Scheme 1.3 The general classes of organic chelating/bridging ligands discussed in the text (R = various substituents with donor or non-donor atoms).

Finally, what is clear is that the dichotomy between “designed” and “serendipitous” assembly can be exaggerated. Much interesting synthetic work is now arising where

results, originally obtained by chance, are being exploited through design, or where careful design has not completely excluded the possibility of a fortunate accident. However, the potential of the bottom-up approach to the nanoscale is immense. Exploiting this potential will require the skills of a traditional synthetic chemist, i.e., an ability to design and test new procedures, and a capacity to develop results obtained by serendipitous to maximize our good fortune. It is irrational to restrict ourselves to "rational synthesis" of cluster compounds. Excluding serendipity from the available synthetic tools is both impossible and undesirable. As Winpenny elegantly said 'the most successful tool for a chemist is undoubtedly luck'.[49] And he was not wrong.

1.5 The Choice of the 3*d*-Metal Ion: The Case of Ni(II)

The choice of the 3*d*-metal ion for the synthesis of nanoscale molecular magnetic compounds is of significant importance because it dictates the overall magnetic behavior and chemical reactivity towards the construction of large families of different cluster compounds with dissimilar properties, i.e. high-spin molecules and SMMs. The metal ion of choice needs to be paramagnetic ($S \neq 0$) and also possess a non-zero magnetic anisotropy as reflected in an appreciable zero-field splitting parameter, D.[32] To this end, the 3*d*-metal ion of choice for the present research project was Ni^{II} which is known to often adopt a distorted octahedral coordination geometry when surrounded by O- and/or N-donor ligands, thus possessing an [Ar]$3d^8$ electronic configuration with 2 unpaired electrons and an $S = 1$ spin-only value. Furthermore, mononuclear nickel(II) complexes

have been shown to possess appreciable $|D|$, e.g., >10 cm^{-1},[41b] thus allowing us to consider Ni^{II} as a promising candidate for the delivery of SMM behavior in its corresponding cluster compounds.

1.6 The Choice of the Organic Chelating/Bridging ligands: Carboxylates and Schiff Bases

An important factor in the construction of new polynuclear 3*d*-metal complexes is the choice of the primary organic chelating/bridging ligands or "ligand blends", since this often dictates not only cluster symmetry, topology and the number of paramagnetic metal ions present, but also the nature of the intramolecular magnetic exchange interactions.[58] Schiff bases belong to one of the most well-known families of ligands in coordination chemistry as a result of their ease formation and remarkable versatility. They readily form stable complexes with most of the transition metals. The research field that deals with metal complexes of Schiff bases is very broad, covering a large number of interdisciplinary research areas such as bioinorganic chemistry, catalysis, optics, and magnetochemistry.[59]

Imines, known as azomethines or Schiff bases, are compounds with a functional group that contains a carbon-nitrogen double bond. They received their name from Hugo Schiff, a German chemist who devoted most of his research into aldehydes.[60] Schiff bases are represented by the general formula RR′C=NR″, where R and R′ may be alkyl,

aryl or heteroaryl groups, or a hydrogen atom. The substituent, R″, at the imino N-atom may also be alkyl, aryl, heteroaryl or hydrogen but also another element, such as Si, Al, B or Sn. Schiff bases that contain aryl substituents are more stable and more easy to synthesize them, while those that contain alkyl substituents are relatively unstable. The physical properties and reactivity of imines have been studied for many decades and still remain a "hot" topic in the field of coordination and inorganic chemistry. The physicochemical and spectroscopic properties of a large variety of Schiff bases have been extensively studied through IR, NMR, Raman and UV/Vis techniques; the corresponding data can be found in any textbook related to Schiff bases.[61]

The general method for the preparation of Schiff bases is quite straightforward and consists of the condensation reaction of primary amines with a carbonyl-based precursor (aldehydes or ketones), usually in alcoholic solvent media and under reflux conditions (Scheme 1.4). This reaction is reversible, progressing through a carbinolamine intermediate, and requires the removal of water, often by azeotropic distillation with benzene, to achieve high overall yields. The reaction is acid-catalyzed but catalysts are not generally required when aliphatic amines are involved. The resulting compounds contain an imine or azomethine group (>C=N).

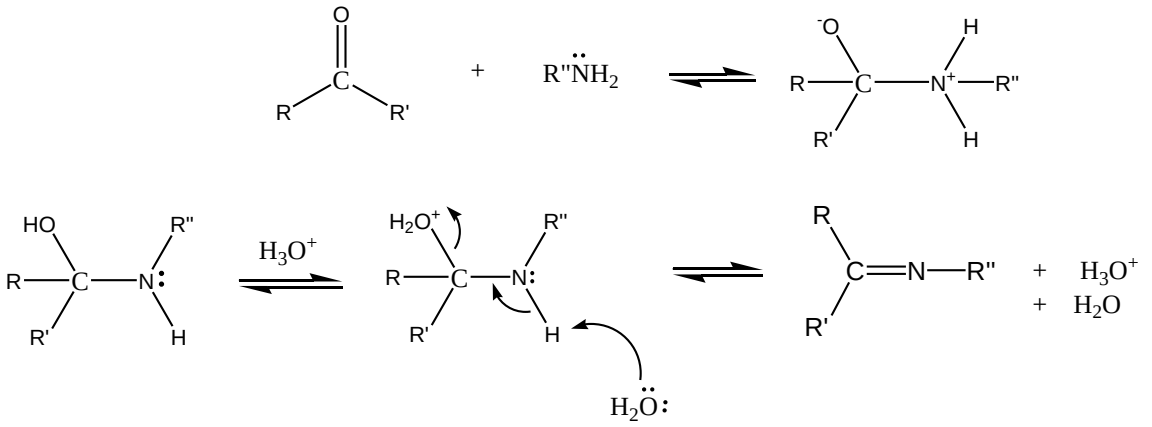

Scheme 1.4 General synthesis and mechanism of formation of Schiff bases. R, R′ and R″ are various substituents.

The first step in the reaction shown in Scheme 1.4 is the attack of the nucleophilic nitrogen atom of the amine on the carbonyl carbon, resulting in a normally unstable carbinolamine intermediate. The hydroxyl group of carbinolamine becomes protonated and the resulting OH_2^+ group is readily eliminated to produce a water molecule with the subsequent formation of an imine (carbon-nitrogen double bond).[62] Many factors affect the condensation reaction, for example the pH of the solution as well as the steric and electronic effects of the carbonyl precursor and amine. Under acidic conditions, the amine is protonated and cannot function as nucleophile; thus, the reaction cannot proceed. Furthermore, in very basic conditions the reaction is blocked because protons are not available to catalyze the elimination of the carbinolamine hydroxyl group. In general, aldehydes react faster than ketones in Schiff base condensation reactions as the reaction center of an aldehyde is sterically less hindered than that of a ketone. Under certain conditions, the additional R-substituent on a ketone

(in place of the H atom of an aldehyde) may also donate electron density to the carbonyl C atom, thus making the ketone less electrophilic than the aldehyde. Since free Schiff bases are not always stable, many coordination complexes with such organic ligands are prepared through template synthetic approaches, which imply the performance of the condensation reaction in the presence of a metal ion. This is a very common route for the preparation of macrocyclic-type Schiff base complexes. For these type of complexes, large in size alkaline or rare earth metal ions have proved to be efficient templates.[63,64]

The compounds that contain the carbon-nitrogen double bond can be easily hydrolyzed to the corresponding aldehydes or ketones. For imines, in general, the hydrolysis in the presence of water is easy. When X = H (Scheme 1.5), the hydrolysis occurs *in situ* because the imine is not stable enough to exist in solution. Schiff bases require an acid or base catalyst for that reaction to proceed. Provided that metal ions are Lewis acids, such a hydrolysis reaction is often observed in many coordination compounds bearing Schiff bases as ligands, where the role of the catalyst is carried out by the metal ion.[65] In terms of spectroscopic characterization, the IR stretching vibrations of the C=N unit of Schiff base ligands, when H, alkyl or aryl groups are bound to the C and N atoms, are shown in the region of 1680-1603 cm^{-1}.[66] The nature of the different substituents on the C_{imine} and N_{imine} atoms determines the position and shift of the IR stretching frequency. For instance, aryl groups bound to the C_{imine} and N_{imine} atoms cause a shift of the IR frequency towards lower wavenumbers. Upon coordination to metal ions, a decrease of the *ν*(C-N) IR frequency is generally observed.

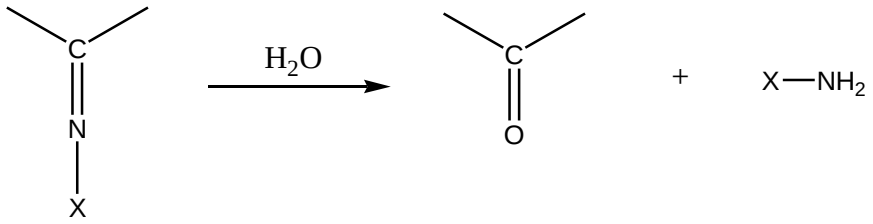

Scheme 1.5 Hydrolysis reaction of imines (X= various substituents).

Our group has recently begun a program aiming at the employment of polydentate chelating/bridging Schiff base ligands in cluster chemistry, as a means of obtaining new polynuclear metal compounds with interesting magnetic and optical properties.[67] Of particular interest is the family of Schiff bases that are based on the scaffold of *N*-salicylidene-*o*-aminophenol (saphH_2, Scheme 1.6). This is due to the ability of the relatively soft N atom and the two hard, upon deprotonation, O atoms to bind to a single or multiple metal centers. Our group has recently reported the employment of saphH_2 in high nuclearity 3*d*/4*f*-metal cluster chemistry which has successfully led to the isolation of $\{Mn^{III}_4Dy^{III}_5\}$ and $\{Mn^{III}_4Dy^{III}_3\}$ complexes with unprecedented metal topologies and SMM behaviors (Figure 1.19).[68]

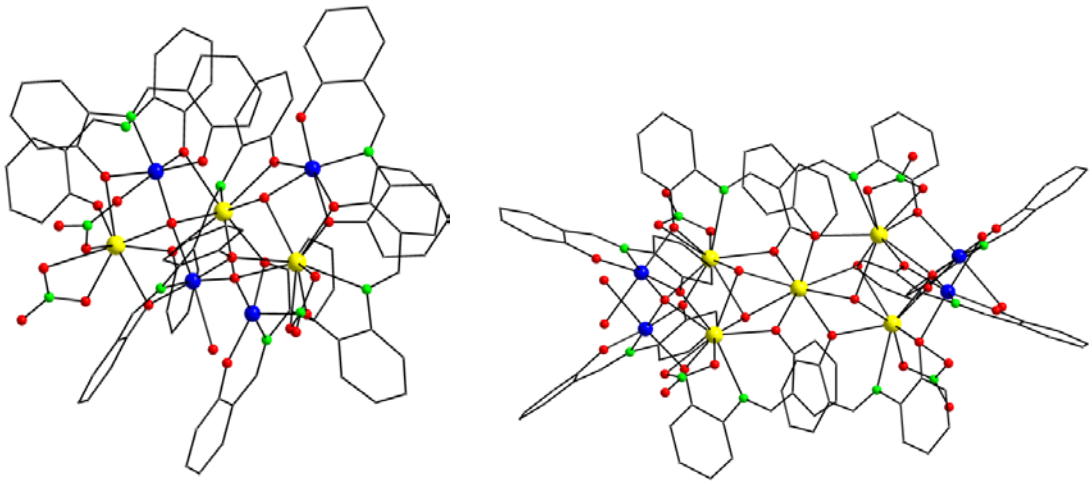

Figure 1.19 Molecular structures of the $\{Mn^{III}_4Dy^{III}_3\}$ (left) and $\{Mn^{III}_4Dy^{III}_5\}$ (right) cluster compounds from the use of *N*-salicylidene-*o*-aminophenol Schiff base ligand. Color scheme: Mn^{III} blue, Dy^{III} yellow, O red, N green, C grey.

Since then, we have been seeking new routes to polynuclear, homometallic Ni^{II} metal complexes with unique motifs and potentially interesting magnetic properties. However, all of our synthetic attempts with the Schiff base ligand saphH_2 failed to give us any crystalline products other than very soluble complexes that remain in solution and oily materials that could not be further analyzed. Thus, we decided to turn our attention into ring-substituted derivatives of saphH_2 with both donor and non-donor groups. We attempted to replace the -OH donor group of the *o*-aminophenol moiety with a carboxylate (-COOH) functionality which could potentially coordinate to more metal centers than saphH_2 through the two O donor atoms and therefore foster the formation of very high nuclearity metal species. In addition, we included a non-donor chloride group in place of a phenyl H atom at the fifth position which could, in principle, differentiate the electronic and steric properties, and hydrogen bonding and crystallization effects. Furthermore, we anticipated a lower solubility of the resulting metal clusters in common organic solvents. The resulting ligand *N*-salicylidene-2-amino-5-chlorobenzoic acid (sacbH_2, Scheme 1.6) has never been previously used in coordination and cluster chemistry either in its neutral or deprotonated forms.

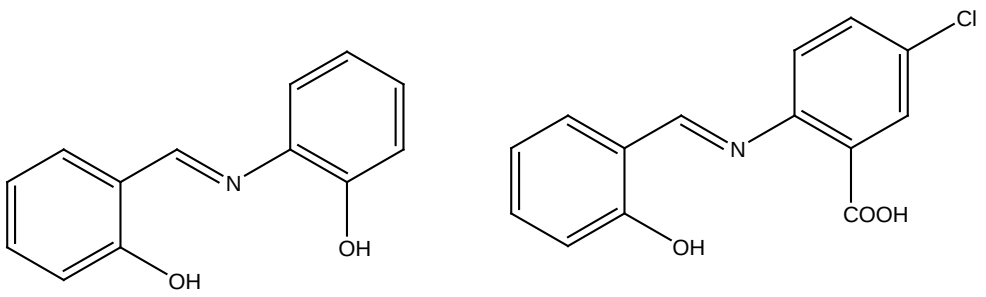

saphH$_2$ **sacbH$_2$**

Scheme 1.6 Structural formulas and abbreviations of the ligands *N*-salicylidene-*o*-aminophenol (saphH$_2$) and *N*-salicylidene-2-amino-5-chlorobenzoic acid (sacbH$_2$) discussed in the text.

Carboxylates (RCO_2^-; R = various) are widely used in metal cluster chemistry since they display a variety of advantages upon coordination. They are bidentate bridging ligands, potentially capable of coordinating up to five metal centers and thus fostering the formation of polynuclear metal clusters. They are also flexible and versatile bridging ligands adopting a variety of different ligation modes (Scheme 1.7).[49b] Furthermore, they often occupy peripheral sites of a coordination cluster, thus providing some additional thermodynamic and kinetic stability to the resulting crystalline products. Finally, they can also act as strong bases facilitating the deprotonation of OH-containing groups.

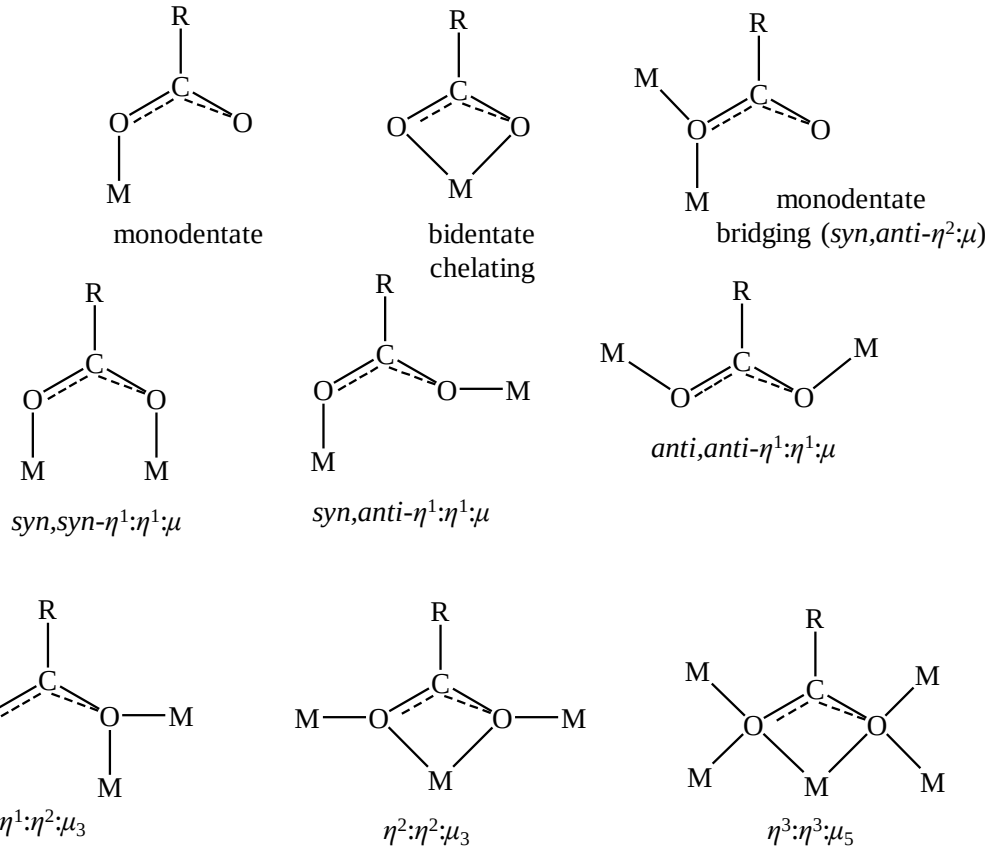

Scheme 1.7 The crystallographically established coordination modes of carboxylate ligands in metal cluster chemistry (R = various; M = metal). Symbols "η" and "μ" denote to the "hapticity" of the donor atoms and the "bridging" fashion of the entire entity, respectively.

The wide variety of coordination modes for the RCO_2^- ions arises from the presence of four lone pairs on the two oxygen atoms which are donated to the metal ions for bond(s) formation. Each lone pair is located on the plane of the carboxylate group. Due to steric and electronic effects it has been proposed that the *syn*-lone pairs are more basic than the ones adopting the *anti*-conformation; this observation has been later on confirmed by theoretical calculations.[49b] The preference of 3*d*-metal ions to bind to the

syn-lone pair(s) of the RCO_2^- moiety is due to their basicity. The *syn*-lone pairs are involved in all usual coordination modes of carboxylates, such as terminally-monodentate, bidentate-chelating, and bidentate-bridging. Most likely due to the lower basicity of the *anti*-lone pairs, coordination modes such as *anti*-(terminal-monodentate), *syn*-*anti*-(bidentate-bridging) and *anti*-*anti*-(bidentate-bridging) are rather scarce. Coordination upon the presence of a monoatomic bridge (Scheme 1.7, top right) is the only one that uses both *syn*- and *anti*-lone pairs of an O atom for the formation of a coordination bond.

In conclusion, the most important point of this section was the negligible previous use of the Schiff base ligand $sacbH_2$ in metal cluster chemistry, either in the presence or absence of any other ancillary/peripheral ligand, such as simple inorganic anions (halides, pseudohalides, etc.), carboxylates, or β-diketones. We thus undertook the challenge to employ for a first time $sacbH_2$ in Ni^{II} cluster chemistry as a means of obtaining new polynuclear compounds with large nuclearities and nanoscale dimensions, exciting structures, and interesting magnetic properties. The following two chapters of this thesis summarize all of our research endeavors toward these objectives.

CHAPTER 2: Investigation of the General $Ni^{2+}/RCO_2^-/sacbH_2$ Reaction System

2.1 Experimental Section

2.1.1 Physical Measurements

General considerations: All experiments were performed under ambient conditions. All chemicals were purchased from Sigma Aldrich and Alfa Aesar. Chemicals and solvents were used as received without further purification.

Elemental Analysis: Elemental analyses (C, H, and N) were performed on a Perkin-Elmer 2400 Series II Analyzer.

FT-IR spectroscopy: Infrared (IR) spectra were recorded in the solid state on a Bruker FT-IR spectrometer (ALPHA Platinum ATR single reflection) in the 4000-450 cm^{-1} range. Notation for IR bands: vs = very strong; s = strong; m = medium; w = weak; b = broad.

Magnetic susceptibility measurements: Direct current (*dc*) magnetic susceptibility studies were performed at the University of Barcelona Chemistry Department on a Quantum Design SQUID magnetometer equipped with a 7 T magnet and operating in the

1.9-300 K range. Samples were embedded in solid eicosane to prevent torquing. Pascal's constants were used to estimate the diamagnetic correction, which was subtracted from the experimental susceptibility to give the molar paramagnetic susceptibility (χ_M).[69]

2.1.2 Synthesis

Synthesis of *N*-salicylidene-2-amino-5-chlorobenzoic acid (sacbH_2): The organic ligand sacbH_2 was prepared in quantitative yields (~95-97%) by the condensation reaction of 2-amino-5-chlorobenzoic acid with salicylaldehyde in a molar ratio of 1:1 in refluxing MeOH. The resulting yellow microcrystalline solid was washed with copious amounts of cold MeOH, dried under vacuum, and analyzed as solvent-free. Elemental analysis (%) calcd for sacbH_2: C 60.99, H 3.66, N 5.08; found: C 61.06, H 3.78, N 5.04. A small amount of the yellow microcrystalline solid was dissolved in CH_2Cl_2 and the resulting yellow solution was left undisturbed to slowly evaporate at room temperature. After 2 days, small yellow, needle-like crystals were appeared and a rough X-ray structural analysis revealed the desired sacbH_2 compound.

Synthesis of metal cluster compounds: Safety note: Perchlorate salts are potentially explosive; such compounds should be synthesized and used in small quantities, and treated with utmost care at all times.

$(NHEt_3)[Ni_{26}(OH)_4(O_2CMe)_{19}(sald)_2(sacb)_{14}(MeOH)_2(H_2O)_6]$ (1): To a stirred, yellow solution of $sacbH_2$ (0.06 g, 0.2 mmol) and NEt_3 (0.17 mL, 1.20 mmol) in MeCN/MeOH (20 mL, 5:1 v/v) was added solid $Ni(ClO_4)_2 \cdot 6H_2O$ (0.15 g, 0.40 mmol) followed by glacial $MeCO_2H$ (23 μL, 0.40 mmol). The resulting green solution was stirred for 20 min, during which time all the solids dissolved and the color of the solution changed to olive-green. The solution was filtered, and the filtrate was left to evaporate slowly at room temperature. After 30 days, X-ray quality yellow-green plate-like crystals of **1**·9MeCN·xMeOH·yH_2O had appeared and were collected by filtration, washed with cold MeCN (2 × 2 mL) and dried under vacuum. The yield was 20 %. Elemental analysis (%) calcd for **1**·10H_2O: C 42.45, H 3.33, N 2.90; found: C 42.59, H 3.46, N 2.62. Selected IR data (ATR): ν = 2980 (m), 2926 (w), 1586 (s), 1536 (vs), 1460 (m), 1439 (s), 1404 (vs), 1349 (m), 1178 (m), 1149 (m), 1115 (m), 1034 (m), 896 (m), 848 (m), 819 (m), 791 (s), 739 (m), 674 (m), 618 (mb), 430 (m).

$(H_3O)[Ni_{18}(OH)_7(O_2CBu^t)_8(sacb)_{10}(MeCN)_4(H_2O)_2](ClO_4)_2$ (2): This complex was prepared in the same manner as complex **1** but using melted Bu^tCO_2H (46 μL, 0.40 mmol) in place of glacial $MeCO_2H$. After 24 days, X-ray quality green plate-like crystals of **2**·11MeCN were collected by filtration, washed with cold MeCN (2 × 2 mL) and dried under vacuum. The yield was 28 %. Elemental analysis (%) calcd for **2**·2MeCN: C 44.32, H 3.53, N 4.31; found: C 44.45, H 3.66, N 4.18. Selected IR data (ATR): ν = 2957 (m), 2946 (mb), 1630 (s), 1596 (vs), 1479 (m), 1459 (m), 1440 (s), 1410 (vs), 1359 (s), 1223 (m), 1176 (m), 1150 (m), 1118 (m), 976 (m), 924 (m), 850 (m), 819 (m), 785 (s), 611 (mb), 530 (m), 459 (m).

$[Ni_{11}(OH)_4(O_2CCH_2Bu^t)_8(sacb)_5(MeCN)_3(H_2O)]$ (3): To a stirred, yellow solution of $sacbH_2$ (0.06 g, 0.20 mmol) and NEt_3 (0.17 mL, 1.20 mmol) in MeCN (20 mL) were added $Ni(ClO_4)_2 \cdot 6H_2O$ (0.15 g, 0.40 mmol) and $Bu^tCH_2CO_2H$ (0.05 mL, 0.40 mmol). The resulting green-yellow solution was stirred for 20 min, during which time all the solids dissolved and the color of the solution changed to dark green. The solution was filtered, and the filtrate was left to evaporate slowly at room temperature. After 10 days, X-ray quality dark-green plate-like crystals of **3**·4.5MeCN·1.5H_2O had appeared and were collected by filtration, washed with cold MeCN (2 × 2 mL) and dried in air. Note that the crystalline product **3** is extremely soluble in Et_2O and thus avoidance of washing with such solvent is strongly recommended. The yield was 65 %. Elemental analysis (%) calcd for **3**·3H_2O: C 46.57, H 4.70, N 3.50; found: C 46.69, H 4.82, N 3.37. Selected IR data (ATR): ν = 2949 (mb), 1587 (vs), 1536 (vs), 1460 (m), 1440 (s), 1407 (s), 1360 (s), 1300 (m), 1229 (w), 1177 (m), 1150 (m), 1119 (m), 1038 (w), 899 (w), 850 (m), 820 (m), 792 (s), 740 (m), 553 (m), 460 (mb).

2.1.3 Single-crystal X-ray Crystallography

Single-crystal X-ray diffraction measurements were carried out for all three complexes **1**-**3**. The corresponding crystals of **1**-**3** were manually harvested and mounted on cryoloops using inert oil.[70] Diffraction data were collected at 150.0(2) K on a Bruker X8 Kappa APEX II Charge-Coupled Device (CCD) area-detector diffractometer controlled by the APEX2 software package[71] (Mo Kα graphite-monochromated radiation,

$\lambda = 0.71073$ Å), and equipped with an Oxford Cryosystems Series 700 cryostream monitored remotely with the software interface Cryopad.[72] Images were processed with the software SAINT,[73] and absorption was corrected using the multi-scan semi-empirical method implemented in SADABS.[74] The structures were solved by the direct or Patterson methods employed in SHELXS-97,[75,76] allowing the immediate location of the heavy metal ions. The remaining, non-H atoms of the complexes were located from difference Fourier maps calculated by full-matrix least-squares refinement cycles on F^2 using SHELXL-2013,[76] and refined with anisotropic displacement parameters. For complexes **1** and **2**, the lattice groups were disordered and could not be modeled properly; thus the program SQUEEZE,[77] a part of the PLATON package of crystallographic software, was used to calculate the solvent disorder area and remove its contribution to the overall intensity data.

In the structures of **1** and **2**, the H-atoms bound to the C-atoms of organic ligands were placed at their geometrical positions using *HFIX* instructions in SHELXL[76] (*43* for the aromatic, *23* for the CH_2 and *137* for the terminal CH_3 groups) and included in subsequent refinement cycles in riding-motion approximation with isotropic thermal displacements parameters (U_{iso}) fixed at 1.2 or $1.5 \times U_{eq}$ of the C-atom to which they are attached. In the structure of **3**, all H-atoms were introduced at calculated positions as riding on bonded atoms, except of those on hydroxido ions and aqua molecules which were located by difference maps and refined with $1.3 \times U_{eq}$ of their riding atom. There are five MeCN and two H_2O solvate molecules per $\{Ni_{11}\}$ cluster. One of the MeCN and one of the H_2O solvate molecules were refined with partial occupancy fixed at 0.50; no H-atoms for these molecules were included in the refinement. The programs used for

molecular graphics of all structures were MERCURY[78] and DIAMOND.[79] Unit cell parameters and structure solution and refinement data for all complexes are listed in Table 2.1.

Table 2.1 Crystallographic data for complexes **1-3**

Parameter	**1**·9MeCN·xMeOH·yH_2	**2**·11MeCN	**3**·4.5MeCN·1.5H_2O
Formula	$C_{275}H_{232}N_{24}Ni_{26}O_{123}Cl_{14}$	$C_{210}H_{211}N_{25}Ni_{18}O_{64}Cl_{12}$	$C_{133}H_{159.5}N_{12.5}Ni_{11}O_{37.5}Cl_5$
Formula weight / g mol^{-1}	7374.48	5591.22	3356.29
Crystal type	Yellow-green plates	Green plates	Dark-green plates
Crystal size / mm^3	0.21 × 0.21 × 0.09	0.28 × 0.08 × 0.05	0.28 × 0.09 × 0.05
Crystal system	Monoclinic	Monoclinic	Monoclinic
Space group	$P2_1/n$	$C2/c$	$P2_1/c$
a / Å	25.959(1)	22.442(2)	27.090(3)
b / Å	45.854(2)	21.074(2)	22.251(2)
c / Å	32.608(2)	52.993(5)	28.725(3)
α / º	90	90	90
β / º	94.904(3)	90.197(4)	114.718(4)
γ / º	90	90	90
Volume / $Å^3$	38671(3)	25063(4)	15728(3)
Z	4	4	4
ρ_{calc} / g cm^{-3}	1.267	1.482	1.417
μ / mm^{-1}	1.398	1.524	1.443
θ range / °	2.42 - 26.37	1.76 - 25.00	2.37 - 29.54

Index ranges	$-30 \le h \le 30$	$-26 \le h \le 26$	$-32 \le h \le 32$
	$-54 \le k \le 54$	$-24 \le k \le 25$	$-26 \le k \le 26$
	$-38 \le l \le 38$	$-62 \le l \le 62$	$-34 \le l \le 34$
Reflections collected	371801	179512	466517
Independent reflections	68057 (R_{int} = 0.0923)	21874 (R_{int} = 0.0832)	27654 (R_{int} = 0.0744)
Final *R* indices $[I>2\sigma(I)]^{a,b}$	*R*1 = 0.0838 *wR*2 = 0.1875	*R*1 = 0.0917 *wR*2 = 0.2066	*R*1 = 0.0594 *wR*2 = 0.1240
Final *R* indices (all data)	*R*1 = 0.1328 *wR*2 = 0.2176	*R*1 = 0.1230 *wR*2 = 0.2201	*R*1 = 0.0775 *wR*2 = 0.1325
$(\Delta\rho)_{max,min}$ / e Å^{-3}	2.564 and -1.994	1.143 and -0.925	1.637 and -0.765

[a] $R1 = \Sigma(||F_o| - |F_c||)/\Sigma|F_o|$.

[b] $wR2 = [\Sigma[w(F_o^2 - F_c^2)^2]/ \Sigma[w(F_o^2)^2]]^{1/2}$, $w = 1/[\sigma^2(F_o^2) + [(ap)^2 + bp]$, where $p = [\max(F_o^2, 0) + 2F_c^2]/3$.

2.2 Results and Discussion

2.2.1 Synthetic Comments and IR Spectra

Many synthetic procedures to polynuclear Ni(II) complexes rely on the reactions of simple NiX_2 starting materials (X^- = various) with a potentially chelating/bridging organic ligand (LH_x; $x \ge 1$).[40-47] The nature of both the X^- group and the organic ligand, LH_x, is of significant synthetic importance. When the X^- belongs to the carboxylate or β-diketonate

groups, additional bridging ligation from these groups might be provided, resulting in the formation of higher nuclearity molecular species. Additionally, their strong basic nature fosters the deprotonation of the organic chelating/bridging ligand, LH_x, without requiring the use of an external base. On the other hand, when the choice of X^- is one of the halides, NO_3^-, ClO_4^- or $CF_3SO_3^-$, all with limited bridging affinity, the employment of an external organic base which would carry the role of proton acceptor seems necessary to facilitate deprotonation of the organic chelating/bridging ligand and therefore increase the chances of metal cluster formation. Finally, a third synthetic approach with negligible previous use in Ni(II) cluster chemistry involves the co-presence of neutral LH_x organic chelates and flexible carboxylic acids; such a reaction mixture undoubtedly requires the use of an external base to subtract the protons and unveil the bridging capabilities of all the organic anionic groups. The latter route was followed in the present study, using as organic chelating/bridging ligand the unexplored in metal cluster chemistry Schiff base *N*-salicylidene-2-amino-5-chlorobenzoic acid ($sacbH_2$) in conjunction with various carboxylic acids.

A variety of reactions differing in the Ni:$sacbH_2$ ratio, the carboxylic acids, the inorganic ions present, the organic base, and/or the reaction solvent(s) were explored in identifying the following successful systems. The reaction of $Ni(ClO_4)_2{\cdot}6H_2O$, $sacbH_2$, NEt_3, and $MeCO_2H$ in a 2:1:6:2 molar ratio in a solvent mixture comprising MeCN/MeOH (5/1, v/v) gave a yellow-green solution that, upon filtration and slow evaporation at room temperature, afforded yellow-green crystals of $(NHEt_3)[Ni_{26}(OH)_4(O_2CMe)_{19}(sald)_2(sacb)_{14}(MeOH)_2(H_2O)_6]$ (**1**) in 20% yield after approximately one month. The coordinated salicylaldehyde ($sald^-$) anions in **1** (*vide infra*)

are presumably derived from the metal-assisted, partial hydrolysis of $sacbH_2$.[80] The base NEt_3 has the role of proton acceptor to facilitate the deprotonation of the $sacbH_2$ and $MeCO_2H$ groups, as well as the deprotonation of H_2O-containing solvents and starting materials towards the *in situ* generation of OH^- groups. Employment of different organic bases, such as NMe_3, $^nBu_3N$ and Me_4NOH, did not afford crystalline materials but only amorphous precipitates or oily products that we were not able to further characterize. The reaction solvents or solvent mixtures were found to be of critical importance for the crystallization of all reported compounds **1**-**3**; various other reactions in more polar or non-polar solvent media gave either very soluble compounds that was infeasible to grow single-crystals from the corresponding solutions or non-crystalline precipitates that were probably mixtures of different products. Once the identity of **1** was established by single-crystal X-ray diffraction studies (*vide infra*), we attempted to optimize the synthesis and increase the yield of the crystalline compound by adding salicylaldehyde (saldH) *in situ* and adjusting the Ni^{II}:$sacbH_2$:saldH:$MeCO_2H$:NEt_3 molar ratio close to the stoichiometric one (i.e., 13:7:1:10:27). Unfortunately, we didn't manage to isolate the $\{Ni_{26}\}$ compound in higher yields. As with many reactions in high-nuclearity *3d*-metal cluster chemistry, the solution likely contains a mixture of species in equilibrium, and what crystallizes out is determined by the relative solubilities, the nature of counterions, lattice energies, and other related factors.[81]

In the next step of our synthetic attempts, we decided to replace the flexible acetate ions with the more bulky pivalates. It is known that in metal cluster chemistry the nature of the carboxylate ions often affects the chemical identity of the crystalline compounds yielding products with different structural motifs and physical properties.[82] That was

indeed turned out to be the case in Ni^{II}/$sacbH_2$ coordination chemistry. The analogous reaction of **1** but with Bu^tCO_2H instead of $MeCO_2H$ afforded single crystals of a different octadecanuclear product. Hence, the reaction of $Ni(ClO_4)_2{\cdot}6H_2O$, $sacbH_2$, NEt_3, and Bu^tCO_2H in a 2:1:6:2 molar ratio in MeCN gave a dark-green solution that, upon filtration and slow evaporation at room temperature, afforded green crystals of $(H_3O)[Ni_{18}(OH)_7(O_2CBu^t)_8(sacb)_{10}(MeCN)_4(H_2O)_2](ClO_4)_2$ (**2**) in 28% yield after ~3 weeks. The formation of **2** can be represented by the balanced equation 2.1.

$$18\ Ni(ClO_4)_2{\cdot}6H_2O + 10\ sacbH_2 + 8\ Bu^tCO_2H + 34\ NEt_3 + 4\ MeCN \longrightarrow$$

$$(H_3O)[Ni_{18}(OH)_7(O_2CBu^t)_8(sacb)_{10}(MeCN)_4(H_2O)_2](ClO_4)_2$$

2

$$+ 34\ (NHEt_3)(ClO_4) + 98\ H_2O \quad (2.1)$$

This time, our attempts to increase the yield and improve the synthesis of crystalline **2** by adjusting the Ni^{II}:$sacbH_2$:Bu^tCO_2H:NEt_3 molar ratio to 18:10:8:34 (see, equation 2.1) were successful, and the product was isolated in yields as high as 70%. Following up with the reported efficient reaction scheme, the last step was to check for any potentially different cluster products from the employment of $Bu^tCH_2CO_2H$ in place of Bu^tCO_2H. Although simple and flexible carboxylates (i.e., $MeCO_2^-$, Bu^tCO_2H), as well as sterically-demanding and robust ones (i.e., aromatic RCO_2^-), have been widely and successfully used in 3*d*-metal cluster chemistry,[48] *tert*-butylacetate ion ($Bu^tCH_2CO_2^-$) has not yet attracted similar attention. Reasons that differentiate $Bu^tCH_2CO_2^-$ group from its related pivalate ion ($Bu^tCO_2^-$) are mainly steric and partially electronic. For instance, *tert*-butylacetate ion is larger in size but more flexible (i.e., free rotation around the C_{Bu}-CH_2 single bond) than the pivalate ion. Furthermore, although $Bu^tCH_2CO_2H$ and Bu^tCO_2H

have similar *p*k_a values (close to 5.0), the acidity of the former is higher than that of the latter due to solvation effects.[83]

Thus, the reaction of $Ni(ClO_4)_2 \cdot 6H_2O$, $sacbH_2$, $Bu^tCH_2CO_2H$, and NEt_3 in a 2:1:2:6 molar ratio in MeCN gave a dark-green solution that, upon slow evaporation at room temperature, afforded dark-green crystals of the undecanuclear compound $[Ni_{11}(OH)_4(O_2CCH_2Bu^t)_8(sacb)_5(MeCN)_3(H_2O)]$ (**3**) in 65% yield. This further emphasizes the importance of carboxylate ions in the clusters' formation and the major role they play in the structural identity of the products. The formation of **3** can be represented by the balanced equation 2.2. Finally, it is essential to mention that a wide variety of similar reactions with different RCO_2H, where R = H, Et or Ph, were performed but we were unable to isolate any crystalline product under various crystallization techniques and work-up conditions. Compounds **1**-**3** are all stable and crystalline solids at room temperature, and nonsensitive toward air and moisture. Unless otherwise stated, they are all soluble in MeOH, DMF and CH_2Cl_2, and partially soluble in almost all other organic solvents such as THF and toluene.

$$11\ Ni(ClO_4)_2 \cdot 6H_2O + 5\ sacbH_2 + 8\ Bu^tCH_2CO_2H + 22\ NEt_3 + 3\ MeCN \longrightarrow$$

$$[Ni_{11}(OH)_4(O_2CCH_2Bu^t)_8(sacb)_5(MeCN)_3(H_2O)]$$

3

$$+ 22\ (NHEt_3)(ClO_4) + 61\ H_2O \quad (2.2)$$

All complexes **1**-**3** have very similar IR spectra. Several bands appear in the ~1596-1380 cm^{-1} range, assigned to contributions from the stretching vibrations of the aromatic rings of $sacb^{2-}$, which overlap with stretches of the carboxylate bands;[84] they, thus, do not represent pure vibrations and render exact assignments difficult. Contributions from the

ν(C=N)$_{imino}$ modes of sacb^{2-} would be also expected in this region. The bands at ~2980 and ~2926 cm^{-1} for complex **1** can be assigned to the stretching vibrations of ν(N-H) modes from the presence of Et_3NH^+ countercation.[85] For complexes **2** and **3**, the intense bands at ~2957 and ~2949 cm^{-1} can be tentatively assigned to the stretching vibrations of ν(C-H) modes from the -CH_3 groups of the *tert*-butyl moiety of Bu^{t}CO$_2$H and Bu^{t}CH$_2$CO$_2$H, respectively.

2.2.2 Description of structures

The formula of complex **1** was based on metric parameters, charge balance considerations and oxygen bond-valence sum (BVS)[86] calculations. The structure of the anion of **1** (Figure 2.1) consists of 26 Ni^{II} atoms bridged by four μ_3-OH$^-$ ions (BVS 1.11-1.20)[86] and the alkoxido and carboxylate fragments of fourteen, doubly-deprotonated sacb^{2-} ligands, two anionic sald$^-$ groups and nineteen acetates. Impressively, sacb^{2-} ions bind in three different modes (Scheme 2.1); two ligands coordinate in an η^3:η^1:η^1:μ_3 manner, a further two adopt the η^2:η^1:η^2:μ_3 modes, while the remaining ten ligands bind in an η^2:η^1:η^2:η^1:μ_4 fashion, acting as O,N,O,O-tetradentate chelates to a Ni^{II} center, simultaneously bridging three additional Ni^{II} atoms through the phenolate and both carboxylate O atoms. This emphasizes the binding affinity and rich bridging versatility of the sacb^{2-} dianionic ligand. In addition, peripheral ligation is provided by nine η^1:η^1:μ, eight η^1:η^2:μ_3 and two η^2:η^2:μ_4 MeCO$_2^-$ groups, two η^1:η^1:μ bidentate chelating/bridging sald$^-$ ligands, and two MeOH and six H$_2$O (BVS 0.32-0.35)[86] molecules terminally bound

to a total of six Ni^{II} atoms; the two MeOH and one H_2O molecules are disordered over three positions. All of the Ni^{II} atoms are six-coordinate with distorted octahedral geometries (orange thick bonds in Figure 2.1).

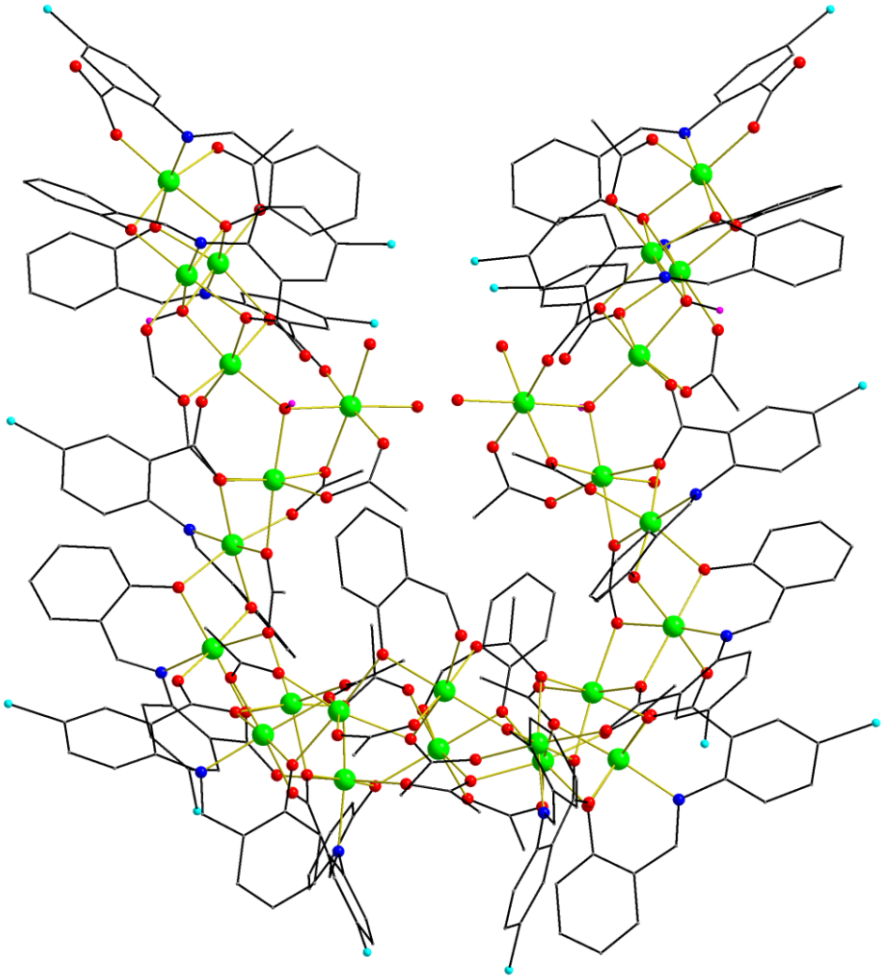

Figure 2.1 Complete structure of the anion of **1**. All H atoms except from the ones belonging to the μ_3-OH^- groups are omitted for clarity. Color scheme: Ni^{II} green, O red, N blue, C dark gray, Cl cyan, H magenta.

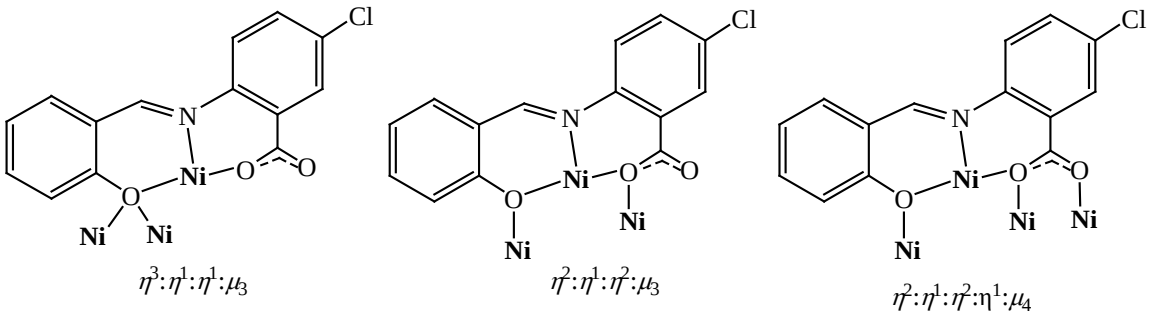

Scheme 2.1 The crystallographically established coordination modes of $sacb^{2-}$ in complex **1**.

The $[Ni_{26}(\mu_3\text{-}OH)_4(\mu_3\text{-}OR)_2(\mu\text{-}OR)_{38}]^{8+}$ core topology of **1** (Figure 2.2, top) resembles the face of a 'bunny-rabbit', with two opposite-side $\{Ni_4(\mu_3\text{-}OH)(\mu_3\text{-}OR)(\mu\text{-}OR)_4\}^{2+}$ defective-dicubane subunits as the 'ears' and a central $\{Ni_{18}\}$ unit solely bridged by μ-OR^- groups providing the 'head' (Figure 2.2, bottom). The $\{Ni_{18}\}$ 'head' can be further divided into two $\{Ni_4\}$ *zigzag* subunits and a non-planar, 'crown'-like $\{Ni_{10}\}$ moiety with a single-strand wheel topology. Furthermore, the $\{Ni_{18}\}$ subunit is nicely "closed out" by two strong intramolecular H-bonds; these involve the aqua O atoms, O74 and O18, as donors and the carboxylate O atoms, O19 and O72, as acceptors [O74···O19 = 2.77 Å and O18···O72 = 2.73 Å] (Figure 2.3). A close examination of the crystal packing of **1** reveals that there are no significant intermolecular interactions between neighboring $\{Ni_{26}\}$ anions; the shortest Ni···Ni distance between neighboring units is ~7.23 Å, with nearest neighbours oriented perpendicular to one another.

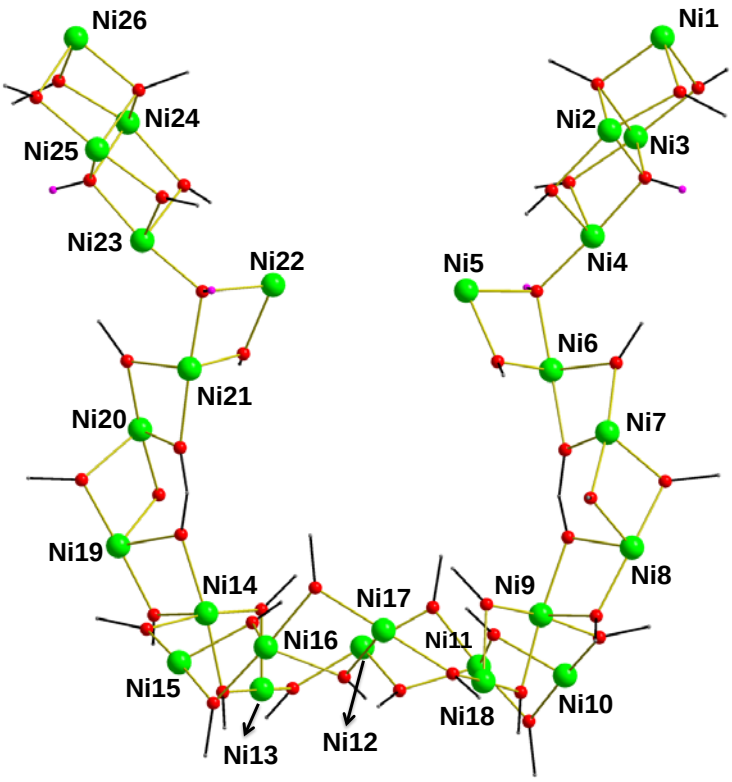
Ni26
Ni24
Ni25
Ni23
Ni22
Ni21
Ni20
Ni19
Ni14
Ni15
Ni13
Ni16
Ni17
Ni12
Ni11
Ni18
Ni9
Ni10
Ni8
Ni7
Ni6
Ni5
Ni4
Ni2
Ni3
Ni1

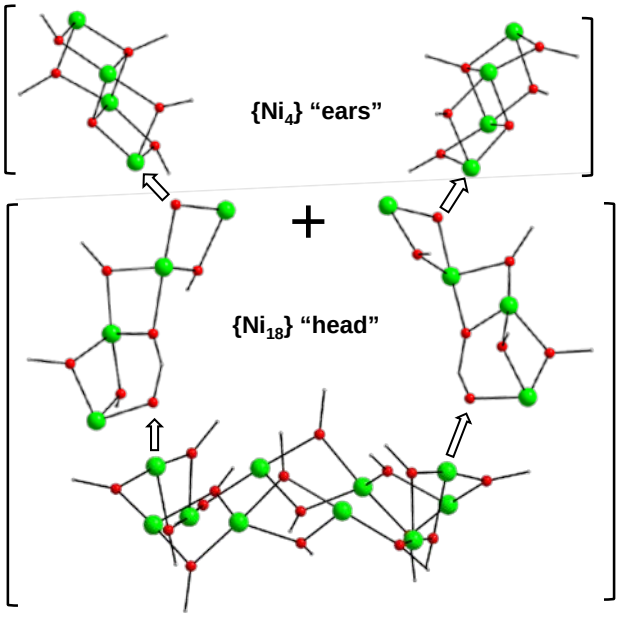
{Ni4} “ears”
+
{Ni18} “head”

Figure 2.2 (top) Partially-labeled structure of the 'rabbit-face'-like core of **1**. (bottom) 'Building up' the $\{Ni_{26}\}$ core from smaller fragments. The arrows indicate the 'nodal' atoms. Color scheme as in Figure 2.1.

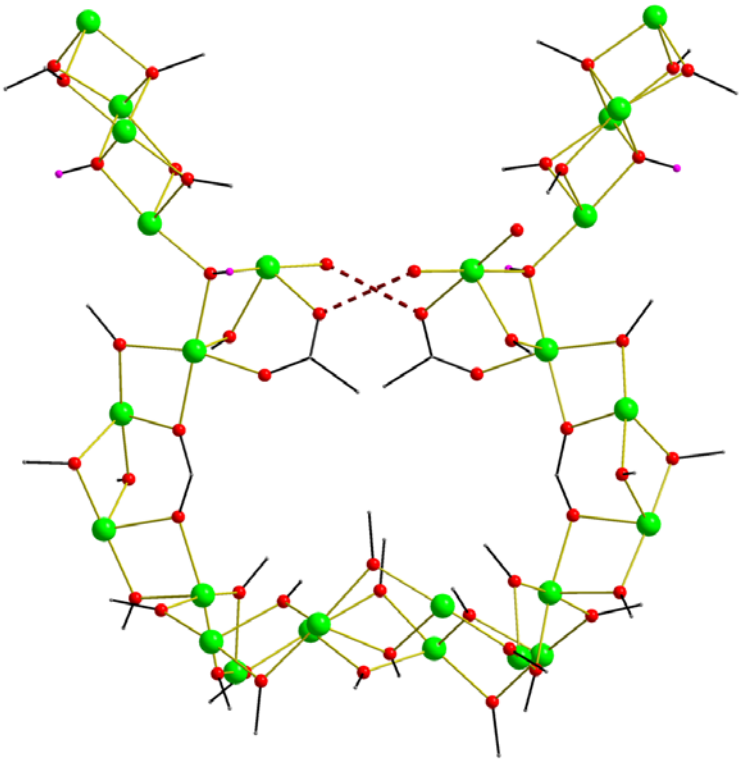

Figure 2.3 The $\{Ni_{26}\}$ core emphasizing the two strong intramolecular H-bonding interactions (brown dashed lines) which serve to "close out" the $\{Ni_{18}\}$ "head".

The space-filling representation (Figure 2.4) shows that **1** adopts a saddle-shaped conformation with a diameter of ~24 Å, defined by the longest Cl···Cl distance. The nanoscale dimensions of this aesthetically bautiful molecular compound place it in the forefront of molecular nanoscience. Furthermore, the $\{Ni_{26}\}$ compound is the highest nuclearity, non-organometallic Ni^{II} cluster reported in the literature to date[16,17] and possesses a unique 'rabbit-face' structural topology.[87]

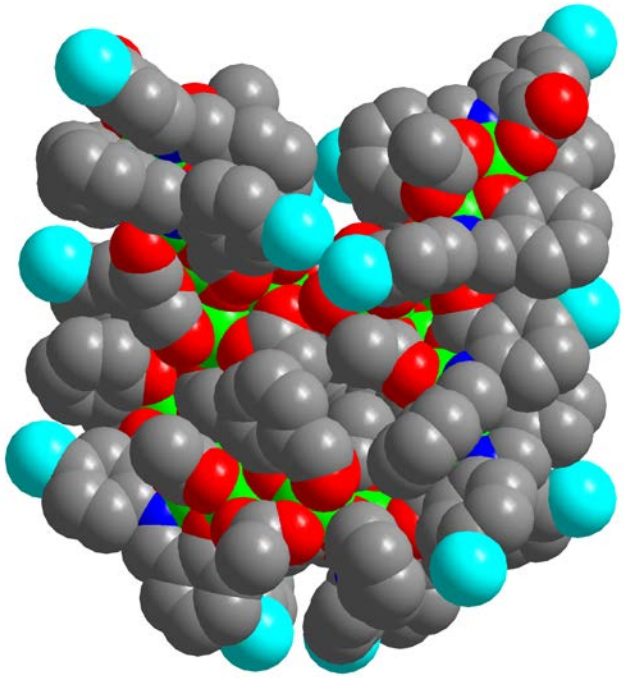

Figure 2.4 Space-filling representation of the $\{Ni_{26}\}$ cluster anion. Color scheme as in Figure 2.1.

Complex **2** crystallizes in the monoclinic space group *C*2/*c* with the asymmetric unit containing a $[Ni_{18}(OH)_7(O_2CBu^t)_8(sacb)_{10}(MeCN)_4(H_2O)_2]^+$ cation, stabilized by the presence of an H_3O^+, two ClO_4^- anions, as well as eleven MeCN solvate molecules, all of which are severely disordered. The formula of the compound was derived based on metric parameters, charge balance considerations and O BVS calculations; the latter confirmed that all bridging, inorganic O atoms belong to OH^- groups. Thus, the charge of the $\{Ni_{18}\}$ cluster is undoubtedly +1. Given the clear presence of two ClO_4^- counterions in the crystal lattice and the absence of any organic cation to counterbalance the overall -1 charge, we assigned that role to a disordered H_3O^+ unit located in the crystal lattice.

The structure of the centrosymmetric cation of **2** (Figure 2.5) comprises a remarkable $\{Ni_{18}\}$ cluster that can be described as consisting of a consecutive array of Ni_4-Ni_3-Ni_4-Ni_3-Ni_4 subunits linked into a discrete 'molecular chain' topology.

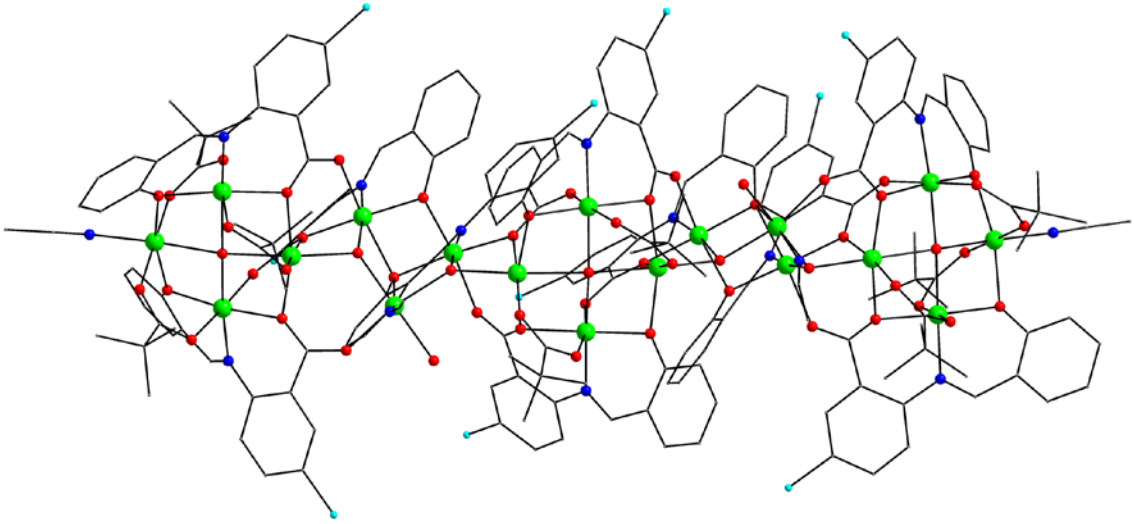

Figure 2.5 Complete molecular structure of the cation of **2**. All H atoms are omitted for clarity. Color scheme: Ni^{II} green, O red, N blue, C dark gray, Cl cyan.

The eighteen Ni^{II} atoms are held together by three μ_4-OH^- (O51, O51′, O52) and four μ_3-OH^- (O53, O53′, O54, O54′) ions (BVS 1.03-1.18), as well as the alkoxido and carboxylate moieties from ten $sacb^{2-}$ ligands. Eight ligands bind in the common η^2:η^1:η^2:η^1:μ_4 mode (as was shown in **1**) and two in the unique η^3:η^1:η^2:η^1:μ_5 fashion, all acting as N,O,O-tridentate chelates to a Ni^{II} center and simultaneously bridging three or four additional Ni^{II} atoms, respectively, through their phenolate and carboxylate O atoms (Scheme 2.2).

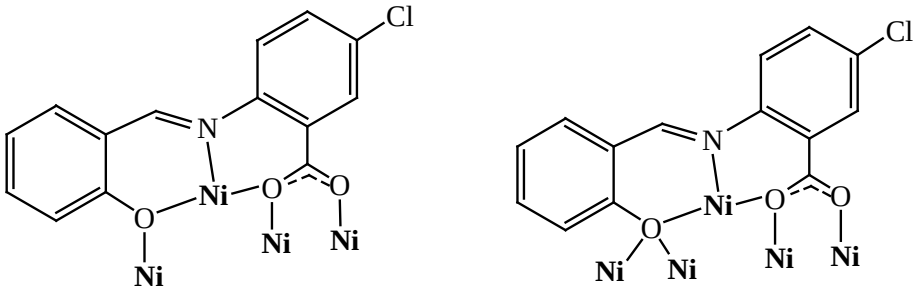

$\eta^2:\eta^1:\eta^2:\eta^1:\mu_4$ $\eta^3:\eta^1:\eta^2:\eta^1:\mu_5$

Scheme 2.2 The crystallographically established coordination modes of $sacb^{2-}$ in complex **2**.

Thus, complex **2** possesses a complete $[Ni_{18}(\mu_4\text{-}OH)_3(\mu_3\text{-}OH)_4(\mu_3\text{-}OR)_2(\mu\text{-}OR)_{18}]^{9+}$ core (Figure 2.6) with peripheral ligation provided by eight $\eta^1:\eta^1:\mu$ $Bu^tCO_2^-$ groups, four MeCN and two H_2O molecules, terminally bound to Ni(4,4′,9,9′) and Ni(4,4′), respectively. The three $\{Ni_4\}$ fragments of the 'molecular $\{Ni_{18}\}$ chain' form similar, near-planar $\{Ni_4(\mu_4\text{-}OH)(\mu\text{-}OR)_4\}^{3+}$ square topologies. The μ_4-OH^- groups are slightly displaced out of the $\{Ni_4\}$ mean planes by 0.221 and 0.268 Å. The Ni-(μ_4-OH^-)-Ni angles span the range 87.9(2)-92.3(2)°, deviating only slightly from the ideal 90°. The two, symmetry-related $\{Ni_3\}$ fragments adopt a scalene triangular $\{Ni_3(\mu_3\text{-}OR)(\mu\text{-}OH)_2(\mu\text{-}OR)\}^{2+}$ motif, with the two edge-bridging μ-OH^- groups becoming μ_3 and linking the $\{Ni_3\}$ triangles with adjacent $\{Ni_4\}$ squares. Finally, all Ni^{II} atoms are six-coordinate with distorted octahedral geometries.

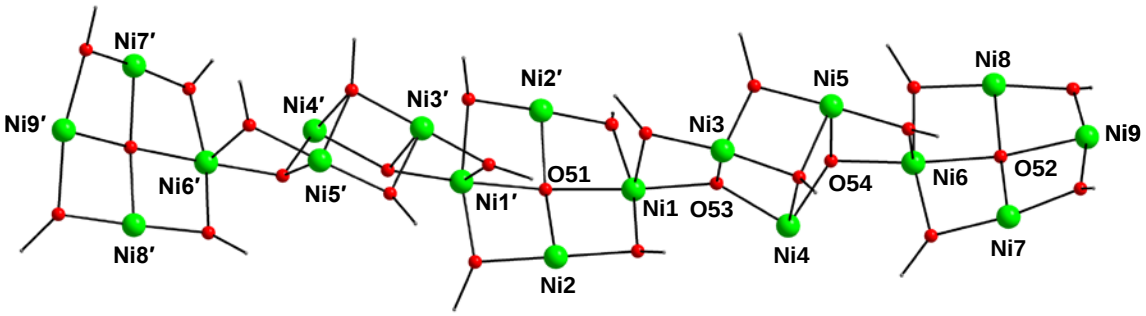

Figure 2.6 The partially-labeled structure of the 'molecular chain'-like core of **2**. Color scheme as in Figure 2.5.

The space-filling representation (Figure 2.7) shows that the cation of **2** has a nanotubular structure with a length of 35 Å, as defined by the longest C···C distance of the externally bound MeCN molecules, and a thickness of ~16 Å as determined by the longest intracluster Cl···Cl separation. Complex **2** is the second $\{Ni^{II}_{18}\}$ cluster reported to date, the first being a planar, disk-like $\{Ni_{18}\}$ compound assembled from the hexadentate ligand N-(2-pyridylmethyl)iminodipropionic acid.[88] Thus, the topology of **2** is not only unprecedented in Ni chemistry but it also represents the highest-nuclearity, chain-like metal complex discovered to date, and can reasonably be called a 'molecular chain'. A 'molecular chain' of the same length, but with Fe^{III} atoms, has been reported by Christou and coworkers,[89] and consists of an $\{Fe_{18}\}$ cluster with a double-headed serpent topology that has an $S = 0$ spin ground state.

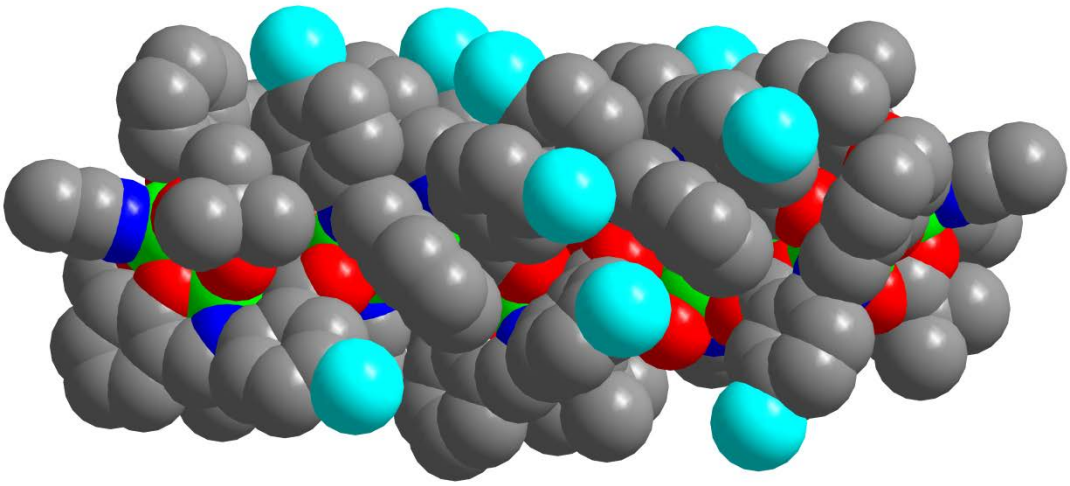

Figure 2.7 Space-filling representation of the nanotubular $\{Ni_{18}\}$ cluster cation. Color scheme: Ni^{II} green, O red, N blue, C dark gray, Cl cyan.

Complex **3** crystallizes in the monoclinic space group $P2_1/c$ with the $[Ni_{11}(OH)_4(O_2CCH_2Bu^t)_8(sacb)_5(MeCN)_3(H_2O)]$ molecule in a general position. The undecanuclear cage-like complex **3** (Figure 2.8) has also a 'molecular chain'-like structure, similar to **2** but of smaller size and shorter length. It consists of eleven Ni^{II} atoms held together by two μ_4-OH^- (O4, O5) and two μ_3-OH^- (O6, O7) ions (Scheme 2.3), as well as the alkoxido and carboxylate fragments of five, double-deprotonated $sacb^{2-}$ ligands. All $sacb^{2-}$ ions bind in the same η^2:η^1:η^2:η^1:μ_4 mode, acting as N,O,O-tridentate chelates to a Ni^{II} center and simultaneously bridging three additional Ni^{II} atoms through the phenolate and carboxylate O atoms.

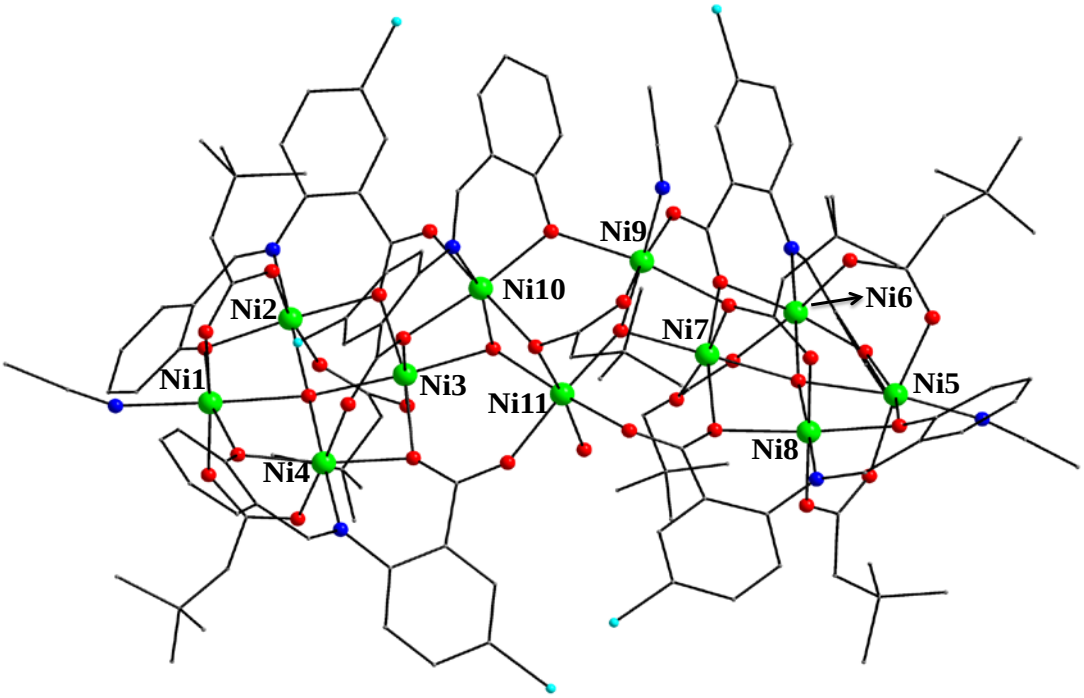

Figure 2.8 Partially-labeled plot of the {Ni_{11}} molecule of **3**, with H atoms omitted for clarity. Colour scheme: Ni^{II} green, O red, N blue, Cl cyan, C dark gray.

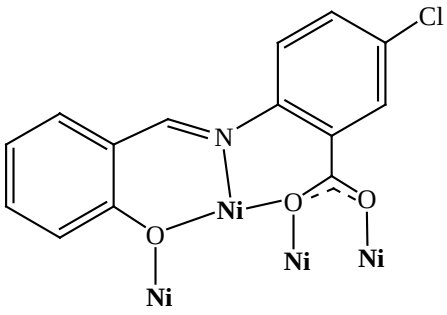

$\eta^2:\eta^1:\eta^2:\eta^1:\mu_4$

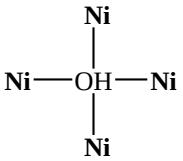

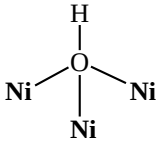

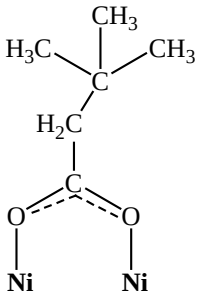

$\eta^1:\eta^1:\mu$

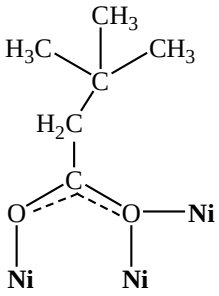

$\eta^1:\eta^2:\mu_3$

Scheme 2.3 The crystallographically established coordination modes of all bridging ligands present in complex **3**.

As expected and seen in all three reported compounds **1**-**3**, the Cl-substituent on the sacb^{2-} groups does not participate in coordination, although it is involved in very weak intermolecular interactions with H atoms of phenyl and *tert*-butyl groups of the coordinated ligands. Peripheral ligation is provided by six η^1:η^1:μ and two η^1:η^2:μ_3 Bu^{t}CH$_2$CO$_2^-$ groups (Scheme 2.3), and three MeCN and one H_2O molecules terminally bound to Ni(1,5,9) and Ni(11), respectively. The space-filling representation (Figure 2.9) shows that **3** has a saddle-shaped or sinusoidal conformation with a diameter of 24.9 Å, defined by the longest H···H distance. It also encapsulates one MeCN and one H_2O solvate molecules which are held *via* hydrogen bonding interactions (Table 2.2); these involve the two μ_3-OH$^-$ (O6, O7) ions, the coordinated H_2O and one carboxylate O-atom (Figure 2.10).

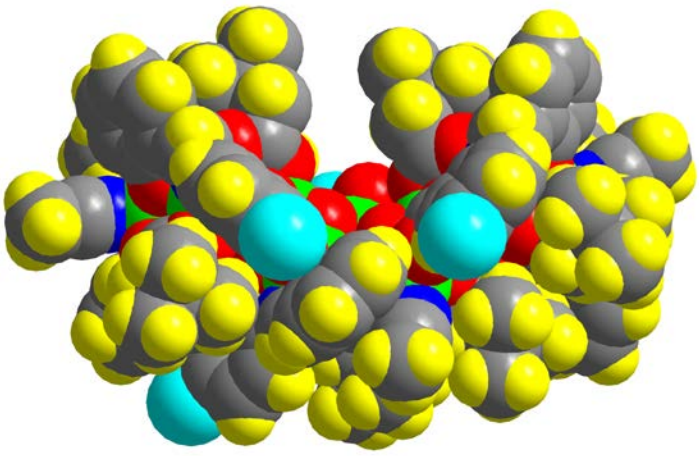

Figure 2.9 Space-filling representation of **3** showing its saddle-shaped conformation. Colour scheme: Ni^{II} green, O red, N blue, Cl cyan, C dark gray, H yellow.

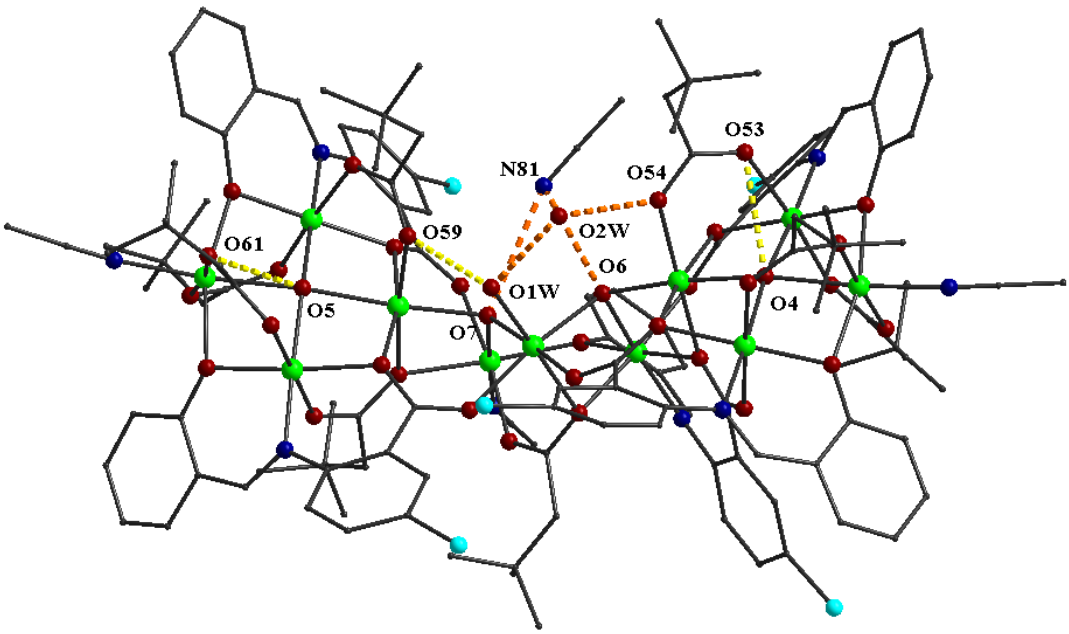

Figure 2.10 Hydrogen bonding interactions in the crystal structure of **3**. Intra- and inter-molecular H-bonds are shown as yellow and orange dashed lines, respectively.

Table 2.2 Hydrogen bonding interactions in **3**·4.5MeCN·1.5H_2O

Interaction	D···A (Å)	H···A (Å)	D-H···A (°)	symmetry operation
O(4)-H(4O)···O(53)	2.846	2.355	123.8	*x*, *y*, *z*
O(5)-H(5O)···O(61)	2.920	2.462	114.5	*x*, *y*, *z*
O(6)-H(6O)···N(81)	3.068	2.365	157.3	*x*, *y*, *z*
O(7)-H(7O)···N(81)	3.170	2.436	164.8	*x*, *y*, *z*
O(1w)-H(1wA)···O(2w)	2.695	1.888	170.8	*x*, *y*, *z*
O(1w)-H(1wB)···O(59)	2.634	1.868	156.6	*x*, *y*, *z*

O(2w)-H(2wB)···O(54)	2.748	2.191	123.0	*x*, *y*, *z*

Complex **3** contains an overall $[Ni_{11}(\mu_4\text{-}OH)_2(\mu_3\text{-}OH)_2(\mu\text{-}OR)_{12}]^{6+}$ core (Figure 2.11), which can be described as two external, almost planar $\{Ni_4(\mu_4\text{-}OH)(\mu\text{-}OR)_4\}^{3+}$ squares [Ni(1,2,3,4) and Ni(5,6,7,8)] at each end, fused to two internal $\{Ni_3(\mu_3\text{-}OH)(\mu\text{-}OR)_2\}^{3+}$ triangles [Ni(3,10,11) and Ni(7,9,11)] which share a common vertex (Ni11) and two edges (Ni10···Ni11 and Ni9···Ni11) with a central $\{Ni_3\}$ scalene triangle that comprises Ni(9,10,11). The average displacement of the Ni^{II} centers from the mean plane of the Ni(1,2,3,4) and Ni(5,6,7,8) squares is only 0.029 and 0.044 Å, respectively. The μ_4-OH^- groups (O4 and O5) are only slightly displaced out of the $\{Ni_4\}$ mean planes by 0.209 and 0.218 Å, respectively. Thus, they have a distorted geometry, closer to that of square-planar, which is rare and has been seen only twice before in Ni(II) chemistry.[90] The Ni-(μ_4-OH^-)-Ni angles (88.0-92.4º) deviate only slightly from the ideal 90º. The two $\{Ni_3(\mu_3\text{-}OH)(\mu\text{-}OR)_2\}^{3+}$ triangular units are essentially isosceles, the almost equal separations being the Ni3···Ni10, Ni10···Ni11, Ni7···Ni9 and Ni7···Ni11 edges. This is also reflected in the geometry at the μ_3-OH^- ions, O6 and O7, which have a Y-shaped geometry (largest Ni-O-Ni angles of 125.5(2) and 121.0(2)º, respectively) rather than the trigonal planar geometry usually seen in triangular metal carboxylates.[91] The protonation levels of OH^- and H_2O groups were confirmed by oxygen BVS calculations which gave values of 1.16 (O4 and O5), 1.10 (O6), 1.13 (O7) and 0.35 (O1W), respectively.[86] Finally, all Ni^{II} atoms are six-coordinate with distorted octahedral geometries.

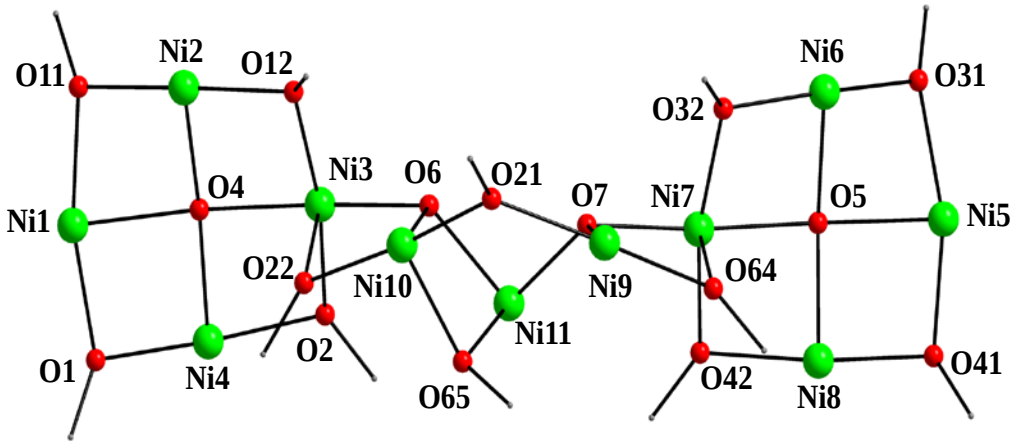

Figure 2.11 Labeled representation of the $[Ni_{11}(\mu_4\text{-}OH)_2(\mu_3\text{-}OH)_2(\mu\text{-}OR)_{12}]^{6+}$ core of **3**. Colour scheme as in Figure 2.8.

While the number of polynuclear Ni^{II} complexes continues to grow rapidly, some nuclearities remain rare. Undecanuclear Ni^{II} clusters are particularly scarce; complex **3** belongs to a small family of $\{Ni_{11}\}$ clusters reported to date,[92,93,94,95,96] and is the first with such a structural topology. The majority of the previously reported $\{Ni_{11}\}$ clusters contain pyridonates as bridging ligands,[93,94,95] except from the mixed-valence $\{Ni^{II/III}{}_{11}\}$ metal chain, which was made from the use of a polydentate tetranaphthyridyltriamine ligand,[92] a $\{Ni_{11}\}$ cluster with metal-metal bonds and a *cyclo*-$\{Ni_{11}\}$ cluster.[96]

2.2.3 Solid-state Magnetic Susceptibility Studies

Variable-temperature direct-current (*dc*) magnetic susceptibility measurements were performed on freshly-prepared and analytically-pure microcrystalline solids of **1**·10H_2O, **2**·2MeCN and **3**·3H_2O in the temperature range 2-300 K; a *dc* field of 0.2 T was applied from 30 to 300 K and a weaker *dc* field of 0.02 T was applied from 2 to 30 K to avoid saturation effects. The data for complex **1**·10H_2O are shown as $\chi_M T$ *vs. T* plot in Figure 2.12. The value of the $\chi_M T$ product at 300 K is 31.34 $cm^3 \cdot mol^{-1} \cdot K$, in excellent agreement with the value of 31.46 $cm^3 \cdot mol^{-1} \cdot K$ (calculated with g = 2.2) expected for twenty-six non-interacting, high-spin Ni^{II} (S = 1) atoms. The $\chi_M T$ product for the {Ni_{26}} complex remains essentially constant in the 300-50 K region and then slightly increases to a value of 32.20 $cm^3 \cdot mol^{-1} \cdot K$ at 35 K, before dropping sharply to a value of 21.25 $cm^3 \cdot mol^{-1} \cdot K$ at 2 K. The shape of the curve suggests that both ferro- and antiferromagnetic exchange interactions are likely present within **1**. The $\chi_M T$ value at the lowest temperature and smallest possible *dc* fields suggests a non-zero ground state spin for the complex, with the value at 2 K being consistent with an S = 6 or 5 ground state depending on g. Given the size and low-symmetry of the {Ni_{26}} cluster, and the resulting number of inequivalent exchange constants, it was not possible to determine the individual pairwise Ni_2 exchange interaction parameters. Thus, we concentrated instead on characterizing the ground state spin, *S*, by performing magnetization (*M*) *vs*. *dc* field measurements in a magnetic field and temperature ranges 1-50 kG and 2-10.0 K, respectively.

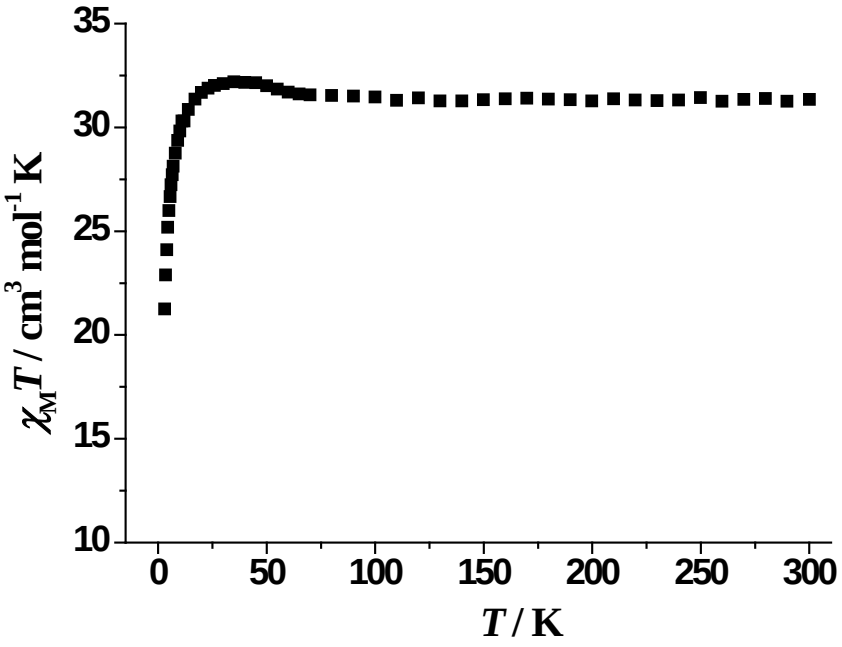

Figure 2.12 $\chi_M T$ *vs.* T plot for complex **1**·10H_2O.

Magnetization (*M*) *vs.* field (*H*) measurements for complex **1**·10H_2O (Figure 2.13) at 2 K show a continuous increase of *M* as the field increases; this is likely due to the presence of low-lying excited states, as reported previously for other high-nuclearity Ni^{II} complexes.[16,17,93,94] As a result, attempts to fit the reduced magnetization data assuming that only the ground state is populated were very poor. However, the *M vs. H* plot at 2 K, and for very small fields of < 5000 G, was nicely reproduced upon application of the Brillouin function for an $S = 6$ ground state with $g = 2.2$.

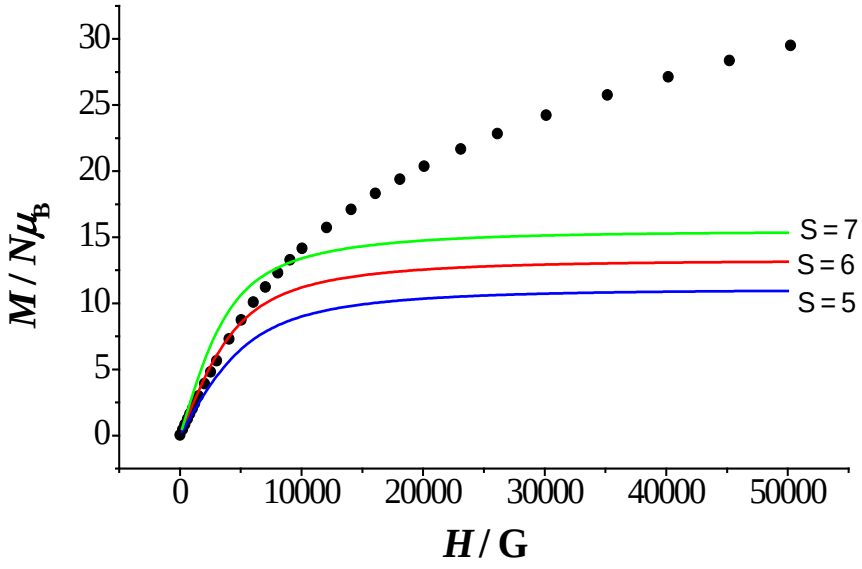

Figure 2.13 Plot of magnetization (*M*) *vs.* field (*H*) for complex **1**·10H_2O at 2 K. The solid, colored lines are the different fits of the data to the corresponding Brillouin functions for S = 5, 6 and 7 with g = 2.2.

A powerful complement to *dc* studies for determining the ground state of a system, and also for studying magnetization dynamics, are alternating-current (*ac*) magnetic susceptibility measurements, which preclude any complications arising from the presence of a *dc* field. These were performed for complex **1** in a 4.0 G *ac* field oscillating at different frequencies. The in-phase susceptibility (χ_M') is shown as $\chi_M'T$ *vs.* T plot in Figure 2.14, and reveals several pertinent features: (i) $\chi_M'T$ decreases almost linearly with decreasing temperature in the 2-10 K range, indicating depopulation of a high density of excited states with spin S greater than that of the ground state, in agreement with the conclusion from the *dc* studies;[34] (ii) extrapolation of the $\chi_M'T$ data from above ~3.0 K to 0 K gives a value of ~24 $cm^3 \cdot K \cdot mol^{-1}$, indicative of an S = 6 ground state with g = ~2.2-

2.0; (iii) even at the lowest accessible temperature and for three different *ac* frequencies, there is no frequency-dependent decrease in the $\chi_M'T$ plot and no out-of-phase χ_M'' signals, thus suggesting that complex **1** is not an SMM.

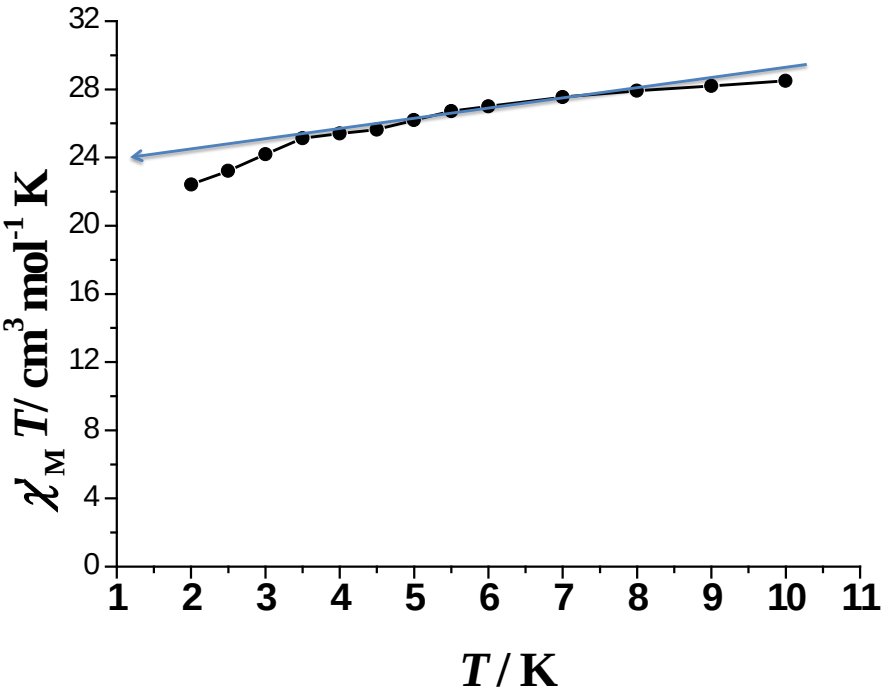

Figure 2.14 The in-phase (as $\chi_M'T$) *vs. T ac* susceptibility signals for **1**·10H_2O under a 4 G oscillating field operating at a frequency of 1000 Hz.

In contrast to the magnetic behavior of **1**, the χ_MT product of the {Ni_{18}} cluster shows a rapid decrease as the temperature is lowered in the range of 300-10 K and then a more gradual decrease to a value of 7.33 $cm^3 \cdot mol^{-1} \cdot K$ at 2.0 K (Figure 2.15). The shape of the plot indicates an overall antiferromagnetic behavior with different strength of magnetic couplings at different temperature regions, presumably deriving from the different fragments ({Ni_4} squares and {Ni_3} triangles) of the {Ni_{18}} cluster. In cases

such as **2** (and **1**), as well as for the majority of polynuclear *3d*-metal clusters with a non-zero ground state, the resultant molecular *S* value is a consequence of the many competing (predominantly) antiferromagnetic interactions that prevent (frustrate) perfectly antiparallel spin alignments.[31] This is particularly true when triangular subunits are present, since an antiferromagnetically-coupled triangle cannot contain spins that are all aligned antiparallel with both neighbours. The ground state then becomes extremely difficult to predict from a structural examination and simple spin-up/spin-down considerations. In fact, the net molecular *S* is dependent on the precise topology of the M_x (M = metal) framework and very sensitive to the relative strengths of the competing interactions. Crucial to the latter in Ni^{II} chemistry is the fact that Ni-OR-Ni interactions within triangular units are often of similar magnitude, either weakly antiferromagnetic or, occasionally, weakly ferromagnetic.[97] For **2**·2MeCN, the value of the $\chi_M T$ product at 300 K is 21.36 $cm^3 \cdot mol^{-1} \cdot K$, again in excellent agreement with the value of 21.78 $cm^3 \cdot mol^{-1} \cdot K$ (calculated with g = 2.2) expected for eighteen non-interacting, high-spin Ni^{II} (S = 1) atoms. Similarly to **1**, the continuous increase of magnetization *vs.* field data for **2**·2MeCN at 2 K (Figure 2.16) indicates the presence of low-lying excited states. No acceptable and reliable fit of magnetization data was feasible.

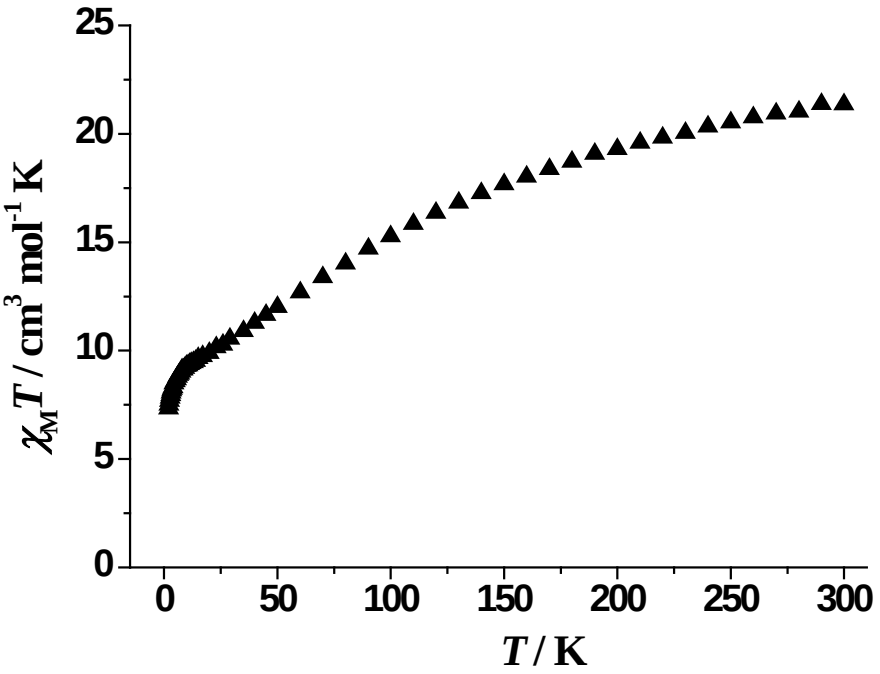

Figure 2.15 $\chi_M T$ *vs.* T plot for complex **2**·2MeCN.

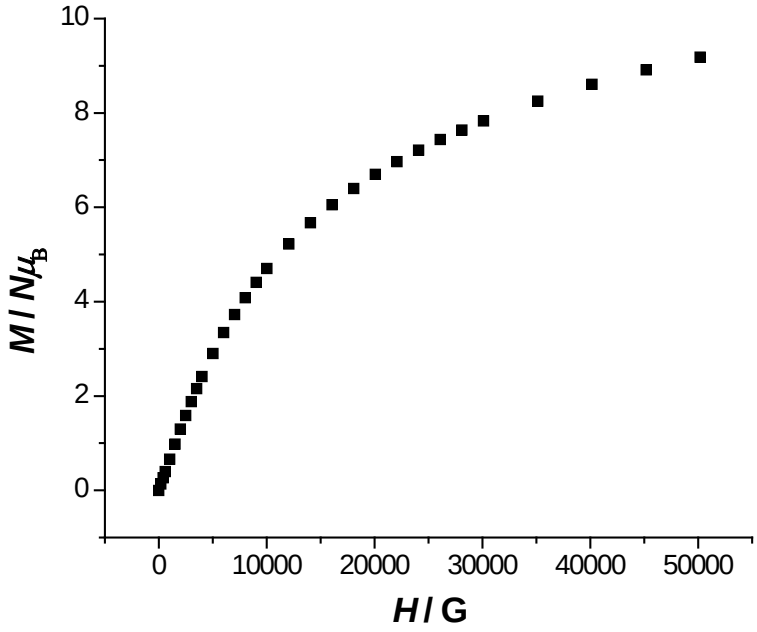

Figure 2.16 Plot of magnetization (*M*) *vs.* field (*H*) for complex **2**·2MeCN at 2 K.

In order to confirm the ground state *S* value for **2**, we carried out alternating-current (*ac*) susceptibility studies, as we have previously done with complex **1**; extrapolation of the in-phase $\chi_M'T$ data from ~3-10 K to 0 K (Figure 2.17) gives a value of ~10 $cm^3 \cdot K \cdot mol^{-1}$, indicative of an $S = 4$ ground state with *g* within the 2.2-2.0 range. No out-of-phase signals were observed in the χ_M'' *vs. T* plot, suggesting **2** is not an SMM.

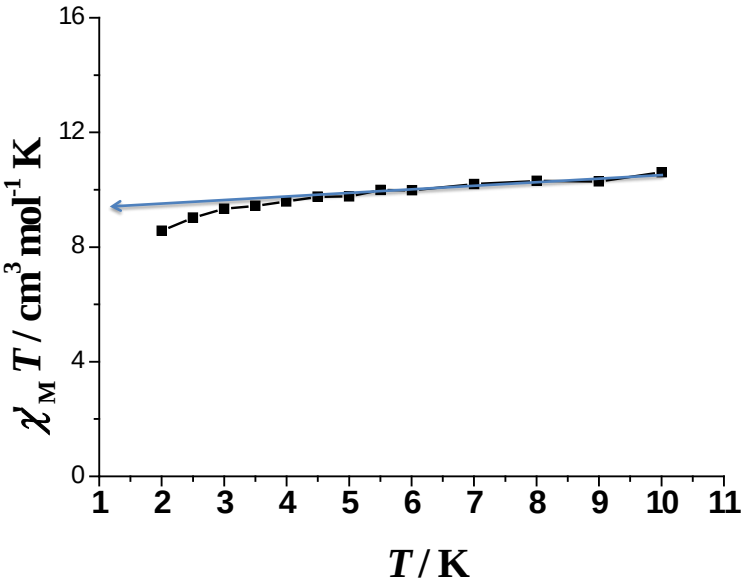

Figure 2.17 The in-phase (as $\chi_M'T$) *vs. T ac* susceptibility signals for **2**·2MeCN under a 4 G oscillating field operating at a frequency of 1000 Hz.

For complex **3**·$3H_2O$, the *dc* magnetic data are shown as χ_MT *vs. T* plot in Figure 2.18.[98] The room temperature χ_MT value is 12.78 $cm^3 \cdot mol^{-1} \cdot K$, slightly lower than the spin-only value of 13.31 $cm^3 \cdot mol^{-1} \cdot K$ with $g = 2.2$ expected for a cluster of eleven non-interacting $S = 1$ Ni^{II} atoms. The χ_MT product for **3**·$3H_2O$ gradually decreases with decreasing *T* in the range 300-25 K, then plateaus to a value of ~4.8 $cm^3 \cdot mol^{-1} \cdot K$ at 20-10

K, before decreasing more rapidly to a value of 3.67 $cm^3 \cdot mol^{-1} \cdot K$ at 2.0 K. The shape of the plot indicates an overall antiferromagnetic behavior with different strength of magnetic couplings at different temperature regions, clearly arising from the different repeating fragments of the $\{Ni_{11}\}$ cage. The low-temperature (T < 20 K) magnetic susceptibility data suggest a small ground state spin value of S = 1 or 2, either of which could be potentially populated at different (or the same) temperatures (*vide infra*).

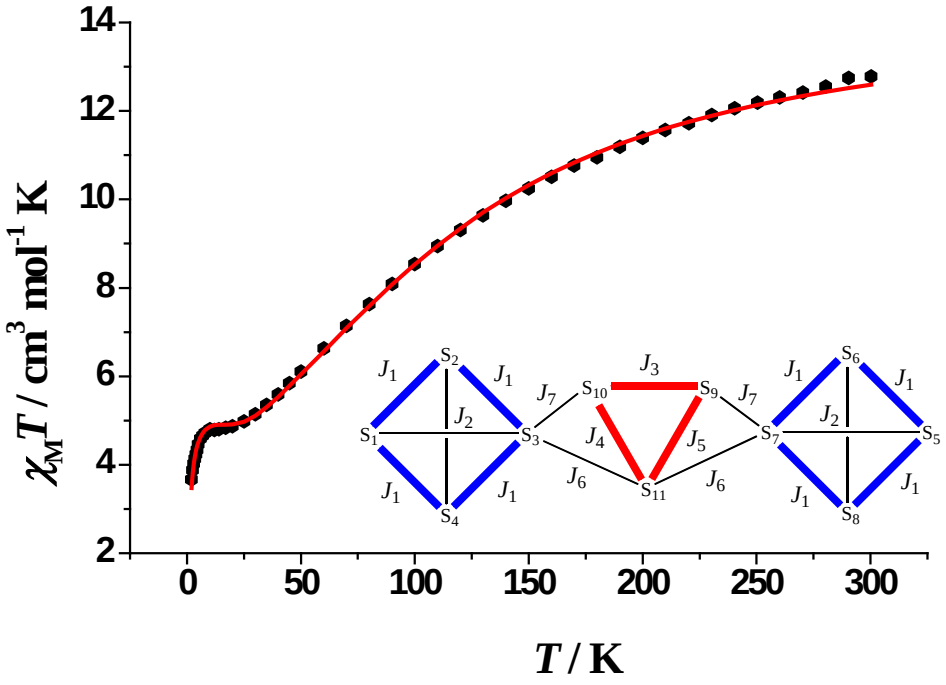

Figure 2.18 Plot of $\chi_M T$ *vs.* T for complex **3**·$3H_2O$. The solid red line is the fit of the data; see the text for the fit parameters. (Inset) Definition of the exchange parameters.

Although complex **3**, as **1** and **2**, is a very complicated, high-nuclearity and low-symmetry system to rationalize its magnetic behavior, we attempted to interpret and fit the magnetic susceptibility data by finding and inspecting all possible magnetic pathways

within the {Ni_4} squares and {Ni_3} triangles. Close inspection of the metric parameters (bond distances and angles) and structural types of the metal fragments in **3** reveals that there are at least seven different exchange pathways and thus seven different *J* coupling constants (from now onward, the numbering scheme that will be used is the same as that used in the molecular structure, see inset of Figure 2.18).

J_1 is associated with the four interactions between the neighboring Ni^{II} centers which comprise the edges of the two {Ni_4} squares; these are bridged by a doubly (μ-OH^-)/(μ-OR^-) pathway with Ni-O-Ni angles in the range 88.0-96.1° (average value close to 90°). Such interactions are expected to be ferromagnetic.[90] J_2 corresponds to the two next-neighboring interactions between Ni1···Ni3 / Ni2···Ni4 and Ni5···Ni7 / Ni6···Ni8 in the diagonal sites of the {Ni_4} squares; these Ni^{II} centers are solely bridged by the central μ_4-OH^- group with the Ni-O-Ni angles spanning the range 165.4-170.8°. Such interactions are expected to be strongly antiferromagnetic,[90] contributing significantly to the high temperature decrease of the $\chi_M T$ product and leading to a local $S = 0$ spin state for the two {Ni_4} squares within **3**. The magnetostructural correlations within the {Ni_3} triangles [Ni(3,10,11), Ni(7,9,11) and Ni(9,10,11)] were expected to be much more complicated due to the possible presence of competing exchange interactions of similar strengths resulting from the different magnetic pathways (i.e., different bridging ligation and metric parameters).[90] Thus, it became difficult to decrease the number of *J* coupling constants (in order to avoid overparameterization problems) by making assumptions which could lead to inaccurate and superficial results. Consequently, J_3, J_4 and J_5 are associated with the three different interactions in the central scalene triangle (Ni9···Ni10 = 3.558 Å, Ni10···Ni11 = 3.072 Å and Ni9···Ni11 = 3.544 Å), deriving from the (μ-OR^-), (μ-OH^-)/(μ-

OR^-) and (μ-OH^-) bridging scheme, respectively. Similarly, J_6 and J_7 stand for the Ni3···Ni11 / Ni7···Ni11 and Ni3···Ni10 / Ni7···Ni9 interactions, within the two fused to the external Ni_4 squares triangles, through a (μ-OH^-) and a doubly (μ-OH^-)/(μ-OR^-) bridging scheme, respectively. The J_3-J_7 superexchange pathways are expected to contribute to the intermediate-to-low temperature region (<20 K) of the $\chi_M T$ *vs.* T plot of **3** and they can be moderate-to-weak ferro- or antiferromagnetic.

The spin Hamiltonian for such a system, illustrated in the inset of Figure 2.18, is given by equation 2.3. An excellent fit of the experimental data (for the entire temperature region) with the program PHI ($H = -2J_{ij}\hat{S}_i \cdot \hat{S}_j$ convention),[99] applying the below Hamiltonian, gave as best-fit parameters: J_1 = +8.4 cm^{-1}, J_2 = -38.5 cm^{-1}, J_3 = +6.7 cm^{-1}, J_4 = +0.2 cm^{-1}, J_5 = -0.6 cm^{-1}, J_6 = +0.1 cm^{-1}, J_7 = +0.9 cm^{-1}, and g = 2.29.

$$H = -2J_1(\hat{S}_1 \cdot \hat{S}_2 + \hat{S}_2 \cdot \hat{S}_3 + \hat{S}_3 \cdot \hat{S}_4 + \hat{S}_4 \cdot \hat{S}_1 + \hat{S}_5 \cdot \hat{S}_6 + \hat{S}_6 \cdot \hat{S}_7 + \hat{S}_7 \cdot \hat{S}_8 + \hat{S}_8 \cdot \hat{S}_5) - 2J_2(\hat{S}_1 \cdot \hat{S}_3 + \hat{S}_2 \cdot \hat{S}_4 + \hat{S}_5 \cdot \hat{S}_7 + \hat{S}_6 \cdot \hat{S}_8) - 2J_3(\hat{S}_9 \cdot \hat{S}_{10}) - 2J_4(\hat{S}_{10} \cdot \hat{S}_{11}) - 2J_5(\hat{S}_9 \cdot \hat{S}_{11}) - 2J_6(\hat{S}_3 \cdot \hat{S}_{11} + \hat{S}_7 \cdot \hat{S}_{11}) - 2J_7(\hat{S}_3 \cdot \hat{S}_{10} + \hat{S}_7 \cdot \hat{S}_9) \qquad (2.3)$$

The obtained J_1 and J_2 values are in satisfactory agreement with the moderate ferromagnetic and strong antiferromagnetic exchange coupling constants, respectively, found in other discrete {Ni_4} square complexes containing the {$Ni_4(\mu_4$-OH)(μ-OR)$_4$}$^{3+}$ core.[90] J_3 is found to be moderately ferromagnetic as a result of the single phenoxido bridge (linking Ni9 and Ni10), which is known to induce ferro- or antiferromagnetic interactions depending on small variations into the nature of the Ni_2 pairwise unit.[100a] The remaining J_4-J_7 coupling constants are weak and lying in the

borderline of ferro-/antiferromagnetic interactions as a result of the wide range of different Ni-O-Ni angles (spanning the range 93.6-125.4°) and countercomplementary effects promoted by the copresence of carboxylate and alkoxido bridging groups within the various Ni_2 subunits.[100b]

The energies of the spin states derived from equation 2.3 *via* the program PHI revealed a very interesting feature which explains the low-temperature magnetic profile of complex **3**. Three well-isolated spin states, namely the S = 1, 2 and 3, are populated at 2 K; S = 1 is the lowest lying spin state (population: 59.6%), with the first S = 2 excited state lying only 0.9 cm^{-1} above the S = 1 level (population: 30.3%) and the second, S = 3, excited state lying 2.5 cm^{-1} above the S = 1 spin state (population: 10.1%). Thus, the plateau of $\chi_M T$ at ~4.8 $cm^3 \cdot mol^{-1} \cdot K$, which does not agree with a well-isolated S = 1, 2 or 3 ground state spin value, corresponds to the simultaneous population of these quasi degenerate spin levels (mixture of spin states). The very low temperature (10-2 K) decay agrees with the population of the lowest in energy, S = 1 ground state for **3**. We should point out that the J_3, J_4 and J_5 coupling constants cannot be joined into a single J value (i.e., treating the central $\{Ni_3\}$ triangle as magnetically equilateral) because in that case the ground state of the system would be the S = 0, in contrast to the experimental data. However, in an attempt to decrease the number of J constants we joined J_6 and J_7 within the Ni(3,10,11) and Ni(7,9,11) triangles and we obtained a similar quality fit with $J_6 = J_7 = 0.5$ cm^{-1}. Based on these findings, we attempted to apply the reported fitting model to the $\{Ni_{18}\}$ complex **2**, which possesses a similar structural motif with that of **3**, in order to interpret its magnetic susceptibility data. However, all our of efforts failed to give any decent

result, which was attributed to the higher nuclearity of **2** and the more exchange coupling constants involved in the overall magnetic behavior.

The magnetization *vs.* field measurements of **3**·3H_2O (Figure 2.19) at 2 K show a continuous increase of *M* as the field increases to a value of ~6 $N\mu_B$ at 5 T, which corresponds to 6 e^- arising from the population of the $S = 3$ spin state. Finally, complex **3** does not exhibit out-of-phase *ac* magnetic susceptibility signals down to 1.8 K, suggesting this is not a SMM.

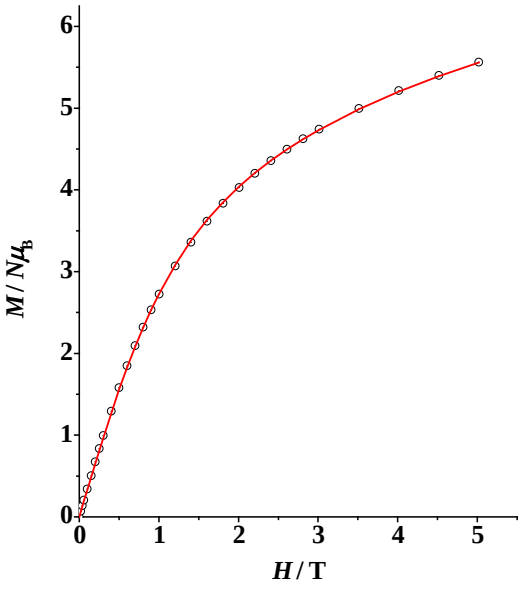

Figure 2.19 Plot of magnetization (*M*) *vs.* field (*H*) for **3**·3H_2O at 2 K. The red line is a guide for the eye.

2.3 Conclusions and Perspectives

It is clear from the above reported results, that the initial use of *N*-salicylidene-2-amino-5-chlorobenzoic acid ($sacbH_2$) in 3*d*-metal cluster chemistry has afforded three novel, diverse molecular clusters with nanoscale dimensions, unprecedented core topologies and record nuclearities. The combined results demonstrate the ability of the doubly deprotonated form of $sacbH_2$ to act as chelating/bridging ligand, fostering the formation of Ni^{II} clusters with unprecedented motifs and structural conformations distinctly different than the ones seen before from the parent *N*-salicylidene-*o*-aminophenol ($saphH_2$) molecule. The structural diversity of complexes **1**-**3** was achieved employing different carboxylate ions as ancillary bridging ligands in the $Ni^{II}/sacbH_2$ general reaction scheme. This emphasizes the rich reactivity of transition metal carboxylate chemistry and the ability of carboxylate ions to yield beautiful complexes with interesting magnetic properties. Although the mechanism of metal cluster formation is impossible to be elucidated, the reported results illustrate the ability of serendipitous assembly to afford nanoscale molecular clusters with sizes similar to the smallest, classical nanoparticles (i.e., metals, metal oxides and alloys). The magnetic properties of the reported Ni^{II} clusters have been studied and revealed interesting results in terms of magnetic exchange interactions and magnetostructural correlations. Moreover, what is really intriguing when comparing the $\{Ni_{26}\}$ complex with other examples of high nuclearity homometallic clusters is that the majority of these complexes tend to crystallize in highly-symmetric, closed-shell topologies with wheel-, grid-, or spherical-like structures, one notable exception being the $\{Co_{36}\}$ cage reported by Alborés and Rentschler.[15] There is no explanation *per se* for this trend, or for the exceptions, but it demonstrates that with the appropriate ligand

choice and under the right experimental conditions the strategy of self-assembly continues to deliver a diverse range of metal topologies that satisfy a broad range of structural tastes.

An obvious future direction for a synthetic inorganic chemist would have been the exploration of the Ni^{II}/sacbH_2 system in the absence of any carboxylate source, and only in the presence of simple inorganic anions (i.e., Cl^-, ClO_4^-, NO_3^-, etc.) with limited binding affinity to Ni^{II} centers. In such a way, sacbH_2 and its anions will reveal their unique bridging versatility and potency, without the additional 'help' of ancillary carboxylate groups. The results of these endeavours will be reported in the next Chapter 3 of this thesis.

CHAPTER 3: Study of the General $Ni^{2+}/X^{-}/sacbH_2$ (X^{-} = inorganic anions) Reaction System

3.1 Experimental Section

3.1.1 Physical measurements

General considerations: All experiments were performed under ambient conditions. All chemicals were purchased from Sigma Aldrich and Alfa Aesar. Chemicals and solvents were used as received without further purification. The organic ligand $sacbH_2$ was prepared as described previously (see, Synthesis of Chapter 2). Safety note: Perchlorate salts are potentially explosive; such compounds should be synthesized and used in small quantities, and treated with utmost care at all times.

Elemental Analysis: Elemental analyses (C, H, and N) were performed on a Perkin-Elmer 2400 Series II Analyzer.

FT-IR spectroscopy: Infrared (IR) spectra were recorded in the solid state on a Bruker FT-IR spectrometer (ALPHA Platinum ATR single reflection) in the 4000-450 cm^{-1} range. Notation for IR bands: vs = very strong; s = strong; m = medium; w = weak; b = broad.

Magnetic susceptibility measurements: Direct current (dc) magnetic susceptibility studies were performed at the University of Barcelona Chemistry Department on a Quantum Design SQUID magnetometer equipped with a 7 T magnet and operating in the 1.9-300 K range. Samples were embedded in solid eicosane to prevent torquing. Pascal's constants were used to estimate the diamagnetic correction, which was subtracted from the experimental susceptibility to give the molar paramagnetic susceptibility (χ_M).[69]

3.1.2 Synthesis

$[Ni_4(sacb)_4(EtOH)_4]$ (4): To a stirred, yellow solution of $sacbH_2$ (0.06 g, 0.20 mmol) and NEt_3 (56 μL, 0.40 mmol) in EtOH (20 mL) was added solid $Ni(ClO_4)_2{\cdot}6H_2O$ (0.07 g, 0.20 mmol). The resulting green-yellow mixture was stirred for 20 min, during which time all the solids dissolved and the color of the solution changed to dark green. The solution was filtered and the filtrate was left to evaporate slowly at room temperature. After four days, X-ray quality green plate-like crystals of **4**·6EtOH had appeared and were collected by filtration, washed with cold EtOH (2 × 2 mL) and Et_2O (2 × 3 mL), and dried in air. The yield was 60 %. Elemental analysis (%) calcd for **4**·2EtOH: C 50.86, H 4.27, N 3.49; found: C 50.97, H 4.41, N 3.24. Selected IR data (ATR): ν = 3299 (mb), 1579 (vs), 1550 (s), 1462 (s), 1439 (s), 1409 (s), 1358 (s), 1287 (m), 1177 (m), 1151 (m), 1117 (m), 1042 (m), 984 (w), 925 (m), 895 (m), 846 (m), 742 (m), 592 (w), 460 (w).

$[Ni_8(sacb)_8(EtOH)_2]$ (5): To a stirred yellow solution of $sacbH_2$ (0.06 g, 0.20 mmol) and NEt_3 (56 μL, 0.40 mmol) in a solvent mixture of MeCN/EtOH (20 mL, 5:1 v/v) was added solid $Ni(ClO_4)_2 \cdot 6H_2O$ (0.07 g, 0.20 mmol). The resulting green solution was stirred for a further 15 min, filtered, and the filtrate was left to evaporate slowly at room temperature. Next day, X-ray quality green plate-like crystals of **5**·MeCN·$5.5H_2O$ had appeared and were collected by filtration, washed with cold MeCN (2 × 2 mL) and Et_2O (2 × 3 mL), and dried in air. The yield was 75 %. Elemental analysis (%) calcd for **5**·$2H_2O$: C 49.99, H 2.89, N 4.02; found: C 50.21, H 2.96, N 3.84. Selected IR data (ATR): ν = 3100 (mb), 1581 (s), 1540 (s), 1462 (s), 1440 (s), 1410 (s), 1354 (s), 1290 (m), 1150 (m), 1116 (m), 981 (w), 924 (w), 893 (m), 846 (m), 740 (m), 593 (m), 454 (w).

3.1.3 Single-crystal X-ray Crystallography

Crystals of **4**·6EtOH (0.03 × 0.12 × 0.13 mm) and **5**·MeCN·$5.5H_2O$ (0.06 × 0.11 × 0.14 mm) were taken from the mother liquor and immediately cooled at -113°C. Diffraction measurements were conducted on a Rigaku R-AXIS SPIDER Image Plate diffractometer using graphite-monochromated Mo Kα (for **4**·6EtOH) or Cu Kα (for **5**·MeCN·$5.5H_2O$) radiation. Data collection (ω-scans) and processing (cell refinement, data reduction and empirical absorption correction) were performed using the CrystalClear program package.[101] Important crystallographic data are listed in Table 3.1. Both structures were solved by direct methods using SHELXS-97[75] and refined by full-matrix least-squares techniques on F^2 with SHELXL-97.[76] All H atoms were located by

difference maps and were refined isotropically or were introduced at calculated positions as riding on their respective atoms. All non-H atoms were refined anisotropically. The programs used for molecular graphics were MERCURY[78] and DIAMOND.[79]

Table 3.1 Crystallographic data for complexes **4** and **5**

Parameter	**4**·6EtOH	**5**·MeCN·5.5H_2O
Formula	$C_{76}H_{92}N_4Ni_4O_{22}Cl_4$	$C_{118}H_{90}N_9Ni_8O_{31.5}Cl_8$
Formula weight / g mol^{-1}	1790.18	2891.25
Crystal type	Green plates	Green plates
Crystal system	Triclinic	Orthorhombic
Space group	*P*-1	*Pcab*
a / Å	11.0498(6)	20.2109(4)
b / Å	11.4157(6)	24.7311(5)
c / Å	17.5861(10)	27.1630(5)
α / º	99.067(2)	90
β / º	94.192(3)	90
γ / º	113.463(2)	90
Volume / $Å^3$	1986.76(19)	13577.1(5)
Z	1	8

ρ_{calc} / g cm^{-3}	1.496	1.423
μ / mm^{-1}	1.143	3.200
$2\theta_{max}$ / °	50	130
Index ranges	$-13 \le h \le 13$	$-23 \le h \le 23$
	$-13 \le k \le 13$	$-26 \le k \le 26$
	$-20 \le l \le 20$	$-20 \le l \le 20$
Reflections collected	52633	20431
Independent reflections	6987 (R_{int} = 0.0379)	9137 (R_{int} = 0.0458)
Final *R* indices	*R*1 = 0.0326	*R*1 = 0.0762
[$I>2\sigma(I)$][a,b]	*wR*2 = 0.0732	*wR*2 = 0.2355
Final *R* indices (all data)	*R*1 = 0.0369	*R*1 = 0.0905
	*wR*2 = 0.0752	*wR*2 = 0.2568
$(\Delta\rho)_{max,min}$ / e Å^{-3}	1.355 and -0.646	1.901 and -0.660

[a] $R1 = \Sigma(||F_o| - |F_c||)/\Sigma|F_o|$.

[b] $wR2 = [\Sigma[w(F_o^2 - F_c^2)^2]/ \Sigma[w(F_o^2)^2]]^{1/2}$, $w = 1/[\sigma^2(F_o^2) + [(ap)^2 + bp]$, where $p = [\max(F_o^2, 0) + 2F_c^2]/3$.

3.2 Results and Discussion

3.2.1 Synthetic Comments and IR Spectra

Our synthetic attempts toward the in-depth investigation of the NiX_2/$sacbH_2$ system, where X^- are various inorganic ions, were started with the one-pot reactions between $NiCl_2 \cdot 6H_2O$ and $sacbH_2$ in various molar ratios and at different solvent media, always in the presence of an external organic base (i.e., NEt_3) to facilitate the deprotonation of the -OH and $-CO_2H$ groups of $sacbH_2$. However, all these reactions failed to give any crystalline material affording only amorphous yellow-green precipitates that we were not able to crystallize and structurally characterize. We have thus turned our attention into the use of $Ni(ClO_4)_2 \cdot 6H_2O$ in place of $NiCl_2 \cdot 6H_2O$ as a means of enhancing the solubility of the resulting product(s) and consequently our chances to isolate single-crystals suitable for X-ray diffraction studies.

A variety of reactions differing in the $Ni(ClO_4)_2 \cdot 6H_2O$:$sacbH_2$ ratio, the organic base and/or the reaction solvent(s) were explored in identifying the following successful systems. The reaction of $Ni(ClO_4)_2 \cdot 6H_2O$, $sacbH_2$, and NEt_3 in a 1:1:2 molar ratio in solvent EtOH gave a green solution that, upon filtration and slow evaporation at room temperature, led to the isolation of green crystals of a new tetranuclear $[Ni_4(sacb)_4(EtOH)_4]$ (**4**) compound in yields as high as 60 % after approximately four days. The formation of **4** can be represented by the balanced equation 3.1. The base NEt_3 has the role of proton acceptor to facilitate the deprotonation of the $sacbH_2$ ligand and provide in solution the necessary for the stabilization of **4** $sacb^{2-}$ ions (*vide infra*). Employment of different organic bases, such as NMe_3, $^nBu_3N$ and Me_4NOH, did not afford crystalline materials but only green precipitates that were characterized with IR spectroscopy and confirmed their same structural identity as **4**.

$$4\ Ni(ClO_4)_2{\cdot}6H_2O + 4\ sacbH_2 + 8\ NEt_3 + 4\ EtOH \longrightarrow$$

$$[Ni_4(sacb)_4(EtOH)_4] + 8\ (NHEt_3)(ClO_4) + 24\ H_2O \quad (3.1)$$

4

Since 3*d*-metal cluster chemistry is relatively unpredictable, the products' identities often depend on many synthetic variables which are frequently ignored due to the need to discover more new bridging/chelating ligands; such variables are usually the reaction solvent, temperature, "pH", metal-to-ligand ratio and the substitution of a given ligand type with donor- or non-donor functionalities. Within the concept of chemical reactivity on cluster compounds, an important synthetic factor that is worth investigating is the effect of the solvent on the structural identity of the complexes. The volatility, polarity, rigidity and coordination affinity of reaction solvents are some of the features which can directly affect the identity of a product.[102] To that end, the reaction that led to complex **4** was repeated in many other alcohols (ROH; R = Me, ^{i}Pr, ^{n}Bu, etc) under exactly the same conditions. In all cases, the resulting compounds were isostructural to **4** with a general formula of $[Ni_4(sacb)_4(ROH)_4]$. Analogous reactions in nonpolar solvent media, such as CH_2Cl_2 and related solvents, did not yield any products presumably due to the poor solubility of the $Ni(ClO_4)_2{\cdot}6H_2O$ inorganic salt. However, when the solvents employed were a mixture of MeCN/EtOH (5:1 v/v), the 1:1:2 reaction of $Ni(ClO_4)_2{\cdot}6H_2O$:$sacbH_2$:NEt_3 afforded green crystals of a new octanuclear $[Ni_8(sacb)_8(EtOH)_2]$ (**5**) compound in 75 % yield within 24 h. The formation of **5** can be represented by the balanced equation 3.2.

$$8\ Ni(ClO_4)_2\cdot 6H_2O + 8\ sacbH_2 + 16\ NEt_3 + 2\ EtOH \longrightarrow$$

$$[Ni_8(sacb)_8(EtOH)_2] + 16\ (NHEt_3)(ClO_4) + 48\ H_2O \quad (3.2)$$

5

Although it is difficult to understand the solution kinetics and propose a mechanism for the formation of complex **5** over **4**, and *vice versa*, it is clear that the nature of the solvent media affects the structural identity of $Ni^{II}/sacb^{2-}$ clusters. Nuclear Magnetic Resonance (NMR) spectroscopy could not provide any insights into the solution chemistry of this system due to the paramagnetic nature of Ni^{II} ions. Further, electrospray ionization (ESI) mass spectrometry (MS) gave multiple signals that correspond to a variety of different fragments in solution, a common feature of transition metal clusters which rarely preserve their solid-state structures in solution. After numerous reactions performed, it is safe to conclude that the tetranuclear **4** is the most thermodynamically stable compound over a wide variety of alcoholic media, but that stability is perturbed in the presence of MeCN and the octanuclear **5** appears to be the most favored product.

As expected due to the same ligands involved in both structures, complexes **4** and **5** have very similar IR spectra. Several bands appear in the ~1581-1290 cm^{-1} range, attributed to contributions from the stretching vibrations of the aromatic rings of $sacb^{2-}$. Contributions from the $\nu(C{=}N)_{imino}$ modes of $sacb^{2-}$ would be also expected in this region. The presence of coordinated EtOH molecules in dried samples of **4** and **5** is manifested by broad bands of medium intensity at ~3299 and ~3100 cm^{-1}, respectively, are assigned to ν(O-H) stretching vibrations; their broadness and relatively low frequency are both indicative of hydrogen bonding (*vide infra*).

3.2.2 Description of Structures

Complex **4**·6EtOH crystallizes in the triclinic space group *P*-1 with the $\{Ni_4\}$ molecule lying on an inversion center located at the middle-point of the Ni2···Ni2′ vector (Figure 3.1). The $\{Ni_4\}$ compound comprises a non-linear, *zigzag* array of four Ni^{II} atoms (Ni1-Ni2-Ni2′ = 108.56º) with each Ni_2 pair bridged by two μ-O atoms from the deprotonated alkoxido (O1, O1′, O11, O11′) or carboxylate (O12, O12′) functionalities of four $sacb^{2-}$ ligands.

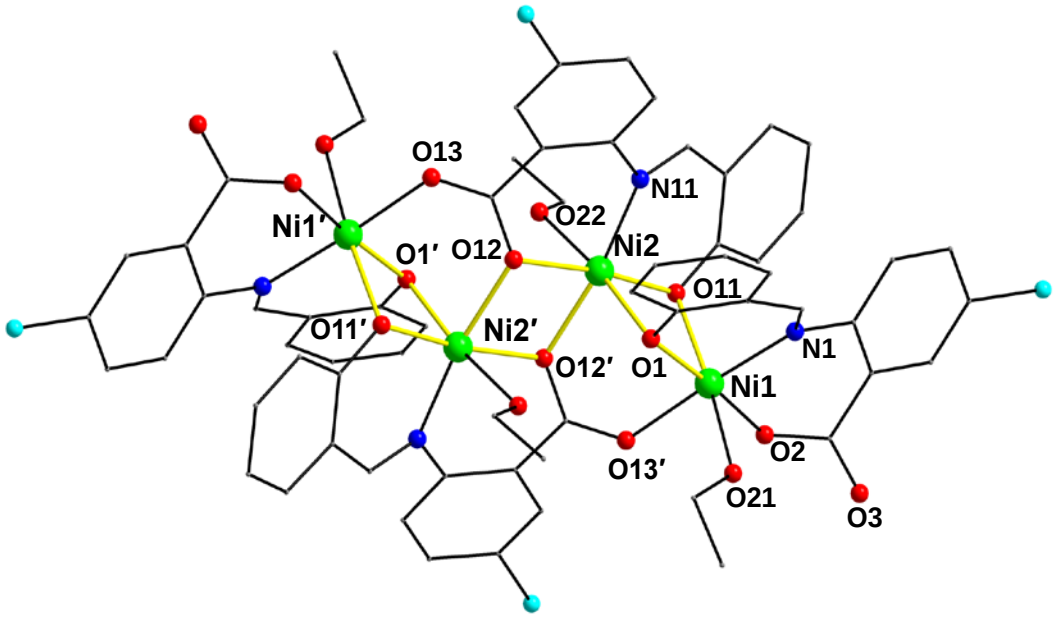

Figure 3.1 Partially-labelled representation of the structure of complex **4** emphasizing the $\{Ni_4(\mu\text{-}OR)_6\}^{2+}$ *zigzag* core. Color scheme: Ni^{II} green, O red, N blue, C gray, Cl cyan. H-atoms are omitted for clarity. Symmetry operation for the primed atoms: 1-*x*, 1-*y*, -*z*.

The sacb^{2-} ligands are of two types (Scheme 3.1): two are binding in an η^2:η^1:η^1:μ mode, acting as N,O,O-tridentate chelates to a Ni^{II} atom (Ni1, Ni1′) and simultaneously bridging an additional Ni^{II} atom (Ni2 or Ni2′) through the phenolate O atom, and the remaining two adopt the more complex η^2:η^1:η^2:η^1:μ_4 binding mode, chelating the central Ni^{II} atoms and bridging all four metal ions through the phenolate and both carboxylate O atoms.

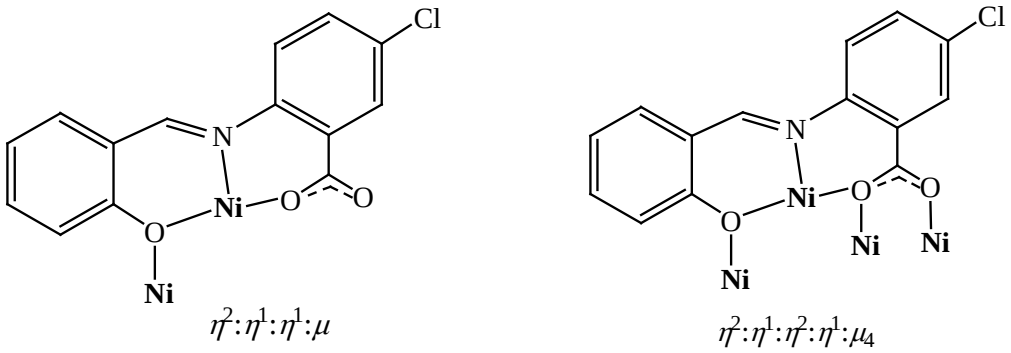

Scheme 3.1 The crystallographically established coordination modes of sacb^{2-} in complex **4**.

Thus, the core of **4** is $\{Ni_4(\mu\text{-}OR)_6\}^{2+}$ (Figure 3.2), with peripheral ligation provided by four terminal EtOH molecules. The central Ni2-O12-Ni2′-O12′ rhombus is strictly planar as a result of the inversion center, but the other two rhombs are quite distorted, with the Ni1-O1-Ni2-O11 torsion angle being 17.1^{o}. The Ni^{II} atoms are all six-coordinate with distorted octahedral geometries.

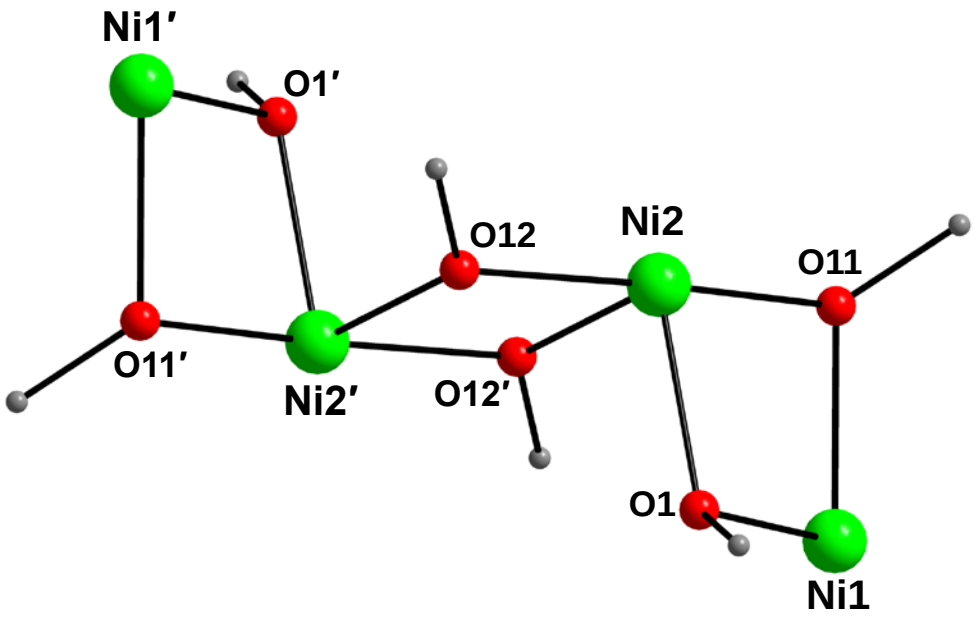

Figure 3.2 The $\{Ni_4(\mu\text{-}OR)_6\}^{2+}$ *zigzag* core of complex **4**.

In the crystal structure of **4**·6EtOH there are H-bonding interactions between the carboxylate and phenolate moieties of $sacb^{2-}$, and the bound EtOH and lattice EtOH solvate molecules (Figure 3.3 and Table 3.2). There are two intramolecular H bonds with the oxygen atoms O22 of coordinated EtOH ligands as donors and the phenolate oxygen atoms O21 as acceptors. Additional H bonds are developed between the oxygen atoms O21 (that belong to coordinated EtOH ligands) and O23, O24, O25 (that belong to lattice EtOH molecules) as donors, and the solvate EtOH oxygen atom O25 and the carboxylate atoms O2 and O3 as acceptors.

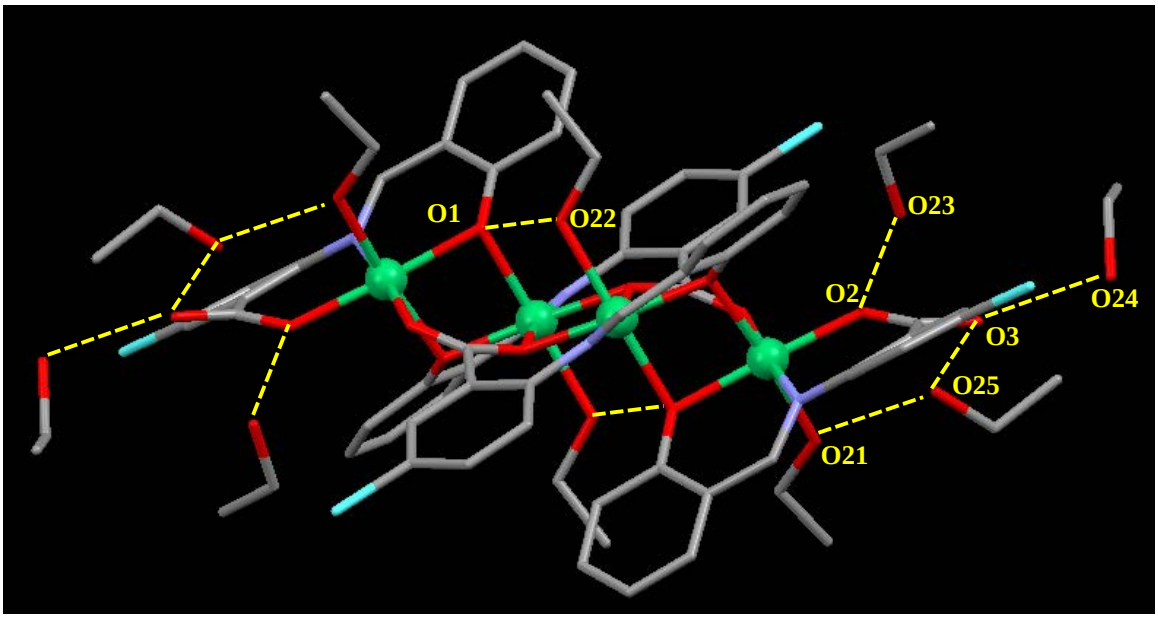

Figure 3.3 The H bonds present in the crystal structure of **4**·6EtOH as illustrated with yellow dashed lines. For further details, see Table 3.2. Color scheme as in Figure 3.1.

Table 3.2 Hydrogen bonds in the crystal structure of **4**·6EtOH

Interaction[a]	D···A (Å)	H···A (Å)	D-H···A (°)	Symmetry operation
O21-H(O21)···O25	2.782	2.001	174.9	*x*, *y*, *z*
O22-H(O22)···O1	2.930	2.184	162.4	1-*x*, 1-*y*, -*z*
O23-H(O23)···O2	2.948	2.162	162.6	*x*, *y*, *z*
O24-H(O24)···O3	2.805	1.862	161.6	*x*, *y*, *z*
O25-H(O25)···O3	2.793	1.946	166.5	*x*, *y*, *z*

[a] O21 and O22 are the oxygen atoms of the crystallographically independent, coordinated EtOH molecules, while O23, O24 and O25 are the oxygen atoms of the crystallographically independent, lattice EtOH molecules. A = acceptor, D = donor.

In addition, weak π-π stacking interactions between the aromatic rings of $sacb^{2-}$ ligands serve to link the $\{Ni_4\}$ clusters into a 2-D network (Figure 3.4).

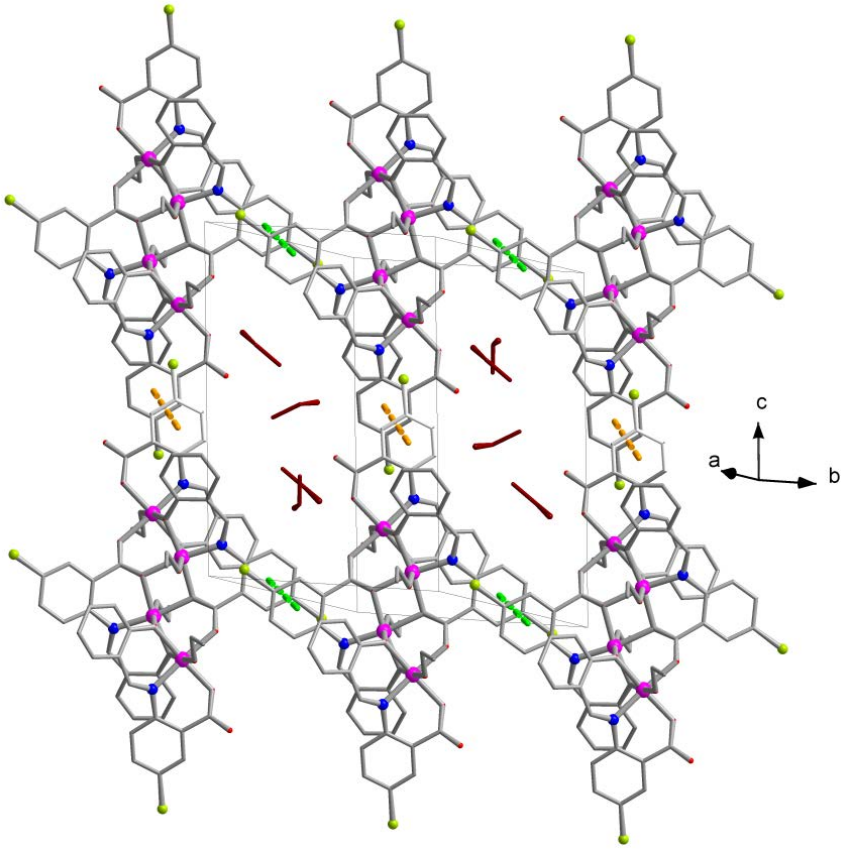

Figure 3.4 A small part of the 2-D network of complex **4** formed by the presence of π-π stacking interactions between the aromatic rings of $sacb^{2-}$ ligands. Bright-green dashed lines indicate the interactions developed between C8···C13 rings along *b*-axis and the orange ones indicate the interactions developed between C28···C33 rings along *c*-axis. The lattice EtOH solvate molecules are indicated with dark red lines. As the overlapping rings are centrosymetrically related, their planes are parallel and the inter-centroid

distance for the C28···C33 rings is 3.652 Å and for the C8···C13 one 4.062 Å. The EtOH solvate molecules reside in the porous of the 2-D network.

Finally, we should mention that although there are hundreds of tetranuclear Ni^{II} complexes structurally and magnetically characterized, compound **4** is only the fourth example of a $\{Ni^{II}_4\}$ cluster with a *zigzag* topology.[103]

Complex **5**·MeCN·5.5H_2O crystallizes in the orthorhombic space group *Pcab* with the $\{Ni_8\}$ molecule lying on an inversion center located at the middle-point of the Ni4···Ni4′ vector (Figure 3.5).

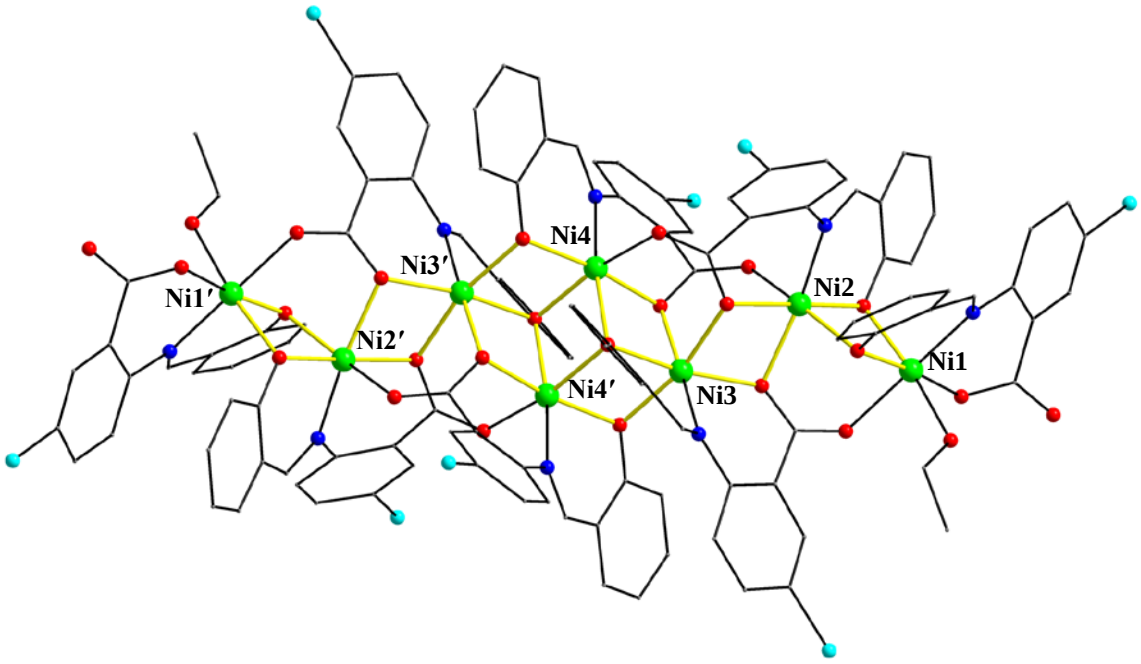

Figure 3.5 Partially-labelled representation of the structure of complex **5** emphasizing the $\{Ni_8(\mu_3\text{-}OR)_2(\mu\text{-}OR)_{12}\}^{2+}$ core. Color scheme: Ni^{II} green, O red, N blue, C gray, Cl cyan. H-atoms are omitted for clarity. Symmetry operation for the primed atoms: 1-*x*, 1-*y*, 2-*z*.

The structure of **5** comprises a $[Ni_8(\mu_3\text{-}OR)_2(\mu\text{-}OR)_{12}]^{2+}$ core (Figure 3.6), which can be described as a central $[Ni_4(\mu_3\text{-}OR)_2(\mu\text{-}OR)_4]^{2+}$ subunit (Ni3, Ni3′, Ni4, Ni4′, O9, O9′, O11, O11′, O12, O12′) attached on either side to two symmetry-related $[Ni_2(\mu\text{-}OR)_4]$ (Ni1, Ni1′, Ni2, Ni2′, O3, O3′, O6, O6′) dimeric moieties. The overall structural conformation of complex **5** can also be described as a *zigzag* molecular chain reminiscent to **4** but larger in nuclearity and dimensions. The linkage between the central $[Ni_4(\mu_3\text{-}OR)_2(\mu\text{-}OR)_4]^{2+}$ unit and the two $[Ni_2(\mu\text{-}OR)_4]$ subunits at opposite ends is provided by four in total alkoxido groups (O5, O5′, O8, O8′) of the $sacb^{2-}$ ligands. The four Ni^{II} ions of the central subunit are located at the four vertices of a defective dicubane, i.e. two cubanes sharing a face (Ni4, O9, Ni4′, O9′) and each missing one metal vertex. The eight Ni^{II} ions are bridged by the alkoxido and carboxylate fragments of eight, doubly deprotonated $sacb^{2-}$ ligands. The $sacb^{2-}$ ions bind in three different ways; two ligands are binding in an $\eta^2\text{:}\eta^1\text{:}\eta^1\text{:}\mu$ manner, four adopt the $\eta^2\text{:}\eta^1\text{:}\eta^2\text{:}\eta^1\text{:}\mu_4$ modes, while the remaining two $sacb^{2-}$ ions bind in an $\eta^3\text{:}\eta^1\text{:}\eta^2\text{:}\eta^1\text{:}\mu_5$ fashion, acting as O,N,O,O-tridentate chelate to a Ni^{II} center and simultaneously bridging four additional Ni^{II} atoms through the phenolate and both carboxylate O atoms (Scheme 3.2). The latter coordination mode of the $sacb^{2-}$ ligand has not been previously seen in any of the reported in this Thesis Ni^{II} clusters, even in the ones with much higher nuclearities. This is most likely due to the co-presence of ancillary carboxylate ligands in complexes **1**-**3** which somehow restrict the bridging capabilities of $sacb^{2-}$ ions. Thus, the decision to investigate the Ni^{II}/$sacbH_2$ system in the absence of any external bridging groups was well deserved, and allowed us to unveil the outright binding affinity and rich bridging versatility of the $sacb^{2-}$ group. The organic

chelate ligand of this work is the sole responsible for bridging up to five metal centers and for yielding the described octanuclear cluster.

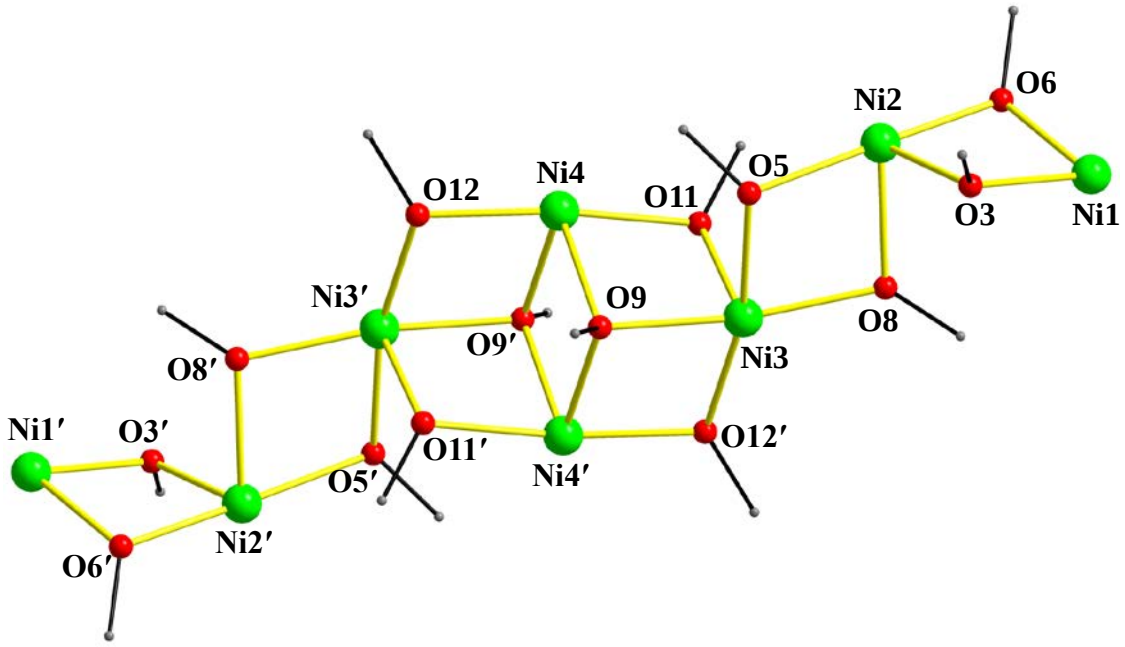

Figure 3.6 Labelled representation of the $[Ni_8(\mu_3\text{-}OR)_2(\mu\text{-}OR)_{12}]^{2+}$ core of complex **5**. Color scheme and symmetry operation for the primed atoms as in Figure 3.5.

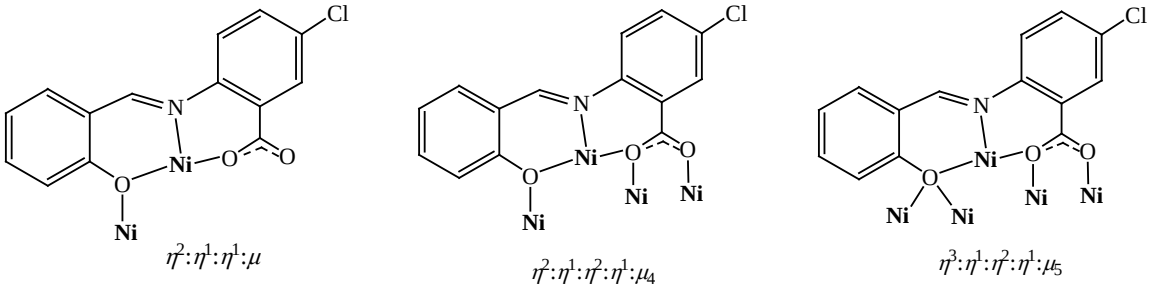

Scheme 3.2 The crystallographically established coordination modes of $sacb^{2-}$ in complex **5**.

Peripheral ligation about the core is provided by two EtOH molecules terminally bound to Ni1 and Ni1′ and hydrogen bonded to aqua lattice solvate molecules; the latter are severally disordered and therefore we avoided extensive discussions on intermolecular H bonding interactions. Finally, all Ni^{II} atoms are six-coordinate with distorted octahedral geometries. In contrast to the tetranuclear complex **4**, the crystal packing of **5** does not reveal any significant π-π stacking effects, either intra- or intermolecularly. An alternative description of the structure of **5** could be that one related to the *zigzag* topology of the tetranuclear cluster **4**. Hence, the octanuclear **5** can be described as two symmetry-related $[Ni_4(\mu\text{-OR})_6]^{2+}$ *zigzag* molecular chains held together by four μ-OR groups, two of which becoming μ_3 and providing the 'hinges' to the overall $\{Ni_8\}$ topology. A space-filling representation (Figure 3.7) shows that **5** has a length of 27.3 Å and a width of 18.7 Å, as calculated by the longest intramolecular Cl···Cl distance, further highlighting the ability of $sacb^{2-}$ to yield molecular compounds with nanoscale dimensions.

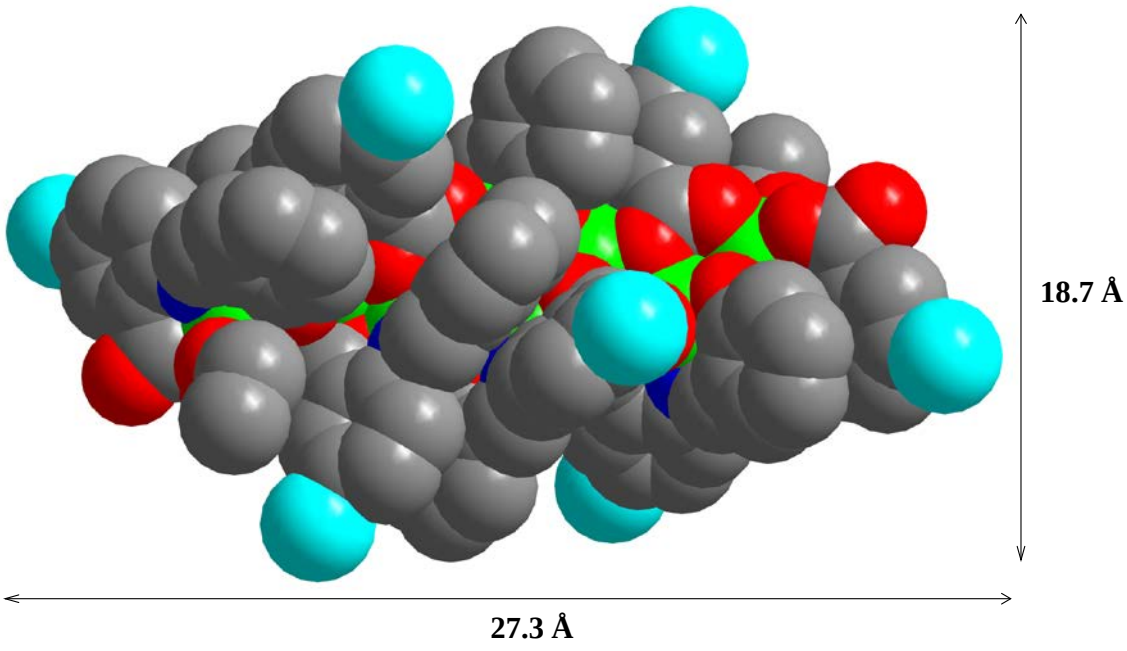

Figure 3.7 Space-filling representation of **5** with its corresponding nanoscale dimensions. Color scheme: Ni green, O red, N blue, C gray, Cl cyan.

Octanuclear Ni^{II} complexes are quite widespread in metal cluster chemistry with N- and/or O-donor ligands. However, none of the previously reported $\{Ni_8\}$ clusters has the same or even similar topology with that of **5**. Most of the reported to date $\{Ni_8\}$ complexes possess topologies consisting of (i) consecutive arrays of $\{Ni_3\}$ triangles fused into an overall rod-like 'closed' motif,[104] (ii) cyclic, wheel-like conformations,[105] and (iii) layers of linear repeating units.[106]

3.2.3 Solid-state Magnetic Susceptibility Studies

Variable-temperature *dc* magnetic susceptibility measurements were performed on freshly-prepared microcrystalline solids of **4**·2EtOH and **5**·$2H_2O$ in the temperature range 2.0-300 K; a *dc* field of 0.3 T was applied from 30 to 300 K and a weaker *dc* field of 0.03 T was applied from 2 to 30 K to avoid magnetization saturation effects. The data for complex **4**·2EtOH are shown as $\chi_M T$ *vs.* *T* plot in Figure 3.8 (top). The value of the $\chi_M T$ product for **4**·2EtOH at 300 K is 5.80 $cm^3 \cdot mol^{-1} \cdot K$, slightly higher than the value of 4.84 $cm^3 \cdot mol^{-1} \cdot K$ (calculated with g = 2.2) expected for four non-interacting Ni^{II} (S = 1) atoms. The $\chi_M T$ product steadily increases in the 300-17 K range to reach a maximum value of 7.31 $cm^3 \cdot mol^{-1} \cdot K$ at 17 K and then more rapidly decreases with decreasing *T* to

reach the value of 4.40 $cm^3 \cdot mol^{-1} \cdot K$ at 2 K (Figure 3.8, top). The data and shape of plot indicate predominant ferromagnetic exchange interactions between the four metal centers in **4**, suggestive of an $S = 4$ ground state spin value.

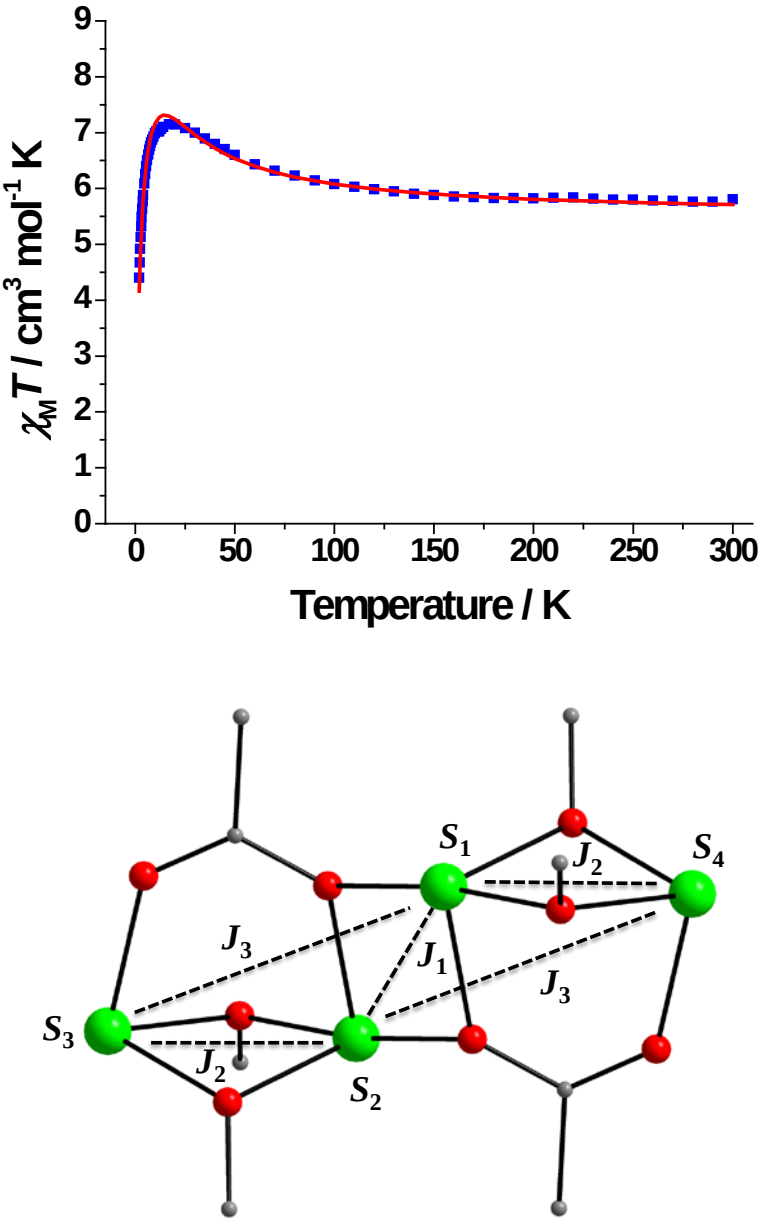

Figure 3.8 (top) $\chi_M T$ *vs.* T plot for complex **4**·2EtOH. The solid red line is the fit of the data; see the text for the fit parameters. (bottom) *J*-coupling scheme employed for the

elucidation of the magnetic exchange interactions in **4**; see the text for the corresponding spin-Hamiltonian.

In order to quantify the nature of the magnetic exchange interactions within **4**, theoretical expressions of χ_M as a function of T were derived and fitted to the experimental data. Complex **4** exhibits a *zigzag* structure, and magnetically it can be treated by the *J*-coupling scheme shown at the bottom of Figure 3.8. On the basis of Figure 3.8 (bottom), the applied Heisenberg spin-Hamiltonian for complex **4** is shown in equation 3.3.

$$\hat{\mathcal{H}} = -J_1(\hat{S}_1 \cdot \hat{S}_2) - J_2(\hat{S}_1 \cdot \hat{S}_4 + \hat{S}_2 \cdot \hat{S}_3) - J_3(\hat{S}_1 \cdot \hat{S}_3 + \hat{S}_2 \cdot \hat{S}_4) \quad (3.3)$$

The PHI program[99] was used to fit both the susceptibility and magnetization data. The quality of the fits was quantified by the agreement factor R, defined as $(\chi_M T_{exp} - \chi_M T_{calc})^2/(\chi_M T_{exp})^2$. An excellent fit of the experimental data (red line of Figure 3.8, top) gave the following best-fit parameters: $J_1 = +12.5$ cm^{-1}, $J_2 = -5.2$ cm^{-1}, $J_3 = +1.8$ cm^{-1} and $g = 2.35$ ($R = 6.7 \times 10^{-5}$).

Magnetization *vs.* field measurements were performed at 2 K and the corresponding plot (Figure 3.9) shows a continuous increase up to a non-saturated value equivalent to 7.2 electrons for **4**. This value is in agreement with the predominant ferromagnetic interactions observed in susceptibility measurements. To evaluate the accuracy of the susceptibility data, the magnetization data were also fitted using the spin-Hamiltonian expressed in equation 3.3, and including the D_{ion} term. Best-fit parameters were: $J_1 = +10.4$ cm^{-1}, $J_2 = -3.2$ cm^{-1}, $J_3 = +1.6$ cm^{-1}, $D =$

+3.9 cm^{-1} and g = 2.34 ($R = 1.1 \cdot 10^{-4}$), in good agreement with the susceptibility data. Both magnetic susceptibility and magnetization measurements confirmed a quasi-frustrated situation for **4** with a mixture of all possible spin states (S = 4 to 0) being very close in energy and almost equally populated at 2 K. The S = 4 spin state for **4** is still not fully saturated under a 5 T field, but it tends to saturate to a value close to 8 electrons at larger magnetic fields. Applying the J values (without the contribution of D) obtained from the fit of the magnetization data, the resulting spin states, their energies and populations at 2 K are given in Table 3.2.

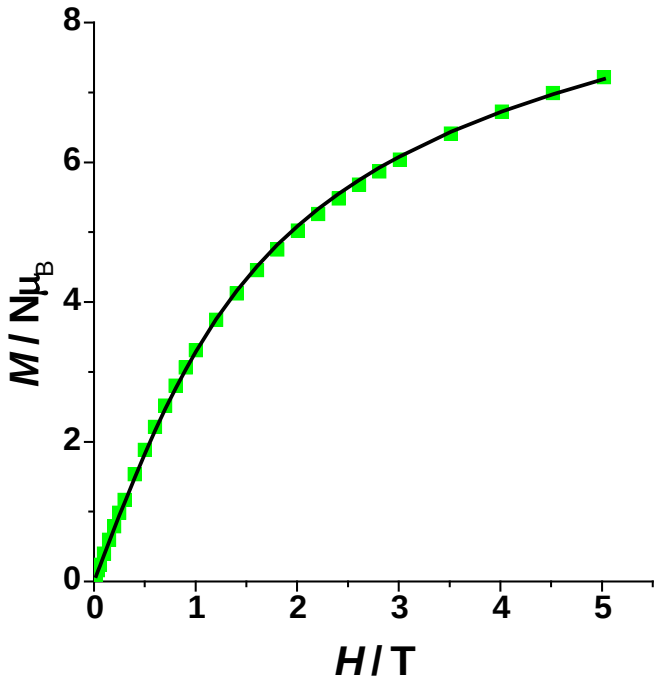

Figure 3.9 Plot of magnetization (M) *vs.* field (H) for complex **4**·2EtOH at 2 K. The solid line is the fit of the data; see the text for the fit parameters.

Table 3.2 Spin states of complex **4**, and their energy values and populations, as

derived from the PHI program suitable for various simulations of magnetic susceptibility and magnetization data

Spin State	Energy (cm^{-1})	Population (%)
2	0	22.21
3	0.76×10^{-3}	22.20
1	0.89×10^{-1}	20.84
0	0.15	19.95
4	0.56	14.80

Rationalization of the magnetic exchange interactions in *zigzag* $\{Ni_4\}$ compounds is unprecedented and thus urged us to undertake magnetostructural correlations on the quasi-frustrated complex **4**. The J_3 coupling constant, which is associated with the next-nearest neighbor interactions of Ni1···Ni2′ and Ni1′···Ni2 (Figures 3.2 and 3.8, bottom) mediated by the carboxylate functionality of $sacb^{2-}$, is undoubtedly necessary and cannot be ignored in order to avoid overparametarization effects. If J_3 was discarded from the fitting model, the ground state should be zero as the result of two external ferromagnetic $\{Ni_2\}$ pairs and a central, antiferromagnetically coupled $\{Ni_2\}$ pair; this is totally against the experimental susceptibility and magnetization data. The most important parameter in the magnetostructural correlations of tetranuclear compounds possessing the $\{Ni_4(\mu_x\text{-}OR)_y\}^{8-y}$ (x = 2 and/or 3; y = various) cores (i.e., cubanes, defective dicubanes, linear,

tetrahedra, etc) has been reported to be the average value of the Ni-O-Ni angles.[97,107] A ferromagnetic exchange is expected for Ni-O-Ni angles lower than 99° and the positive coupling constant value increases as the angle decreases. On the other hand, Ni-O-Ni angles in the vicinity of, and larger than, 99° lead to antiferromagnetic interactions and the absolute value increases as the angle increases. In the *zigzag* complex **4**, J_1 and J_2 constants were employed for the two outer (Ni1-Ni2 and Ni1′-Ni2′) and a central (Ni2-Ni2′) interactions with average Ni-O-Ni angles of 93.8° and 100.2°, respectively. Hence, both J_1 and J_2 were reasonably found to be ferromagnetic and antiferromagnetic, respectively, according to the calculated mean angles. In conclusion, compound **4** exhibits a quasi-frustrated ground state, as a result of the highly competing ferromagnetic and antiferromagnetic exchange interactions. The {Ni_4} compound does not show out-of-phase *ac* magnetic susceptibility signals down to 1.8 K, suggesting that this is not an SMM.

For complex **5**·2H_2O, the magnetic susceptibility data are shown as $\chi_M T$ *vs.* T plot in Figure 3.10. The room temperature $\chi_M T$ value is 10.79 $cm^3 \cdot mol^{-1} \cdot K$, higher than the spin-only value of 9.68 $cm^3 \cdot mol^{-1} \cdot K$ (calculated with g = 2.2) expected for eight non-interacting, high-spin Ni^{II} (S = 1) atoms. The $\chi_M T$ product for **5**·2H_2O steadily increases with decreasing temperature in the range 300-100 K and then rapidly increases to a maximum value of ~28.2 $cm^3 \cdot mol^{-1} \cdot K$ at 3.5 K, before dropping slightly to a value of 27.1 $cm^3 \cdot mol^{-1} \cdot K$ at 2.0 K. The shape of the plot indicates an overall ferromagnetic behavior for the octanuclear compound and a possible S = 8 ground state spin value. The very low-temperature (T < 3.5 K) decrease of the $\chi_M T$ product is mainly due to zero-field

splitting within the ground state, Zeeman effects from the applied *dc* field, and/or weak antiferromagnetic intermolecular interactions.

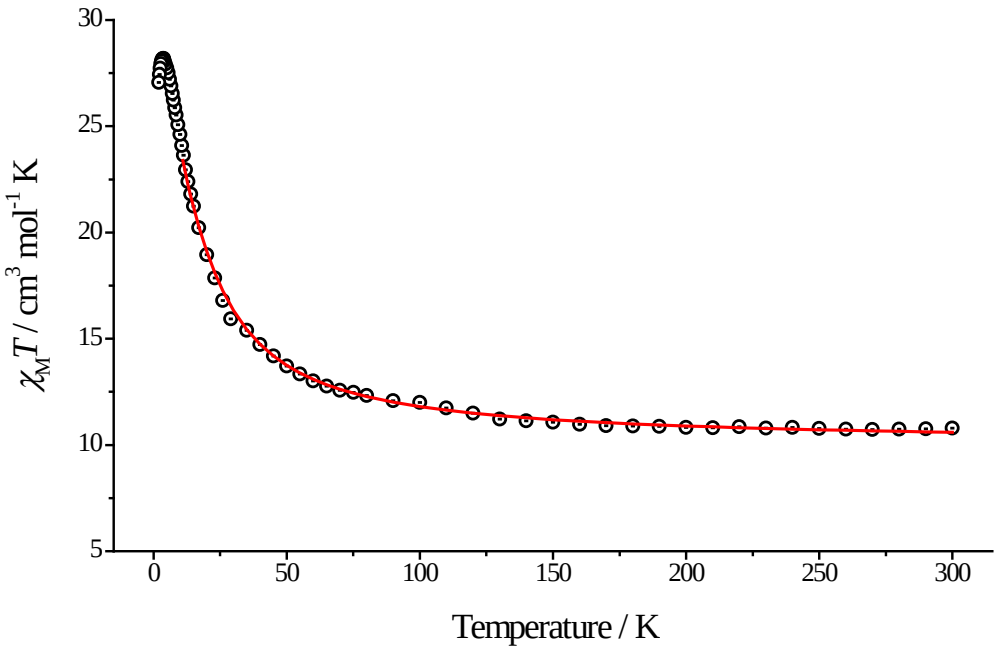

Figure 3.10 $\chi_M T$ *vs. T* plot for complex **5**·2H_2O. The solid red line is the fit of the data; see the text for the fit parameters.

Although the size of the {Ni_8} cluster deter any realistic interpretation of the magnetic susceptibility data, we undertook the challenge of simulating the $\chi_M T$ *vs. T* data using a 3-*J* fitting model which accounts for the similarities of the Ni-O-Ni angles and Ni···Ni distances within the different or similar fragments of the centrosymmetric cluster compound. Based on the metric parameters, we came across the *J*-coupling scheme shown in Figure 3.11. The J_1 coupling constant was used to assess the magnetic interaction between the two central Ni^{II} atoms, bridged exclusively by two μ_3-OR^- groups within the $[Ni_4(\mu_3\text{-OR})_2(\mu\text{-OR})_4]^{2+}$ subunit; the mean Ni-O-Ni angle is 94.9°, much

smaller than the borderline angle of 99°, and was thus expected to lead to a ferromagnetic J_1 coupling constant. The J_2 coupling constant was employed to account for the symmetry-related, opposite $[Ni_2(\mu_3\text{-OR})(\mu\text{-OR})]^{2+}$ faces of the $\{Ni_4\}$ subunit; the mean Ni-O-Ni angles is 94.9°, same as that of J_1 albeit different by means of bridging ligation. Finally, the J_3 coupling constant was considered for six in total $[Ni_2(\mu\text{-OR})_2]^{2+}$ fragments with similar Ni-O-Ni mean angles (94.9°, 96.8° and 98.6°; from left to right in Figure 3.11), Ni···Ni distances, and bridging ligation. These angles are also less than 99°, presaging ferromagnetic exchange interaction between the metal centers. In principle, a different J coupling constant may have been used for each of these $[Ni_2(\mu\text{-OR})_2]^{2+}$ subunits, but this would have led to overparametarization without improving the already good fitting of the susceptibility data (*vide infra*).

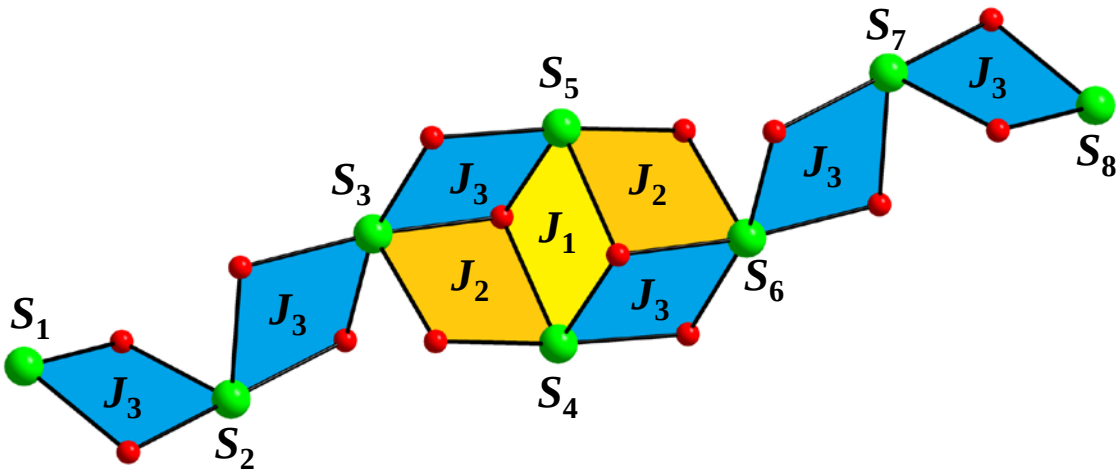

Figure 3.11 The *J*-coupling scheme employed for the elucidation of the magnetic exchange interactions in **5**.

On the basis of Figure 3.11, the applied Heisenberg spin-Hamiltonian for complex **5** is shown in equation 3.4.

$$\mathcal{H} = -J_1(\hat{S}_4 \cdot \hat{S}_5) - J_2(\hat{S}_3 \cdot \hat{S}_4 + \hat{S}_5 \cdot \hat{S}_6) - J_3(\hat{S}_1 \cdot \hat{S}_2 + \hat{S}_2 \cdot \hat{S}_3 + \hat{S}_3 \cdot \hat{S}_5 + \hat{S}_4 \cdot \hat{S}_6 + \hat{S}_6 \cdot \hat{S}_7 + \hat{S}_7 \cdot \hat{S}_8) \quad (3.4)$$

Similarly to the tetranuclear complex **4**, the PHI program[99] was used to fit the magnetic susceptibility data of the octanuclear complex **5**. A very good fit of the experimental data (red line of Figure 3.10) in the 10-300 K temperature range, and not at lower temperatures in order to avoid magnetic effects and parameters that were not included in the employed spin Hamiltonian, gave the following best-fit parameters: J_1 = +6.7 cm^{-1}, J_2 = +7.6 cm^{-1}, J_3 = +2.2 cm^{-1} and g = 2.24 ($R = 6.4 \times 10^{-5}$). All J coupling constants were positive, thus justifying the overall ferromagnetic behavior of the $\{Ni_8\}$ cluster and confirming the expected from the above described magnetostructural criteria S = 8 ground state spin value.

Magnetization (M) *vs.* field (H) measurements for complex **5** were also performed at 2 K, and the corresponding plot (Figure 3.12) shows a continuous increase of M as the field increases to reach a non-saturated value of ~14 $N\mu_B$ at 5 T; such behavior is consistent with an S = 8 ground state with low-lying excited states close in energy with the ground state. It is now well-known that centrosymmetric Ni^{II} clusters possess small to negligible magnetic anisotropy of the Ising-type due to the cancellation of the individual, Ni^{II} single-ion magnetic anisotropies as projected in the z (easy-axis) direction.[108] To that end, complex **5** was expected to also have a negligible molecular magnetic anisotropy, and that was confirmed by the absence of any visible out-of-phase signals in the

imaginary part of the *ac* magnetic susceptibility studies; thus, although **5** exhibited an appreciable ground state spin value, was not an SMM.

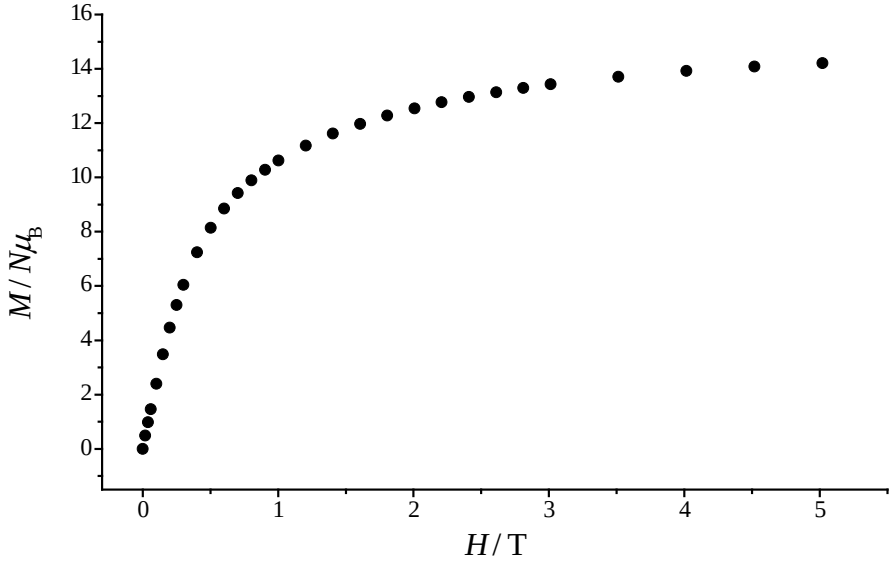

Figure 3.12 Plot of magnetization (*M*) *vs.* field (*H*) for complex **5**·2H_2O at 2 K.

Although there are numerous {Ni_8} paramagnetic clusters reported to date,[104-106] only two[43] of them are ferromagnetically-coupled with S = 8 spin ground states. In particular, Winpenny's group developed the use of 3-methyl-2-pyrazolin-5-one (Hmpo) in Ni(II)/azido cluster chemistry and was able to isolate the isostructural complexes $[Ni_8Na_2(\mu_{1,1,1}\text{-}N_3)_6(\mu_{1,1}\text{-}N_3)_2(\mu_{1,1,3}\text{-}N_3)_4(mpo)_4(O_2CPhBu^t)_2(Hmpo)_6(EtOAc)_6]$ and $[Ni_8Na_2(\mu_{1,1,1}\text{-}N_3)_6(\mu_{1,1}\text{-}N_3)_2(\mu_{1,1,3}\text{-}N_3)_4(mpo)_4(O_2CPh)_2(Hmpo)_6(EtOAc)_6]$. Both complexes feature the $\{Ni_8Na_2(\mu_{1,1,1}\text{-}N_3)_6(\mu_{1,1}\text{-}N_3)_2(\mu_{1,1,3}\text{-}N_3)_4\}^{6+}$ azido-rich core in the form of four fused defective cubanes bound to two additional peripheral Ni^{II} ions. The Ni-N-Ni angles at the bridging azides range from 90.4 to 124.1°. The value of $\chi_M T$ product increases as the temperature decreases, demonstrating that ferromagnetic

exchange interactions are operative through the end-on N_3^- groups. Isofield magnetization data were consistent with an $S = 8$ ground state and a very small D value of -0.066 cm^{-1} and $g = 2.35$. Single-crystal measurements on a micro-SQUID array confirmed SMM behavior with hysteresis seen below 0.4 K; the energy barrier for reorientation of magnetization was very small (~2.8 cm^{-1}).

3.3 Conclusions and Perspectives

In conclusion, we have isolated and characterized two new polynuclear Ni^{II} complexes with rare or unprecedented tetranuclear or octanuclear *zigzag* topologies, respectively. Both $\{Ni_4\}$ and $\{Ni_8\}$ molecular compounds were resulted from similar one-pot reactions of simple inorganic Ni^{II} precursors with the sole use of Schiff-base ligand $sacbH_2$ without requiring the co-presence of any external bridging ligand, such as carboxylate ions or preudohalides. The nature of the reaction solvent(s) was found to be the 'key' point of this research project, leading to molecular cluster compounds of different nuclearities, nanoscale dimensions and structural topologies. The similarities in the *zigzag* motifs of both complexes **4** and **5** were also reflected on their overall magnetic behaviors; both complexes are ferromagnetically-coupled with a quasi-frustrated magnetic system, resulting in a mixture of spin states populated at very low temperatures, for complex **4**, and an $S = 8$ ground state for complex **5**. One of the salient features of this work is the need to insist on the examination and trial of as many synthetic variables as possible in a given reaction system when seeking ways

to synthesize new polynuclear metal complexes. The search for completely new ligand types is not the only route to obtain structurally unique compounds; re-consideration and thorough investigation of various synthetic factors such as the reaction solvent and ligand substituent(s) can also offer alternative pathways for the emergence of beautiful and magnetically interesting 3*d*-metal clusters.

Finally, the vast majority of the research objectives of the present thesis have been completely accomplished. In summary, we have been indeed able to synthesize and thoroughly characterize five new nanometer-sized polynuclear Ni(II) complexes with record nuclearities and interesting magnetic properties, such as ferromagnetic and high-spin molecular magnetic materials. The use of the novel organic chelating/bridging Schiff base ligand *N*-salicylidene-2-amino-5-chlorobenzoic acid ($sacbH_2$) has opened new avenues in Ni^{II} cluster chemistry, breaking the record in nuclearity for any Ni^{II} molecular compound and yielding one of the largest Ni^{II} ground state spin systems (i.e., $S = 8$) reported to date. We have also been able to grow single-crystals suitable for X-ray diffraction studies for all the reported compounds and fully characterize their structural, physical, and spectroscopic properties using X-ray crystallography, IR spectroscopy, elemental analyses, and all modern susceptometry techniques (i.e., *dc* and *ac* magnetic susceptibility studies, magnetization studies at various fields and temperatures, etc.). We have no reason to believe that this area is exhausted of interesting new results. Indeed, on the basis of our ongoing studies and the results arising from them yet to be published, our own opinion is that we have seen only the tip of the iceberg in this area and that many exciting molecules and properties await discovery.

REFERENCES

[1] (*a*) Moore, G. E. *Electronics* **1965**, *38*, 114; (*b*) Balzani, V.; Credi, A.; Venturi, M. in *Molecular Devices and Machines - A Journey into the Nano World*, **2003**.

[2] Feynman, R. P. *Eng. Sci.* **1960**, *23*, 22.

[3] Balzani, V.; Credi, A.; Raymo, F. M.; Stoddart, J. F. *Angew. Chem. Int. Ed.* **2000**, *39*, 3348.

[4] de Silva, N.; Dahl, L. F. *Inorg. Chem*. **2005**, *44*, 9604.

[5] Christou, G. *Polyhedron* **2005**, *24*, 2065.

[6] Stamatatos, Th. C.; Foguet-Albiol, D.; Poole, K. M.; Wernsdorfer, W.; Abboud, K. A.; O'Brien, T. A.; Christou, G. *Inorg. Chem.* **2009**, *48*, 9831.

[7] Stamatatos, Th. C.; Efthymiou, C. G.; Stoumpos, C. C.; Peplepes, S. P. *Eur. J. Inorg. Chem.* **2009**, 3361.

[8] Cotton, F. A.; Walton, C. A.; Murillo, C. A. *Multiple Bonds Between Metal Atoms*, Springer- Verlag, New York , **2005**.

[9] (*a*) Yoshizawa, M.; Tamura, M.; Fujita, M. *Science* **2006**, *312*, 251. (*b*) Sato, S.; Iida, J.; Suzuki, K.; Kawano, M.; Ozeki, T.; Fujita, M. *Science* **2006**, *313*, 1273.

[10] (*a*) Whitehead, G. F. S.; Moro, F.; Timco, G. A.; Wernsdorfer, W.; Teat, S. J.; Winpenny, R. E. P. *Angew. Chem. Int. Ed.* **2013**, *125*, 10116. (*b*) Scott, R. T. W.; Parsons, S.; Murugesu, M.; Wernsdorfer, W.; Christou, G.; Brechin, E. K. *Angew. Chem. Int. Ed.* **2005**, *44*, 6540. (*c*) Manoli, M.; Inglis, R.; Manos, M. J.; Nastopoulos, V.; Wernsdorfer, W.; Brechin, E. K.; Tasiopoulos, A. J. *Angew. Chem. Int. Ed.* **2011**, *50*, 4441. (*d*) Murugesu, M.; Clérac, R.; Anson, C. E.; Powell, A. K. *Inorg. Chem.* **2004**, *43*,

7269. (*e*) Bi, Y.; Wang, X.- T.; Liao, W.; Wang, X.; Zhang, H.; Gao, S. *J. Am. Chem. Soc.* **2009**, *131*, 11650. (*f*) Liu, T.; Zhang, Y.- J.; Wang, Z.- M.; Gao, S. *J. Am. Chem. Soc.* **2008**, *130*, 10500. (*g*) Langley, S. K.; Scott, R. A.; Chilton, N. F; Moubaraki, B.; Murray, K. S. *Chem. Commun.* **2011**, *47*, 6281. (*h*) Moushi, E. E.; Lampropoulos, C.; Wernsdorfer, W.; Nastopoulos, V.; Christou, G.; Tasiopoulos, A. J. *J. Am. Chem. Soc.* **2010**, *132*, 16146.

[11] Liu, J. P.; Fullerton, E.; Gutfleisch, O.; Sellmyer, D. J. *Nanoscale Magnetic Materials and Applications*, Springer, **2009**.

[12] Kühne, I. A.; Kostakis, G. E.; Anson, C. E.; Powell A. K. *Chem. Commun.* **2015**, *51*, 2702.

[13] Tasiopoulos, A. J.; Vinslava, A.; Wernsdorfer, W.; Abboud, K. A.; Christou, G. *Angew. Chem. Int. Ed.* **2004**, *43*, 2117.

[14] Zhang, Z.- M.; Yao, S.; Li, Y.- G.; Clérac, R.; Lu, Y.; Su, Z.- M.; Wang, E.- B. *J. Am. Chem. Soc.* **2009**, *131*, 14600.

[15] Alborés, P.; Rentschler, E. *Angew. Chem. Int. Ed.* **2009**, *48*, 9366.

[16] Dearden, A. L.; Parsons, S.; Winpenny, R. E. P. *Angew. Chem. Int. Ed.* **2001**, *40*, 152.

[17] Foguet-Albiol, D.; Abboud, K. A; Christou, G. *Chem. Commun.* **2005**, 4282.

[18] Powell, A. K. *Comprehensive Coordination Chemistry II*, (Eds.: Mc Cleverty, J. A.; Meyer, T. J.), Elsevier, Amsterdam, **2004**, *8*, 169-194.

[19] Ciurli, S.; Benini, S.; Rypniewski, W. R.; Wilson, K. S.; Miletti, S.; Mangani, S. *Coord. Chem. Rev.* **1999**, *190*, 331.

[20] (*a*) Kanady, J. S.; Tsui, E. Y.; Day, M. W.; Agapie, Th. *Science* **2011**, *333*, 733. (*b*) Mukherjee, S.; Stull, J. A.; Yano, J.; Stamatatos, Th. C.; Pringouri, K.; Stich, T. A.;

Abboud, K. A.; Britt, R. D.; Yachandra, V.; Christou, G. *Proc. Nat. Acad. Sci.* **2012**, *109*, 2257.

[21] Lippard, S. J. *Science* **1995**, *268*, 996.

[22] Blakeley, R. L.; Hinds, J. A.; Kunze, H. E.; Webb, E. C.; Zerner, B. *Biochemistry* **1969**, *8*, 1991.

[23] Callahan, B. P.; Yuan, Y.; Wolfenden, R. *J. Am. Chem. Soc.* **2005**, *127*, 10828.

[24] Sharma, B.; Mandani, S.; Sarma, T. K. *Scientific Reports* **2013**, *3*, 2601.

[25] Gray, H. B.; Stiefel, E. I.; Valentine, J. S.; Bertini, I. in "*Biological Inorganic Chemistry: Structure and Reactivity*", University Science Books, **2007**.

[26] Benini, S.; Rypniewski, W. R.; Wilson, K. S.; Miletti, S.; Ciurli, S.; Mangani, S. *Structure* **1999**, *7*, 205.

[27] Meyer, F. in "*Progress in Inorganic Chemistry*" (Ed.: Karlin, K. D.), John Wiley & Sons, Inc., Hoboken, New Jersey, USA, **2009**, *Vol. 56*, 487-542.

[28] (*a*) Christou, G.; Gatteschi, D.; Hendrickson, D. N.; Sessoli, R. *MRS Bull.* **2000**, *25*, 66. (*b*) Aromi, G.; Brechin, E. K. *Struct. Bond.* **2006**, *122*, 1. (*c*) Bircher, R.; Chaboussant, G.; Dobe, C.; Gudel, H. U.; Ochsenbein, S. T.; Sieber, A.; Waldman, O. *Adv. Funct. Mater.* **2006**, *16*, 209. (*d*) Murrie, M.; Price, D. J. *Annu. Rep. Prog. Chem., Sect. A* **2007**, *103*, 20.

[29] Gatteschi, D.; Sessoli, R.; Villain, J. *Molecular Nanomagnets*, **2006** (Oxford University Press: Oxford).

[30] Gatteschi, D.; Sessoli, R. *Angew. Chem. Int. Ed.* **2003**, *42*, 268.

[31] Stamatatos, Th. C.; Christou, G. *Phil. Trans. R. Soc. A* **2008**, *366*, 113.

[32] Boca, R. *Coord. Chem. Rev.* **2004**, *248*, 757.

[33] (*a*) Vincent, R.; Klyatskaya, S.; Ruben, M.; Wernsdorfer, W.; Balestro, F. *Nature* **2012**, *488*, 357. (*b*) Urdampilleta, M.; Klyatskaya, S.; Cleuziou, J.- P.; Ruben, M.; Wernsdorfer, W. *Nat. Mater.* **2011**, *10*, 502.

[34] For a tutorial review, see: Bagai, R.; Christou, G. *Chem. Soc. Rev.* **2009**, *38*, 1011.

[35] (*a*) Thomas, L.; Lionti, L.; Ballou, R.; Gatteschi, D.; Sessoli, R.; Barbara, B. *Nature* **1996**, *383*, 145. (*b*) Wernsdorfer, W.; Sessoli, R. *Science*, **2000**, 2417.

[36] Zhang, P.; Guo, Y.- N.; Tang, J. *Coord. Chem. Rev.* **2013**, *257*, 1728.

[37] Guo, Y.- N.; Xu, G.- F.; Guo, Y.; Tang, J. *Dalton Trans.* **2011**, *40*, 9953.

[38] Novak, M. A.; Folly, W. S. D.; Sinnecker, J. P.; Soriano, S.; *J. Mag. Mat.* **2005**, *294*, 133.

[39] (*a*) Sessoli, R.; Tsai, H. L.; Schake, A. R.; Wang, S.; Vincent, J. B.; Folting, K.; Gatteschi, D.; Christou, G.; Hendrickson, D. N. *J. Am. Chem. Soc.* **1993**, *115*, 1804. (*b*) Sessoli, R.; Gatteschi, D.; Novak, M. A.; Caneschi, A. *Nature* **1993**, *356*, 141.

[40] (*a*) Winpenny, R. E. P. *Adv. Inorg. Chem.* **2001**, *52*, 1. (*b*) Winpenny, R. E. P. *J. Chem. Soc., Dalton Trans.* **2002**, 1.

[41] (*a*) Krzystek, J.; Park, J. H.; Meisel, M. W.; Hitchman, M. A.; Stratemeier, H.; Brunel, L. C.; Telser, J. *Inorg. Chem.* **2002**, *41*, 4478. (*b*) Rorez, G.; Rebilly, J. N.; Barra, A. L.; Sorace, L.; Blondin, G.; Kirchner, N.; Duran, M.; van Slageren, J.; Parsons, S.; Richard, L.; Marvilliers, A.; Mallah, T. *Angew. Chem. Int. Ed.* **2005**, *44*, 1876.

[42] (*a*) Yang, E. C.; Wernsdorfer, W.; Zakharov, L. N.; Karaki, Y.; Yamaguchi, A.; Isidro, R. M.; Lu, G.- D.; Wilson, S. A.; Rheingold, A. L.; Ishimoto, H.; Hendrickson, D. N. *Inorg. Chem.* **2006**, *45*, 529. (*b*) Moragues-Cánovas, M.; Helliwell, M.; Ricard, L.;

Rivière, E.; Wernsdorfer, W.; Brechin, E. K.; Mallah, T. *Eur. J. Inorg. Chem.* **2004**, 2219.

[43] Bell, A.; Aromi, G.; Teat, S. J.; Wernsdorfer, W.; Winpenny, R. E. P. *Chem. Commun.* **2005**, 2808.

[44] Aromi, G.; Parsons, S.; Wernsdorfer, W.; Brechin, E. K.; McInnes, E. J. L. *Chem. Commun.* **2005**, 5038.

[45] Cadiou, C.; Murrie, M.; Pailsen, C.; Villar, V.; Wernsdorfer, W.; Winpenny, R. E. P. *Chem. Commun.* **2001**,2666.

[46] Ochsenbein, S. T.; Murie, M; Rusanov, E.; Stoeckli-Evans, H.; Sekine, C.; Güdel, H. U. *Inorg. Chem.* **2002**, *41*, 5133.

[47] Escuer, A.; Esteban, J.; Perlepes, S. P.; Stamatatos, Th. C. *Coord. Chem. Rev.* **2014**, *275*, 87.

[48] Winpenny, R. E. P. in "*Transition Metals in Supramolecular Chemistry*", *Vol. 5*, (ed.: Sauvage, J. P.), Wiley, Chichester, **1999**, pp. 193-223.

[49] (*a*) Brechin, E. K. *Chem. Commun.* **2005**, 5141. (*b*) Papaefstathiou, G. S.; Perlepes, S. P. *Comments Inorg. Chem.* **2002**, *23*, 249. (*c*) Stamatatos, Th. C.; Christou, G. *Inorg. Chem.* **2009**, *48*, 3308.

[50] (*a*) Powell, A. K.; Heath, S. L.; Gatteschi, D.; Pardi, L.; Sessoli, R.; Spina, G.; Del Giallo, F.; Pieralli, F. *J. Am. Chem. Soc.* **1995**, *117*, 2491. (*b*) Goodwin, J. C.; Sessoli, R.; Gatteschi, D.; Wernsdorfer, W.; Powell, A. K.; Heath, S. L. *J. Chem. Soc., Dalton Trans.* **2000**, 1835.

[51] (*a*) Heath, S. L.; Powell, A. K. *Angew. Chem., Int. Ed. Engl.* **1992**, *31*, 191. (*b*) Murugesu, M.; Clérac, R.; Anson, C. E.; Powell, A. K. *Chem. Commun.* **2004**, *43*, 1598.

[52] Murrie, M.; Stoeckli-Evans, H.; Güdel, H. U. *Angew. Chem. Int. Ed.* **2001**, *40*, 1957.

[53] (*a*) Baxter, P. N. W.; Lehn, J.- M.; Fisher, J.; Youinou, M.- T. *Angew. Chem. Int. Ed. Engl.* **1994**, *33*, 2284. (*b*) Lehn, J.- M. *Supramolecular Chemistry*; VCH Publishers: New York, **1995**.

[54] (*a*) Fujita, M.; Umemoto, K.; Yoshizawa, M.; Fujita, N.; Kusukawa, T.; Biradha, K. *Chem. Commun.* **2001**, 509. (*b*) Fujita, M. *Chem. Soc. Rev.* **1998**, *27*, 417.

[55] (*a*) Seidel, S. R.; Stang, P. J. *Acc. Chem. Res.* **2002**, *35*, 972. (*b*) Yuan, Q.- H.; Wan, L.- J.; Jude, H.; Stang, P. J. *J. Am. Chem. Soc.* **2005**, *127*, 16279. (*c*) Leininger, S.; Olenyuk, B.; Stang, P. J.; *Chem. Rev.* **2000**, *100*, 853.

[56] Fielden, J; Cronin, L. in "*Encyclopedia of Supermolecular Chemistry*", Taylor & Francis, doi: 10.1081/E-ESMC-120024346, **2005**.

[57] Winpenny, R. E. P. *Comprehensive Coordination Chemistry II, Vol. 7*, (Eds.: J. A. McCleverty, T. J. Meyer), Elsevier, Amsterdam, **2004**, pp. 125.

[58] (*a*) Tasiopoulos, A. J.; Perlepes, S. P. *Dalton Trans.* **2008**, 5537. (*b*) Milios, C. J.; Piligkos, S.; Brechin, E. K. *Dalton Trans.* **2008**, 1809. (*c*) Milios, C. J.; Stamatatos, Th. C.; Perlepes, S. P. *Polyhedron* **2006**, *25*, 134.

[59] Sreenivasulu, B. in "*Schiff Base and Reduced Schiff Base Ligands. Supramolecular Chemistry: From Molecules to Nanomaterials*", **2012**.

[60] Schiff, H. *Ann. Suppl*. **1864**, *3*, 343.

[61] Qin, W.; Panunzio, M.; Biondi, S. *Molecules* **2013**, *18*, 12264.

[62] Clayden, J.; Greeves, N.; Warren, S. in "*Organic Chemistry*", 2nd ed., Oxford, New York, USA, **2012**, pp. 231.

[63] Okawa, H.; Furutachi, H.; Fenton, D. E. *Coord. Chem. Rev*. **1998**, *174*, 51.

[64] Guerreiro, P.; Tamburini, S.; Vigato, V. A. *Coord. Chem. Rev*. **1995**, *139*, 17.

[65] March, J. in "*Advanced Organic Chemistry*", 4th ed., Wiley, New York, USA, **1992**, pp. 884, 918, 934, 966.

[66] Hernandez-Molina, R.; Mederos, A. in "*Comprehensive Coordination Chemistry II*", eds. McCleverty, J. A.; Meyer, T. J. Elsevier, **2003**, Vol.1, ch.1.19, pp.413.

[67] Mazarakioti, E. C.; Poole, K. M.; Cunha-Silva, L.; Christou, G.; Stamatatos, Th. C. *Dalton Trans.* **2014**, *43*, 11456.

[68] Alexandropoulos, D. I.; Nguyen, T. N.; Cuhna-Silva, L.; Zafiropoulos, T. F.; Escuer, A.; Christou, G.; Stamatatos, Th. C. *Inorg. Chem.* **2013**, *52*, 1179.

[69] Bain, G. A.; Berry, J. F. *J. Chem. Educ.* **2008**, *85*, 532.

[70] Kottke, T.; Stalke, D. *J. App. Cryst.* **1993**, *26*, 615.

[71] APEX2, *Data Collection Software Version 2.1-RC13, Bruker AXS, Delft, The Netherlands*, **2006**.

[72] Cryopad, *Remote monitoring and control, Version 1.451, Oxford Cryosystems, Oxford, United Kingdom* **2006**.

[73] SAINT+, *Data Integration Engine v. 7.23a* © **1997-2005**, Bruker AXS.

[74] Sheldrick, G. M. in *SADABS v.2.01, Bruker/Siemens Area Detector Absorption Correction Program* **1998**, Bruker AXS.

[75] Sheldrick, G. M. in *SHELXS-97, Program for Crystal Structure Solution, University of Göttingen*, **1997**.

[76] Sheldrick, G. M. *Acta Cryst. A* **2008**, *64*, 112.

[77] Van der Sluis, P.; Spek, A. L. *Acta Crystallogr., Sect. A* **1990**, *A46*, 194.

[78] *Mercury;* Bruno, I. J.; Cole, J. C.; Edgington, P. R.; Kessler, M. K.; Macrae, C. F.; McCabe, P.; Pearson, J.; Taylor, R. *Acta Crystallogr., Sect. B* **2002**, *58*, 389.

[79] Bradenburg, K. *DIAMOND, Release 3.1f, Crystal Impact GbR*; Bonn, Germany, **2008**.

[80] Cordes, E. C.; Jencks, W. P. *J. Am. Chem. Soc.* **1963**, *85*, 2843.

[81] Giannopoulos, D. P.; Wilson-Konderka, C.; Gagnon, K. J.; Teat, S. J.; Escuer, A.; Metallinos, C.; Stamatatos, Th. C. *Dalton Trans.* **2015**, *44*, 4318.

[82] Stamatatos, Th. C.; Abboud, K. A.; Wernsdorfer, W.; Christou, G. *Angew. Chem. Int. Ed.* **2008**, *47*, 6694.

[83] Cox, B. G. in "*Acids and Bases: Solvent Effects on Acid-Base Strength*", Oxford University Press, **2013**.

[84] (*a*) Khairy, E. M.; Shoukry, M. M; Khalil, M. M.; Mohamed, M. M. A. *Trans. Met. Chem.* **1996**, *21*, 176. (*b*) Hall, M. D.; Failes, T. W.; Hibbs, D. E.; Hambley, T. W. *Inorg. Chem.* **2002**, *41*, 1223.

[85] (*a*) Alaimo, A. A.; Takahashi, D.; Cunha-Silva, L.; Christou, G.; Stamatatos, Th. C. *Inorg. Chem.* **2015**, *54*, 2137. (*b*) Glazunov, V. P.; Mashkovsky, A. A.; Odinokov, S. E. *J. Chem. Soc., Faraday Trans. 2* **1979**, *75*, 629.

[86] An O BVS in the ~1.8-2.0, ~1.0-1.2, and ~0.2-0.4 ranges is indicative of non-, single- and double-protonation, respectively. (*a*) Brown, I. D.; Altermatt, D.; *Acta Crystallogr.* **1985**, *B41*, 244. (*b*) Liu, W.; Thorp, H. H. *Inorg. Chem.* **1993**, *32*, 4102.

[87] Athanasopoulou, A. A.; Pilkington, M.; Raptopoulou, C. P.; Escuer, A.; Stamatatos, Th. C. *Chem. Commun.* **2014**, *50*, 14942.

[88] Pestov, A. V.; Slepukhin, P. A.; Yatluk, Y. G. *Russ. J. Coord. Chem.* **2011**, *37*, 619.

[89] Bagai, R.; Abboud K. A., Christou, G. *Chem. Commun.* **2007**, 3359.

[90] (*a*) Kajiwara, T.; Kobashi, T.; Shinagawa, R.; Ito, T.; Takaishi, S.; Yamashita M.; Iki, N. *Eur. J. Inorg. Chem.* **2006**, 1765. (*b*) Edwards, A. J.; Hoskins, B. F.; Kachab, E. H.; Markiewicz, A.; Murray, K. S.; Robson, R. *Inorg. Chem.* **1992**, *31*, 3585.

[91] Representative references: (*a*) Vincent, J. B.; Chang, H.- R.; Folting, K.; Huffman, J. C.; Christou, G.; Hendrickson, D. N. *J. Am. Chem. Soc.* **1987**, *109*, 5703. (*b*) Wu, R.; Poyraz, M.; Sowrey, F. E.; Anson, C. E.; Wocadlo, S.; Powell, A. K.; Jayasooriya, U. A.; Cannon, R. D.; Nakamoto, T.; Katada, M.; Sano, H. *Inorg. Chem.* **1998**, *37*, 1913. (*c*) Bhula, R.; Gainsford, G. J.; Weatherburn, D. C. *J. Am. Chem. Soc.* **1988**, *110*, 7550. (*d*) Li, J.; Yang, S.; Zhang, F.; Tang, Z.; Ma, S.; Shi, Q.; Wu, Q.; Huang, Z *Inorg. Chim. Acta* **1999**, *294*, 109. (*e*) Sreerama, S. G.; Pal, S. *Inorg. Chem.* **2002**, *41*, 4843.

[92] Ismayilov, R. H.; Wang, W.- Z.; Lee, G.- H.; Yeh, C.- Y.; Hua, S.- A.; Song, Y.; Rohmer, M.- M.; Benard, M.; Peng, S.- M. *Angew. Chem. Int. Ed.* **2011**, *50*, 2045.

[93] Brechin, E. K.; Clegg, W.; Murrie, M.; Parsons, S.; Teat, S. J.; Winpenny, R. E. P. *J. Am. Chem. Soc.* **1998**, *120*, 7365.

[94] (*a*) Brechin, E. K.; Parsons, S.; Winpenny, R. E. P. *J. Chem. Soc., Dalton Trans.* **1996**, 3745. (*b*) Benelli, C.; Blake, A. J.; Brechin, E. K.; Coles, S. J.; Graham, A.; Harris, S. G.; Meier, S.; Parkin, A.; Parsons, S.; Seddon, A. M.; Winpenny, R. E. P. *Chem. Eur. J.* **2000**, *6*, 883.

[95] Nikiforova, M. E.; Kiskin, M. A.; Bogomyakov, A. S.; Aleksandrov, G. G.; Sidorov, A. A.; Mironov, V. S.; Eremenko, I. L. *Inorg. Chem. Commun.* **2011**, *14*, 362.

[96] (*a*) Decker, A.; Fenske, D.; Maczek, K. *Angew. Chem. Int. Ed.* **1996**, *35*, 2863. (*b*) Ivanov, S. A.; Kozee, M. A.; Merrill, W. A.; Agarwal, S.; Dahl, L. F. *J. Chem. Soc., Dalton Trans.* **2002**, 4105.

[97] (*a*) Ruiz, E.; Cano, J.; Alvarez, S.; Alemany, P. *J. Am. Chem. Soc.* **1998**, *120*, 11122. (*b*) Isele, K.; Gigon, F.; Williams, A. F.; Bernardinelli, G.; Franz, P.; Decurtins, S. *Dalton Trans.* **2007**, 332.

[98] Athanasopoulou, A. A.; Raptopoulou, C. P.; Escuer A.; Stamatatos,Th. C. *RSC Adv.* **2014**, *4*, 12680.

[99] Chilton, N. F.; Anderson, R. P.; Turner, L. D.; Soncini, A.; Murray, K. S. *J. Comput. Chem.* **2013**, *34*, 1164.

[100] (*a*) Greatti, A.; Scarpellini, M.; Peralta, R. A.; Casellato, A.; Bortoluzzi, A. J.; Xavier, F. R.; Jovito, R.; Aires de Brito, M.; Szpoganicz, B.; Tomkowicz, Z.; Rams, M.; Haase, W.; Neves, A. *Inorg. Chem.* **2008**, *47*, 1107. (*b*) El Fallah, M. S.; Badyine, F.; Vicente, R.; Escuer, A.; Solans, X.; Font-Bardia, M. *Dalton Trans.* **2006**, 2934, and references cited therein.

[101] Rigaku/MSC. *CrystalClear*. Rigaku/MSC Inc., The Woodlands, Texas, USA, **2005**.

[102] Stamatatos, Th. C.; Oliver, K.; Abboud, K. A.; Christou, G. *Inorg. Chem.* **2011**, *50*, 5272.

[103] (*a*) Akine, S.; Nagumo H.; Nabeshima, T. *Dalton Trans.* **2013**, *42*, 15974. (*b*) Fondo, M.; Ocampo, N.; Garcia-Deibe, A. M.; Vicente, R.; Corbella, M.; Bermejo M. R.; Sanmartin, J. *Inorg. Chem.* **2006**, *45*, 255. (*c*) Zhao, Z.- G.; Wu, X.- Y.; Zhai, Q.- G.; Chen, L.- J.; Zhang, Q.- Z.; Li, W.; Xie Y.- M.; Lu, C.- Z. *Z. Anorg. Allg. Chem.* **2008**, *634*, 288.

[104] (*a*) Breeze, B. A.; Shanmugam, M.; Tuna, F.; Winpenny, R. E. P. *Chem. Commun.* **2007**, 5185. (*b*) Aromi, G.; Bell, A. R.; Helliwell, M.; Raftery, J.; Teat, S. J.; Timco, G. A.; Roubeau, O.; Winpenny, R. E. P. *Chem.- Eur. J.* **2003**, *9*, 3024. (*c*) Esteban, J.;

Escuer, A.; Font-Bardia, M.; Roubeau, O.; Teat, S. J. *Polyhedron* **2013**, *52*, 339. (*d*) Pons-Balague, A.; Ioanidis, N.; Wernsdorfer, W.; Yamaguchi, A.; Sanudo, E. C. *Dalton Trans.* **2011**, *40*, 11765. (*e*) Scott, R. T. W.; Jones, L. F.; Tidmarsh, I. S.; Breeze, B.; Laye, R. H.; Wolowska, J.; Stone, D. J.; Collins, A.; Parsons, S.; Wernsdorfer, W.; Aromi, G.; McInnes, E. J. L.; Brechin, E. K. *Chem.- Eur. J.* **2009**, *15*, 12389.

[105] (*a*) Perivolaris, A.; Stoumpos, C. C.; Karpinska, J.; Ryder, A. G.; Frost, J. M.; Mason, K.; Prescimone, A.; Slawin, A. M. Z.; Kessler, V. G.; Mathieson, J. S.; Cronin, L.; Brechin, E. K.; Papaefstathiou, G. S. *Inorg. Chem. Front.* **2014**, *1*, 487. (*b*) Liu, Y.; Kravtsov, V.; Walsh, R. D.; Poddar, P.; Srikanth, H.; Eddaoudi, M. *Chem. Commun.* **2004**, 2806. (*c*) Karotsis, G.; Stoumpos, C.; Collins, A.; White, F.; Parsons, S.; Slawin, A. M. Z.; Papaefstathiou, G. S.; Brechin, E. K. *Dalton Trans.* **2009**, 3388. (*d*) Xu, Z.; Thompson, L. K.; Milway, V. A.; Zhao, L.; Kelly, T.; Miller, D.O. *Inorg. Chem.* **2003**, *42*, 2950.

[106] (*a*) Scheurer, A.; Gieb, K.; Alam, M. S.; Heinemann, F. W.; Saalfrank, R. W.; Kroener, W.; Petukhov, K.; Stocker, M.; Muller, P. *Dalton Trans.* **2012**, *41*, 3553. (*b*) Kou, H.- Z.; An, G.- Y.; Ji, C.- M.; Wang, B.- W.; Cui, A.- L. *Dalton Trans.* **2010**, *39*, 9604.

[107] For representative examples of $\{Ni_4\}$ cubanes without additional bridging ligands, see: (*a*) Yang, E.- C.; Wernsdorfer, W.; Hill, S.; Edwards, R. S.; Nakano, M.; Maccagnano, S.; Zakharov, L. N.; Rheingold, A. L.; Christou, G.; Hendrickson, D. N. *Polyhedron* **2003**, *22*, 1727. (*b*) Ferguson, A.; Lawrence, J.; Parkin, A.; Sanchez-Benitez, J.; Kamenev, K. V.; Brechin, E. K.; Wernsdorfer, W.; Hill, S.; Murrie, M. *Dalton Trans.* **2008**, 6409. (*c*) Escuer, A.; Font-Bardia, M.; Kumar, S. B.; Solans, X.; Vicente, R.

Polyhedron **1999**, *18*, 909. (*d*) Halcrow, M. A.; Sun, J.- S.; Huffman, J. C.; Christou, G. *Inorg. Chem.* **1995**, *34*, 4167.

[108] Esteban, J.; Alcázar, L.; Torres-Molina, M.; Monfort, M.; Font-Bardia, M.; Escuer, A. *Inorg. Chem.* **2012**, *51*, 5503.

4. APPENDIX

4.1 IR spectra of sacbH_2 and complexes 1-5 (from the top to the bottom)

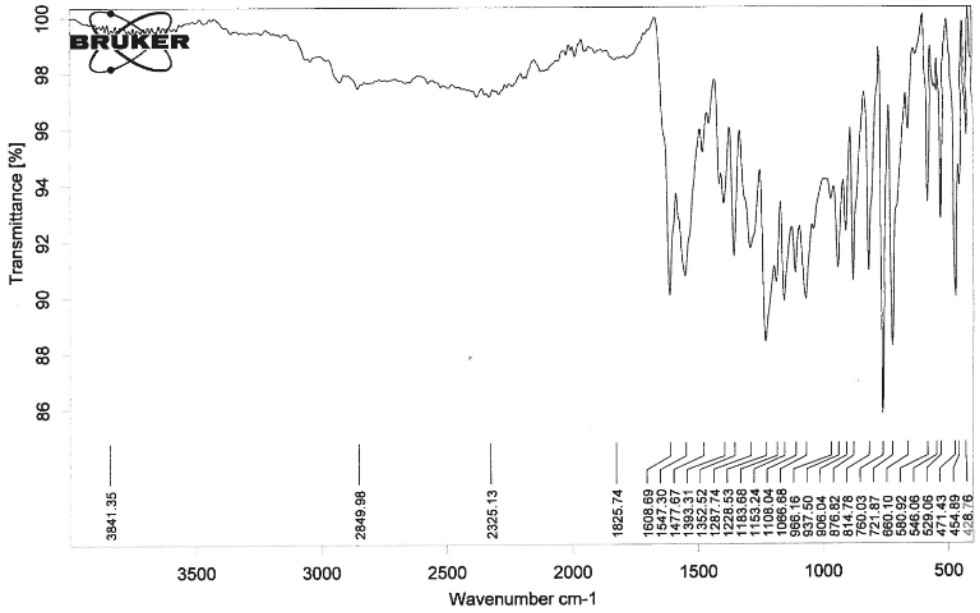

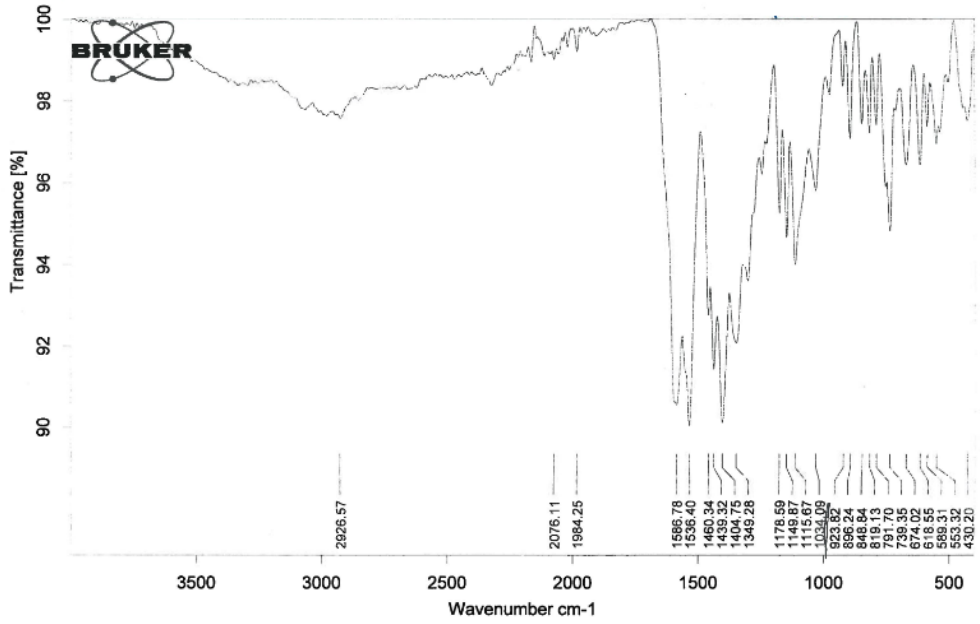

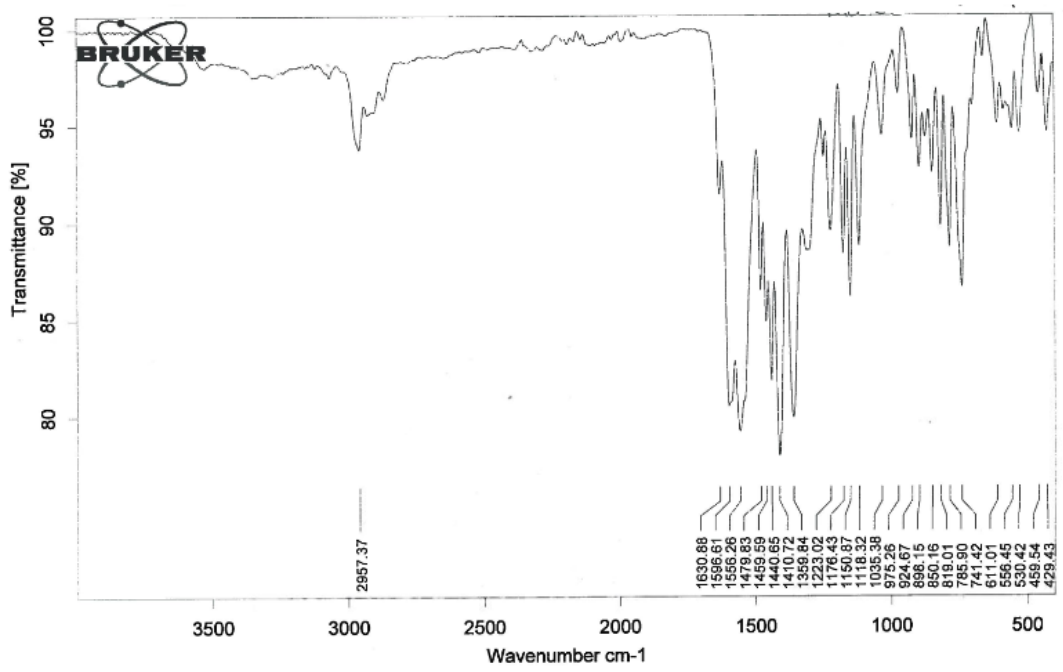
BRUKER
Transmittance [%]
100
95
90
85
80
2957.37
1630.88
1596.61
1556.26
1479.83
1459.59
1440.65
1410.72
1359.84
1223.02
1176.43
1150.87
1118.32
1035.38
975.26
924.67
898.15
850.16
819.01
785.90
741.42
611.01
556.45
530.42
459.54
429.43
3500
3000
2500
2000
1500
1000
500
Wavenumber cm-1

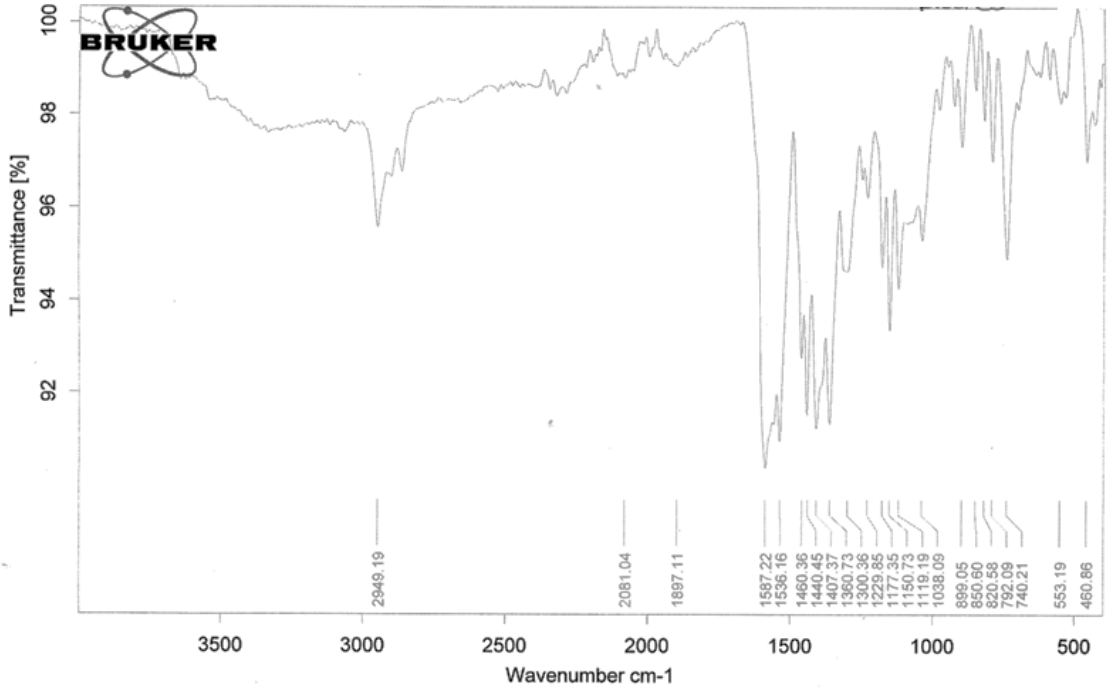
BRUKER
Transmittance [%]
100
98
96
94
92
2949.19
2081.04
1897.11
1587.22
1536.16
1460.36
1440.45
1407.37
1360.73
1300.36
1229.85
1177.35
1150.73
1119.19
1038.09
899.05
850.60
820.58
792.09
740.21
553.19
460.86
3500
3000
2500
2000
1500
1000
500
Wavenumber cm-1

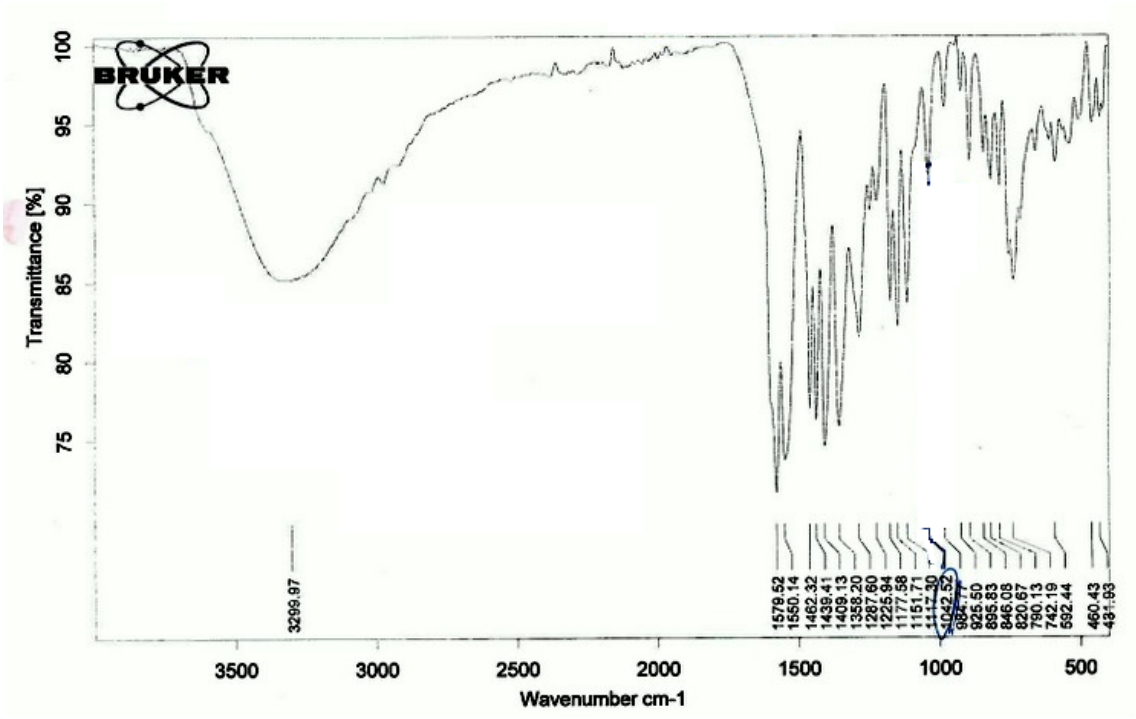
BRUKER
Transmittance [%]
100
95
90
85
80
75
3299.97
1579.52
1550.14
1462.32
1439.41
1409.13
1358.20
1287.60
1225.94
1177.58
1151.71
1117.30
1042.52
984.77
925.50
895.83
846.08
820.67
790.13
742.19
592.44
460.43
431.93
3500
3000
2500
2000
1500
1000
500
Wavenumber cm-1

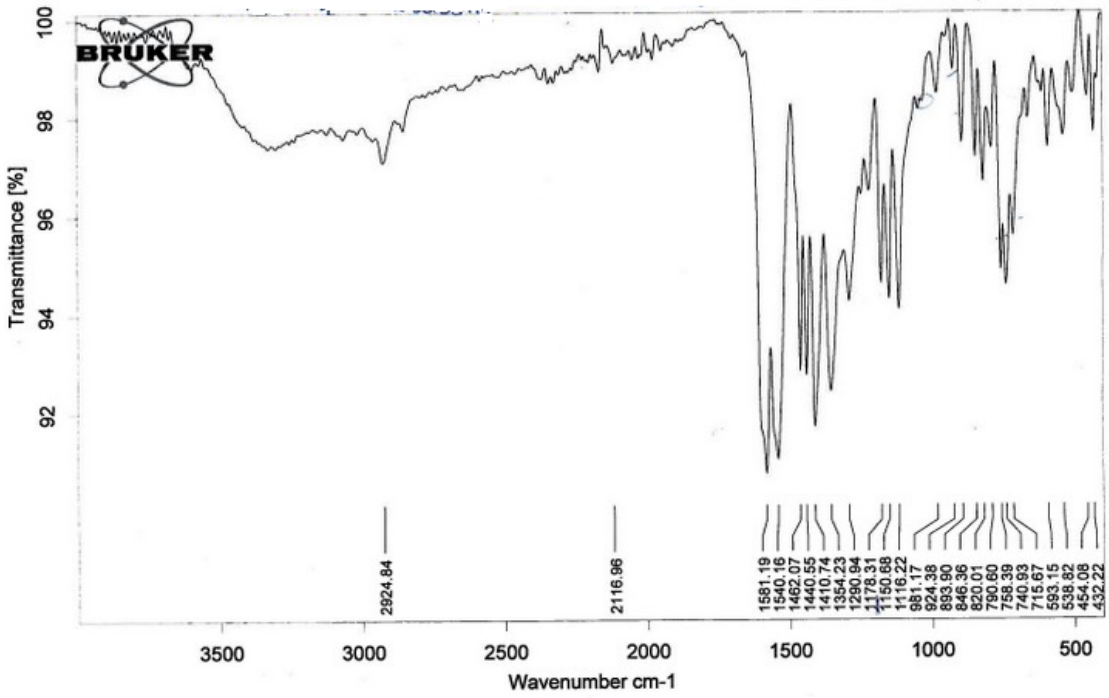
BRUKER
Transmittance [%]
100
98
96
94
92
2924.84
2116.96
1581.19
1540.16
1462.07
1440.55
1410.74
1354.23
1290.94
1178.31
1150.68
1116.22
981.17
924.38
893.90
846.36
820.01
790.60
758.39
740.83
715.67
593.15
538.82
454.08
432.22
3500
3000
2500
2000
1500
1000
500
Wavenumber cm-1